DESIGN OF A SHOCK ABSORBER FOR WEAPON SYSTEMS

A THESIS SUBMITTED TO
THE GRADUATE SCHOOL OF NATURAL AND APPLIED SCIENCES
OF
MIDDLE EAST TECHNICAL UNIVERSITY

BY

ERDEM CANİK

IN PARTIAL FULFILLMENT OF THE REQUIREMENTS
FOR
THE DEGREE OF MASTER OF SCIENCE
IN
MECHANICAL ENGINEERING

JULY 2014

Approval of the thesis:

DESIGN OF A SHOCK ABSORBER FOR WEAPON SYSTEMS

submitted by **ERDEM CANİK** in partial fulfillment of the requirements for the degree of **Master of Science in Mechanical Engineering Department, Middle East Technical University** by,

Prof. Dr. Canan Özgen _____
Dean, Graduate School of **Natural and Applied Sciences**

Prof. Dr. Süha Oral _____
Head of Department, **Mechanical Engineering**

Prof. Dr. Mehmet Çalışkan _____
Supervisor, **Mechanical Engineering Dept., METU**

Examining Committee Members:

Asst. Prof. Dr. Cüneyt Sert _____
Mechanical Engineering Dept., METU

Prof. Dr. Mehmet Çalışkan _____
Mechanical Engineering Dept., METU

Assoc. Prof. Dr. Ender Ciğeroğlu _____
Mechanical Engineering Dept., METU

Assoc. Prof. Dr. M. Metin Yavuz _____
Mechanical Engineering Dept., METU

Serkan Güvey, M. Sc. _____
Lead Design Engineer, ASELSAN

Date: 25.07.2014

I hereby declare that all information in this document has been obtained and presented in accordance with academic rules and ethical conduct. I also declare that, as required by these rules and conduct, I have fully cited and referenced all material and results that are not original to this work.

Name, Last name : Erdem CANİK

Signature :

ABSTRACT

DESIGN OF A SHOCK ABSORBER FOR WEAPON SYSTEMS

CANİK, Erdem
M.S. Department of Mechanical Engineering
Supervisor: Prof. Dr. Mehmet ÇALIŞKAN

August 2014, 132 Pages

Shock absorbing pistons, as the absorbers of the instantaneous shocks and the recoil forces of weapon systems embodying them, are subjected to very high forces. The pistons are required not only to decrease the recoil forces down to favorable values for the other components of the system to function properly and the operator to operate the system comfortable, but also they should not be destructively rigid considering the dynamics of the weapons.

The majority of the shock absorber producers in the local market are suppliers for automotive industry. Considering the life of the items and the loads that they are to be subjected to, the shock absorbers aimed at automotive systems, cannot be satisfactorily integrated to weapon systems.

The dependence on foreign market, as an inevitable result of the insufficiently qualified local suppliers, introduce serious handicaps for the engineering developments where weapons, systems or applications alter; furthermore, is problematic by limiting the shock absorbance capability of the systems since the optimization of these items are out of the clearance of system design and development engineers.

This study; whereby the most efficient piston design, convergent to the ideally desired shock absorbance, is aimed to be obtained by the alteration of design parameters, namely fluid properties, orifice geometry and spring properties, will both provide an opportunity to carry out flexible and unique design by

absorbing recoil forces to lower the effective force down to the levels which would let the other components work properly and operator to control the system comfortably, and end up the dependence on the foreign market.

In the scope of this study, fluid properties, orifice geometry and spring properties are to be investigated for their relation with the shock absorbance characteristics of the piston and the conclusions are to be validated by tests. The software to be developed is aimed to have the capability to finalize the full mathematical modeling of a shock absorber using the recoil force, the desired remainder force after shock absorbing and the correlation coefficients that are to be obtained by tests to validate the mathematical model during its development.

The end product of the study is aimed to be a shock absorber that is designed by the software, produced and validated and is going to be used in the present weapon systems.

Keywords: *Localization, Shock Absorber, Recoil, Weapon Systems*

ÖZ

SİLAH SİSTEMLERİ İÇİN ŞOK SÖNÜMLEYİCİ TASARIMI

CANİK, Erdem
Yüksek Lisans, Makina Mühendisliği Bölümü
Tez Yöneticisi: Prof. Dr. Mehmet Çalışkan

Ağustos 2014, 132 Sayfa

Silah sistemlerinde şok ve geri tepme kuvveti sönümleme işlevlerini sağlayan şok emici pistonlar(damperler), anlık olarak yüksek kuvvetlere maruz kalmaktadır. Pistonların, geri tepme kuvvetini çevre birimler ve kullanıcı için gerekli seviyelere sönümlerken, aynı zamanda silahın dinamiğini bozmayacak şekilde davranmaları gerekmektedir.

Mevcut silah sistemlerinin şok sönümlemesinde kullanılan şok emici pistonlar, yurtdışından hazır ürün olarak satın alınmakta ve uygulamaya yönelik olarak optimizasyonları sağlanamamaktadır. Gerekli mühendislik hesaplamalarında kullanılmak üzere ürünlere ait olan katsayılar ve matematik modellemeler, sağlayıcı firmaların inisiyatifiyle gizli tutulmaktadır.

Yerli pazarda mevcut olan şok emici pistonlar, ağırlıklı olarak otomotiv sektörüne hizmet etmek üzere üretilmektedir. Gerek kullanım ömrü, gerekse maruz kaldıkları kuvvetler açısından, otomotiv sistemlerinde kullanılan şok emici pistonların silah sistemlerine entegrasyonu tatmin edici bir sonuç doğurmamaktadır.

Yerli pazarın yetersizliği sebebiyle yabancı pazara doğan bağlılık, farklı silahlar ve uygulamalar için silah sistemlerinin şok sönümleme kabiliyetini kısıtlamakta ve bu hususta çeşitli sorunlara sebep olmakla beraber, değişen silah, sistem ve uygulamalar için de mühendislik geliştirilmesine engel teşkil etmektedir.

Şok emici pistonların sönümleme karakteristiği pistonlarda kullanılan akışkan özellikleri, piston iç geometrisi ve yay özellikleri gibi değişkenlerle kontrol edilmektedir. Silah sistemleri uygulamalarında arzu edilen sönümlemeyi sağlamak üzere gerçekleştirilecek bu çalışmada atış şoklarının çevre birimlere ve kullanıcıya en az rahatsızlık verecek şekilde sönümlenmesi amaçlanmaktadır. Bu çalışma ile elde edilecek bilgi birikimi esnek ve özgün tasarımı mümkün kılınacağı gibi, aynı zamanda yurtdışı pazarına olan bağımlılığın da önüne geçilecektir.

Çalışma kapsamında, akışkan özelliklerinin, piston iç geometrisi ve yay özelliklerinin, pistonun şok sönümleme katsayıları ile olan bağıntısı araştırılacak, yapılacak testler ile bu bağıntılar doğrulanacaktır. Çalışmanın ardından geliştirilecek sistem ile, silahlara ait olan ölçülmüş geri tepme kuvveti ve isterlerce tanımlanan sönümlenmiş son kuvvet, sistem girdileri olarak kullanılarak, yazılım ortamında şok emici pistonun matematiksel tasarımı yapılacak ve bu tasarımı doğrulamak üzere gerçekleştirilen testler ile geliştirilecek olan korelasyon katsayıları aracılığıyla, sistemin girdileri kullanarak nihai bir şok emici piston tasarımı yapma yetisine sahip olması sağlanacaktır.

Geliştirilen sistem aracılığı ile tasarımı yapılacak olan şok emici piston, çalışmanın sonucunda elde edilecek olan nihai üründür ve mevcut silah sistemlerinde kullanılacaktır.

Anahtar sözcükler: *Yerlileştirme, Şok Sönümleyici, Geri Tepme, Silah Sistemi*

To my family…

ACKNOWLEDGEMENTS

First of all, I would like to express my sincere appreciation to my supervisor Prof. Dr. Mehmet Çalışkan for his guidance and support throughout the study.

This study is funded by ASELSAN Inc. and Ministry of Science, Industry and Technology as a "SANTEZ" project. I am thankful to ASELSAN Inc. and Ministry of Science, Industry and Technology for providing me with the opportunity to perform this research by their funding.

I would like to thank to Assoc. Prof. Dr. Zeki Kıral for his guidance, help and comments throughout the study.

I am in debt of gratitude to my unit leader Serkan Güvey and manager İlhan Başçuhadar for their support and patience.

I am grateful to Gökhan Gürol and PİMAKS Defense and Aerospace Inc. for their help on manufacturing process.

Further, thanks to Berna Öztürk, Merve Bayramusta, Merve Soyarslan, Bahar Cavcar Yayladere, Elif Altuntop, Gökçem Şeker, Canberk Öztoprak, Sait Can Güven and my other colleagues for their support and encouragement.

Finally, I wish to express my sincere thanks to my parents, Zübeyde and Çetin Canik, my sister Didem Canik Orel and her husband Okray Orel for their supports.

TABLE OF CONTENTS

LIST OF FIGURES

LIST OF TABLES

LIST OF SYMBOLS

L	length
E	Young's modulus of material
I	area moment of intertia
A	area
F	force
d	diameter
c	damping coefficient
k	spring stiffness coefficient
m	mass
g	gravitational acceleration
CF	coefficient of critical load for prescribed end conditions
t	time
n	factor of safety
λ	coefficient of heat transmission
c_v	fluid heat capacity
v	velocity
h_r	radiation heat transfer coefficient
h_t	convective heat transfer coefficient
x	displacement
b	thickness
v	kinematic vicosity of fluid
ρ	density
T	temperature
f	frequency
G	shear modulus of material
W	weight
κ_B	Bergstraesser factor
τ_a	alternating shear stress amplitude
p	pressure

σ stress

ζ emprical flow factor

LIST OF ABBREVATIONS

calc	calculated
cyl	cylinder
ammo	ammunition
spr	spring
wnd	winding
cpl	capillary
st	steel
fl	fluid
fund	fundamental
EMI	Electromagnetic Inductance
RFI	Radiofrequency Inductance
cr	Critical
max	Maximum
min	Minimum
t	tangential
r	radial
l	longitudinal

CHAPTER 1

INTRODUCTION

1.1. Overview

Automatic weapons are classified according to their operating principles as gas operated, recoil operated and blowback operated [1]. These three principles provide energy for weapon components to feed, chamber, cock and fire the ammunition by different methods.

In gas operated weapons, the gas pushing the bullet out through the barrel is fed back to bolt group by a hole located on barrel to regenerate the cycle of firing, while in recoil and blowback operated weapons, explosion directly drives the bolt backwards although these two methods have differences in operation.

In the scope of this study, recoil force of a 12.7 mm caliber M2 machine gun is investigated. Therefore, the focus is on recoil operated weapons. Assembled and exploded views of the weapon are presented in Figure 1-1 and Figure 1-2, respectively.

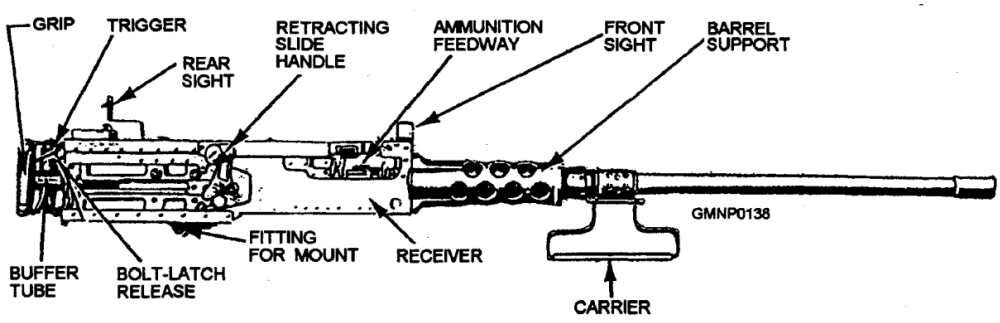

Figure 1-1: 12.7 mm Caliber M2 Machine Gun [1]

The explosion that takes place due to firing of the gun produces gases at high pressure, which forces the round out of the barrel with high velocities. However, the explosion, driving the bullet forward, also acts rearward on the bolt group.

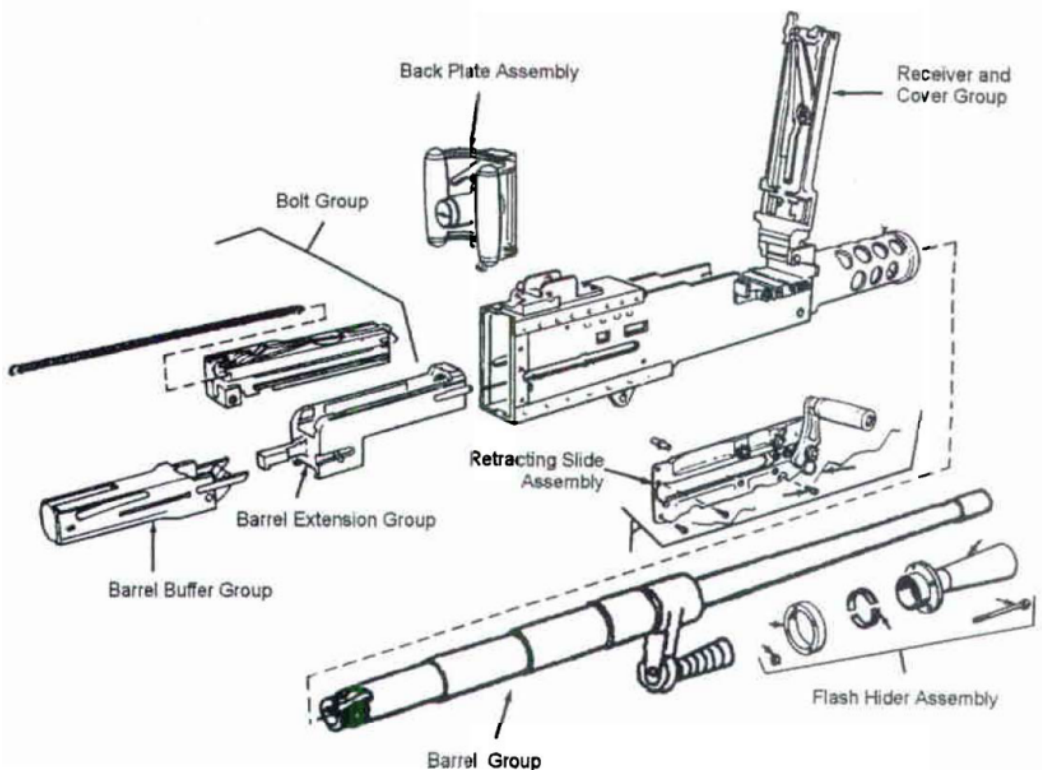

Figure 1-2: Components of M2 Machine Gun [2]

High forces are produced on the weapon mounts after firings due to recoil forces. When the weapon is located on a turret with electronic devices, high levels of vibration and shock may obstruct the functioning of these devices.

In order to be able to prevent incompatibilities with electronic devices, weapons are mounted on recoil mechanisms with shock absorbers. However, coupling a

recoil operated weapon to a system with a shock absorber may affect the dynamics of the weapon causing dispersion and performance issues. Therefore, shock absorbers should be customarily designed for each weapon-turret couplings to obtain sufficient amount of vibration isolation along with stable weapon dynamics.

In the light of the above information, this study aims to develop a software which provides geometric design parameters to obtain required damping and stiffness characteristics and deliver a tangible shock absorber to be integrated in a weapon turret sold commercially.

1.2. Motivation

Shock absorbers must be able to lower the recoil forces received from weapon down to levels required by the electronic units attached on turrets while also providing ease of integration. In present applications, shock absorbers purchased from abroad disables the research and development of a device optimized for systems. Localization of manufacturing and design are the two primary motivations to this study.

In the scope of this study, a shock absorber design tailored for desired performance characteristics is aimed to be conducted by user-friendly software. Mechanical design engineers of limited background regarding the shock absorber design will be able to integrate the correct absorber for their systems by the help of the software, which constitutes another motivation to this study.

1.3. Scope and Objectives

In the scope of this thesis, a software package which is capable of performing a military standard shock absorber design, given required characteristics, and a

shock absorber suitable for a weapon station used in a military project are to be developed.

By the help of the software, weapon stations will be equipped with custom design shock absorbers that are suitable for the coupling of a specific weapon on a specific turret, rather than the off-the-shelf products.

Furthermore, using the design tool, local manufacturers are to be preferred rather than the acquired items from abroad. This study aims to provide the know-how and the ability to localize the manufacturing of shock absorbers. The help of the design software avoids dependence on the foreign market and the research and development capabilities of the foreign providers by localizing the customary shock absorber design.

In present applications of shock absorbers on weapon systems, off-the-shelf products are purchased and the applicability of products is assessed by firing tests, thereby increasing the cost of integration. Software is aimed to design a shock absorber dedicated for the system, therefore, avoids the costs of trial-error method.

1.4. Contribution of Work

This study aims to provide an optimum mathematical shock absorber design for weapon systems and contributes to defense industry by providing localization of design and manufacturing.

Present applications by integrating off-the-shelf products, limit the ability of absorbing shocks. Manufacturers take initiative and request the system and weapon properties to design an appropriate shock absorber, instead of sharing their products' designs. Due to the secrecy of projects, flow of information is limited and products are chosen by trial tests.

Incase shock absorbers attached on recoil mechanisms lack sufficient vibration isolation properties, additional shock mounts on electronic units are required. This study aims to provide sufficient shock absorption in the most compact geometry by the smallest possible number of shock absorbers, thereby contributes for decreasing system size and resolving compatibility issues of electronic devices so that more devices can be implemented on systems.

A tangible outcome of this study is the design of a shock absorber to be used in one of the commercial weapon turrets.

1.5. Outline of Dissertation

In Part 2, literature surveys on various topics relevant to the study are presented.

In Part 3, a 12.7 mm caliber M2 machine gun observation and characterization study is explained. Image processing as a method of characterization is explained in detail.

In Part 4, steps of shock absorber design are explained in detail with formulations. This part constitutes the background for the software development.

In Part 5, prototyping is explained along with know-how's gathered during manufacturing. Failing prototypes and prototype variations are presented.

In Part 6, validation of the mathematical model by prototype tests is explained. Testing scenarios and method are introduced.

In Part 7, concerns about the software development are explained. User-friendly software is introduced in this part.

In the final part, results of previous parts are evaluated and summarized, while conclusion is drawn along with the recommendations for future work.

CHAPTER 2

LITERATURE SURVEY

2.1. Survey on Viscous Heating

Hydraulic dampers consist of spring as a stiffness component and as for the damping component, viscous oil and a piston. While a compression spring is an elastic mechanical energy storage device that simply releases its stored energy when uncompressed, viscous oil forced through the orifices on a piston dissipates energy by converting it to heat.

"In fluid damper, most kinetic energy of vibration and shock transforms into heat due to the fluid viscosity and the energy dissipation results in a temperature rise. This phenomenon is called viscous heating. On the other hand, with the rise of temperature, the fluid viscosity decreases as well as the effectiveness of the damper. This is a cyclic process until a dynamic heat balance is reached." [3]

He and Zheng's derivation [3] of thermal balance equation for a hydraulic damper assumes that viscous fluid has the same temperature everywhere at a given time and the only conduction is through cylinder walls, radially. The formulation of heat transfer includes conduction, convection and radiation.

$$m_f c_v \frac{dT}{dt} = F_c(t) \times v - \frac{\lambda(h_r+h)}{\lambda+h_r+h} A(T(t)-T_{air})$$

Equation (2-1)

2.2. Survey on Viscous Damping Force

Hall [4] discusses damping can be provided by a linear damper, which exerts damping force linearly proportional with the velocity of motion and therefore provides $\alpha=1$ in Equation (2-2).

$$F=cv^{\alpha}$$

Equation (2-2)

According to his study, obtaining linear damping characteristics is possible either by flow in a capillary or in an annulus. Hall states that, annular flow provides about 40 times greater damping force compared to capillary flow, given that capillary flow occurs through a single orifice but is of the same cross sectional area and length as the annular [4].

Hall provides Equation (2-3) for capillary flow and Equation (2-4) for annular flow.

$$F_{damping}=\frac{128\ \rho\ \vartheta\ L_{capillary}A_{hydraulic}^{2}}{\pi d_{capillary}^{4}}v$$

Equation (2-3)

$$F_{damping}=\frac{12\ \rho\ \vartheta\ L_{annular}A_{hydraulic}^{2}}{\pi d_{annulus}b_{annulus}^{3}}v$$

Equation (2-4)

Elaldı and Akçay [5] formulate the damping force for a hydraulic damper as in Equation (2-5).

$$F_{damping} = \frac{\left(1 - \frac{A_{orifice}}{A_{piston}}\right)^2}{\zeta} \frac{\rho_{fl} (A_{piston})^3}{2(A_{orifice})^2} v^2$$

Equation (2-5)

Notice, however, that this study approaches damping as a square law damping since α, damping exponent in Equation (2-2) is equal to 2.

2.3. Survey on Viscous Damper Design Considerations

Annulus type of viscous damper functions by forcing viscous fluid, through the clearance between the cylinder wall and the piston. Mechanical energy is thereby converted into heat. Hall states that changes in viscosity due to viscous heating may be overcome by choosing different materials for the piston and the cylinder wall, so that the difference between material thermal expansion coefficients may compensate the viscosity drop [4].

Hall [4] also recommends oils with viscosity lower than 200 cSt and mentions that any contamination or imperfection in the fluid will distort low frequency response. According to Hall, piston diameter should be at least 3 times greater than the piston rod diameter to allow oil velocity above piston region to approach to zero. In his study, co-centricity of piston and cylinder at all times is advised.

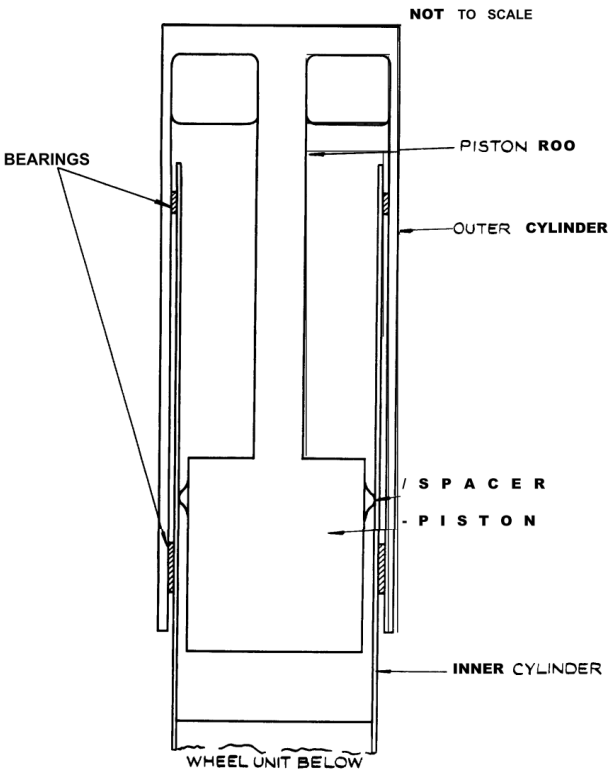

Figure 2-1: Sketch of Annulus Type of Shock Strut Proposed by Hall [4]

Taylor and Duflot [6] suggest practical design tips for hydraulic shock absorbers. Their work sums up many fundamentals regarding the component-wise design considerations. For piston rod, Taylor and Duflot [6] suggest the outer diameter to be highly polished and, as for the material, stainless steel with additional chrome plating for cases where seal material incompatibility is possible. Cylinder is recommended to be manufactured from seamless steel tubing and considering the internal pressure, safety factor of at least 1.5 is advised.

Their study denotes that, seals that are used as leakproofness materials must, for the sake of their function, not allow leakage nor exhibit long-term sticking. Material for seals is advised to be chosen among structural polymers, considering both strength and the issue of eliminating sticking during long periods of inactivity. Typically, Teflon®, stabilized nylon and acetyl resin family materials are advised, since structural polymers do not age, degrade or cold flow over time. Their study mentions about the damping exponent and states that depending on the geometry of orifices, damping exponent can be obtained ranging from 0.3 to 2.

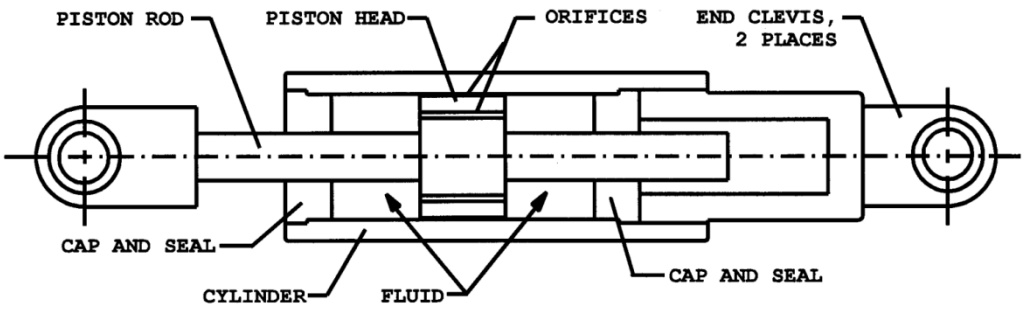

Figure 2-2: Viscous Damper Design Proposed by Taylor and Duflot [6]

Elaldı and Akçay [5] propose 20MnV6, carbon-manganese steel with vanadium, as material for cylinders. Corrosion of internal parts and leakage are prevented by chromium plating.

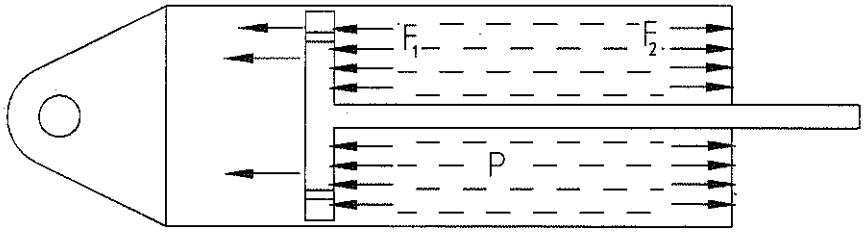

Figure 2-3: Schematic of a Hydraulic Damper by Elaldı and Akçay [5]

2.4. Survey on Mechanical Shock

Mercimek [7] defines mechanical shock as a transient phenomenon where the equilibrium of a system is disturbed by a sudden forcing or change in either the direction or the magnitude of its velocity. Shock input pulse is described in his study by a peak amplitude A_0, duration t_0 and shape form and is expressed in gravitational acceleration g's.

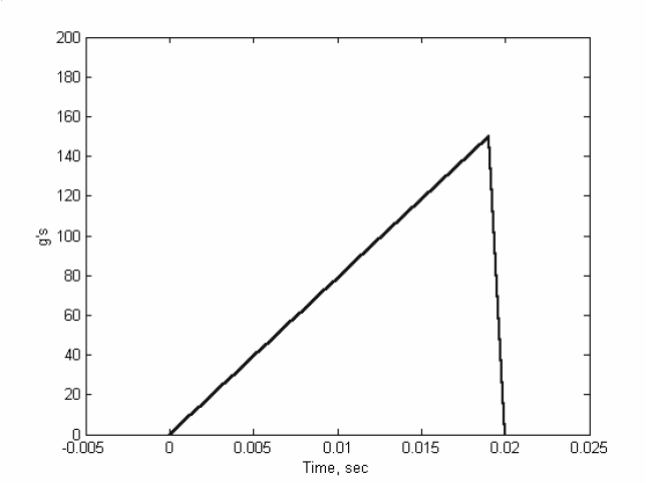

Figure 2-4: Sawtooth Shock Form [7]

As stated in MIL-STD-810G [8], mechanical shock may produce functional or physical damage to materials. Shock may cause, material failure due to increased friction between parts, overstress of structural or non-structural members, ultimate strength of component being exceeded and cracks in fracturing components [8].

2.5. Survey on Shock and Vibration Limits of Electronic Units

Electronic devices used on military systems are required to have better survivability compared to customer products. For weapon systems, electronics satisfying EMI, RFI, environmental conditions and system requirements, must be protected from the shock delivered by firing.

Gyros, for example, are required to provide stable, high resolution angular rate information over wide ranges of angular velocity. Furthermore, they should operate in harsh weather conditions without loss of performance. However, vibration and shock on a gyro causes its outputs to be contaminated with noise.

MaxGyro®, a commercial angular rate measurement product, by Watson Industries is specified to produce lower than 0.1°/sec per 1g at 12g rms vibration limit within a frequency spectrum from 20 Hz to 2 kHz [9]. It is stated in the specifications sheet of the product that, the survival limit of shock is 300g with 2ms endurance and half sine wave configuration or 50g with 11ms endurance and half sine wave configuration.

Figure 2-5: MaxGyro® by Watson Industries [9]

Another off-the-shelf electronic unit that is used in military systems is thermal camera. IMPERX™ states that its thermal camera model B1410 survives 100g of vibration in between 20 Hz and 200 Hz triaxially, while its shock limit is 1000g [10].

Figure 2-6: IMPERX™ Thermal Camera Model B1410 [10]

Most widely used standard in military systems, MIL-STD-810G by US Department of Defense, defines the lower limit of shock in a functional test as 40g with 11ms endurance and of saw-tooth configuration [8].

CHAPTER 3

M2 MACHINE GUN RECOIL CHARACTERIZATION

3.1. Introduction

M2 machine gun uses 12.7 mm caliber ammunition and fires up to 600 rounds per minute. In order to investigate the effect of shock absorbers, three different off-the-shelf shock absorbers are chosen and trial firings are carried out.

Dampers chosen varied according to their spring stiffness coefficients as hard, medium and soft. This part of the study investigates the difference in responses of machine gun when damped with different stiffness dampers. Regime and cyclic speed of the machine gun is observed.

Firing tests are conducted in the firing range located in ASELSAN Inc. using 12.7 mm caliber M2 machine gun manufactured by Manroy Inc. Every damper is tested by firing 10-series bursts. 7 tests are conducted in the scope of this study, starting with the softest damper, followed by medium and lastly hardest damper. High speed camera videos of 30 frames per second speed and 480x640 pixel resolutions in .avi video format are input into the Simulink® model designed for analysis. The model is run on a workstation with dual core Intel® Xeon® 2.8GHz processor, 48GB installed RAM, 160GB installed hard disk drive and 4GB dedicated GDDR3 video memory.

3.2. Image Processing Algorithm

Simulink® image processing tools are used in order to construct a model which is able to follow a selected part in the images over time. Videos that are recorded by the high-speed camera are in .avi video format. These video files for each series burst firings are input into the Simulink® model. Inside the model, image is first transformed into black and white and then tuned for contrast. Using the default values, color and saturation thresholds are edited and optical flow with Horn-Schunk method is generated. Horn-Schunk solver block formulates the displacement of followed blob using the last 6 frames and is programmed to generate data points using 10 successive trial results.

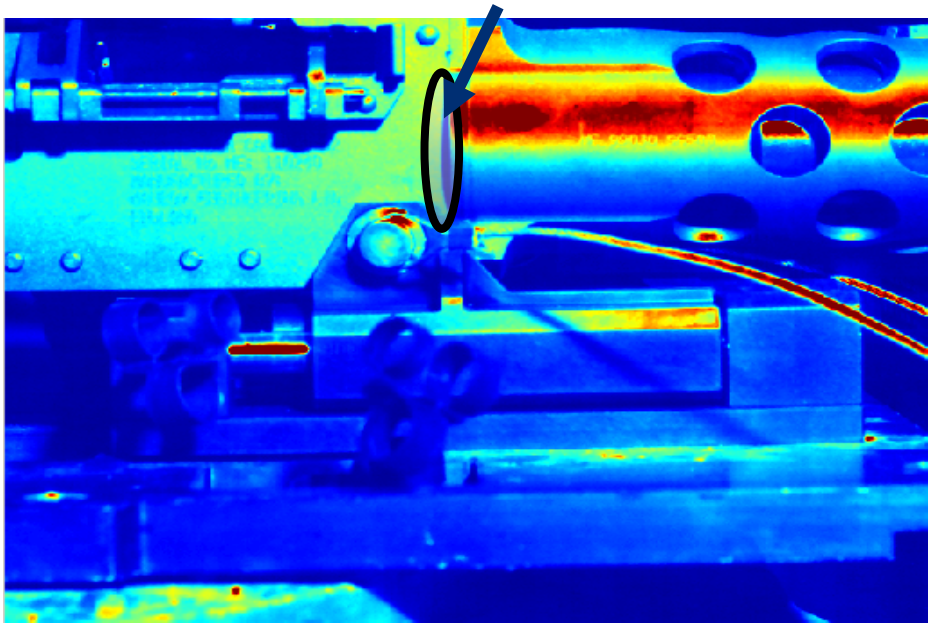

Figure 3-1: Optical Flow Input Image, Single Frame, Flow Region is Marked

Data points that are generated by optical flow are transformed into displacement data using median filter. Using blob analysis function block, then, displacement data are stored in a cell as distinct coordinates. Displacements versus time plots are generated using window function with Blackman algorithm. After applying image cropping, contrast adjustments, auto-threshold, optical flow, median filter and lastly blob analysis function blocks, simplified output image is given in Figure 3-2 for user to follow the process.

Figure 3-2: Processed Image Output

Displacement data that is obtained is in terms of pixels must be transformed into millimeters. Using solid model file information for a specific part in the assembly as shown in Figure 3-3, this conversion is carried out.

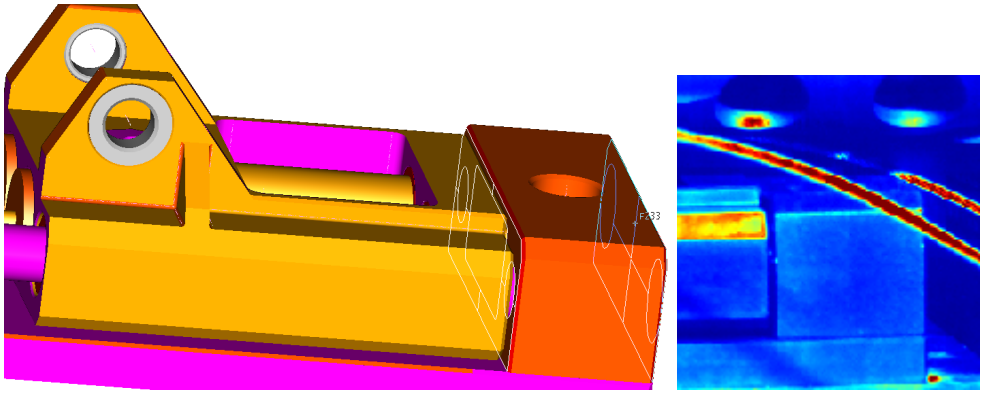

Figure 3-3: Reference Distance on Recoil Assembly for Displacement Conversion

Highlighted surfaces are picked as reference surfaces and the distance between these points is measured. Using the pixel region toolbox of Simulink® the pixel information for these two surfaces is obtained. The distance is measured as 42mm and in pixels from the video files, this corresponded into 98 pixel.

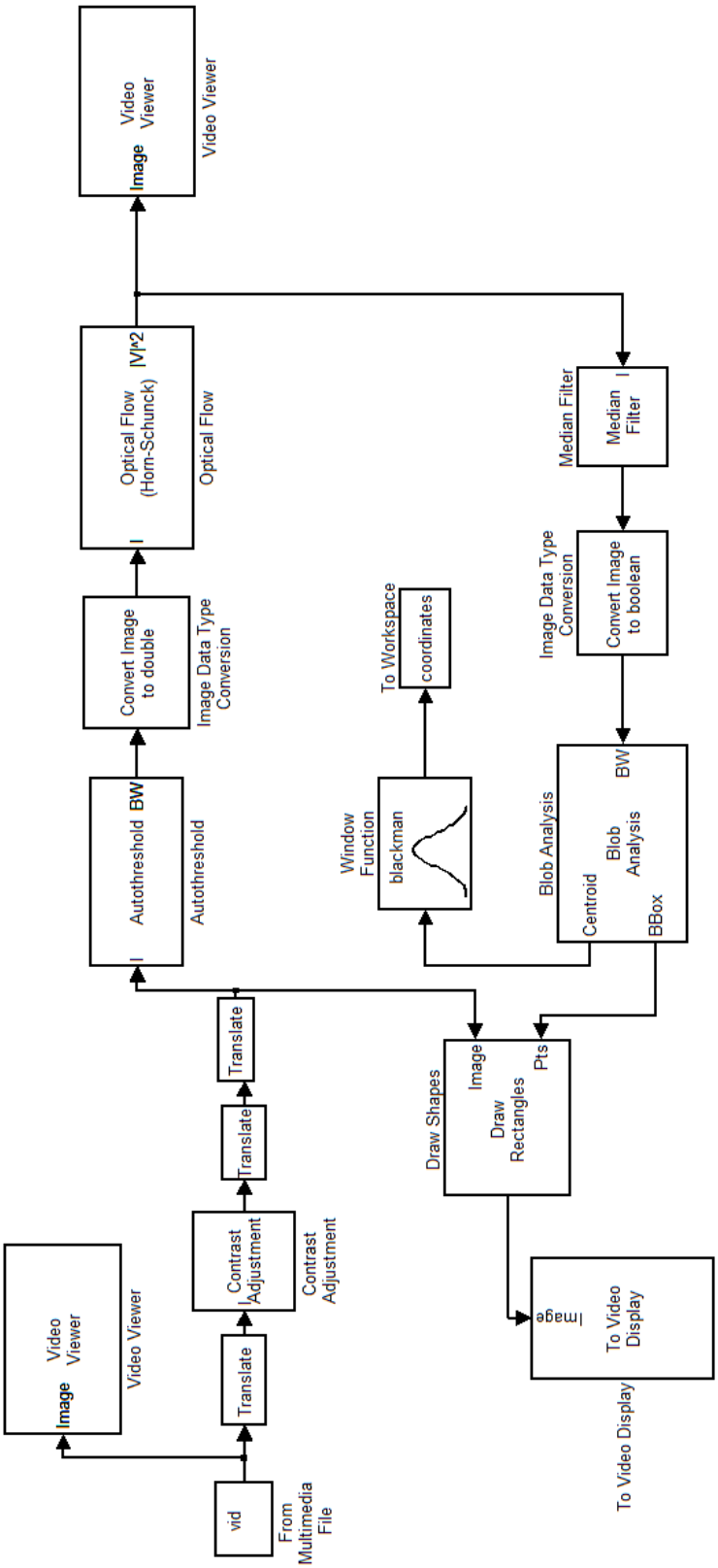

Figure 3-4: Simulink® Model for Image Processing of High Speed Camera Videos

3.4. Observations and Results

Each firing test is conducted using the same recoil assembly which allows 19.5mm stroke. The red lines in Figure 3-5 indicate the region where the measured displacement is in the range of allowed stroke. Any data over or under the red lines are due to the bending of the mounting plates. Since the stiffness of the shock absorber is low, under the action of recoil force, recoil assembly hits its rearmost position and the impact causes the mounting assembly to bend. Bending of the mounting assembly is measured as off-the-limits data and its occurrences are marked with red circles. Total displacement is measured to be 21.8 mm and cyclic firing speed of the machine gun is measured as 504 rpm.

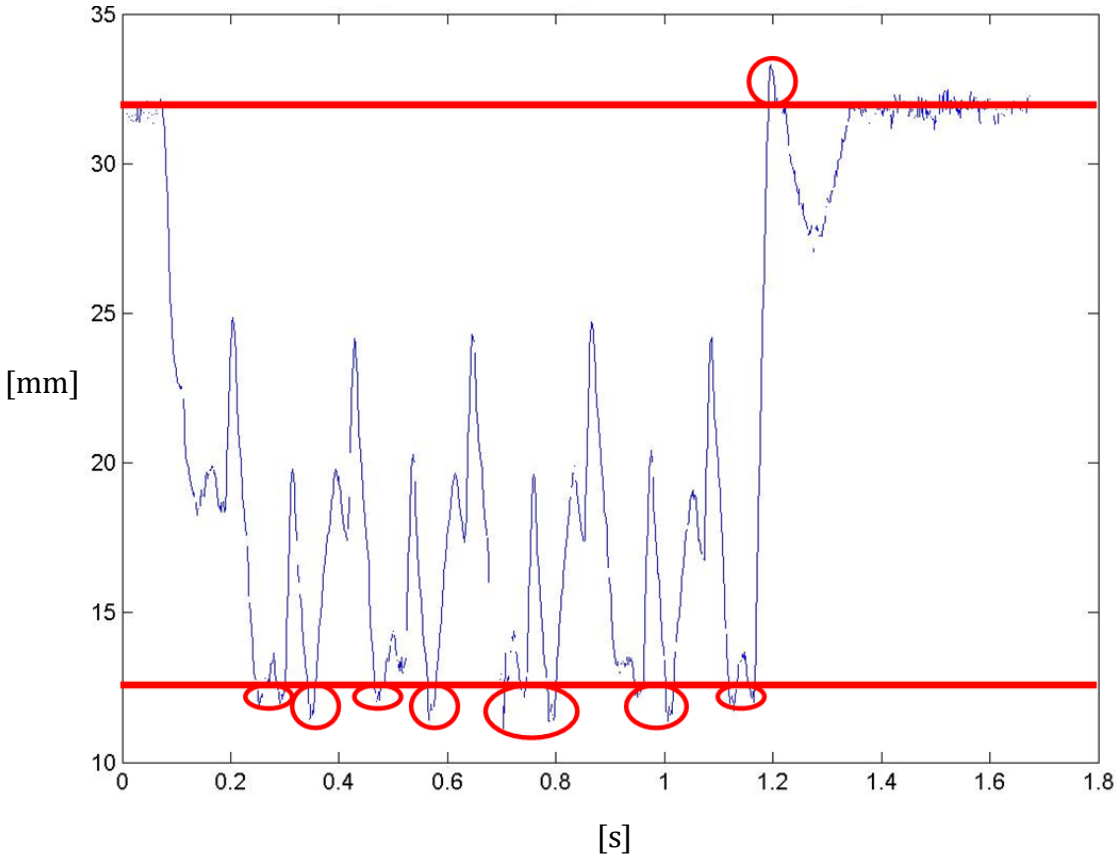

Figure 3-5: Response of Weapon Chassis to 10 Series Burst Firing with Shock Absorber of Low Stiffness

In Table 3-1, hit points of the test and mean point of impact (MPI) is represented. The diameter of the smallest circle enclosing all hit points is found to be 57.7 mm.

Table 3-1: Hit Points of Test Firing with Shock Absorber of Low Stiffness

	X [mm]	Y [mm]
	11	40
	9	29
	8	21
	19	8
	-6	27
	-6	41
	-3	44
	-2	43
	0	34
	0	33
MPI [mm]	3.6667	30.6667
Ø [mm]		57.6888

Firings with medium stiffness shock absorber yielded regular response and one of the firings is represented by Figure 3-6. In between the green lines, machine gun response is observed to be steady. Blue arrows show deviation from the harmonic response. During that firing, the ammunition used is assessed to have less powder charge, resulting in lower recoil force. Machine gun resulted in the same displacement in the following firings appropriate with the regular response.

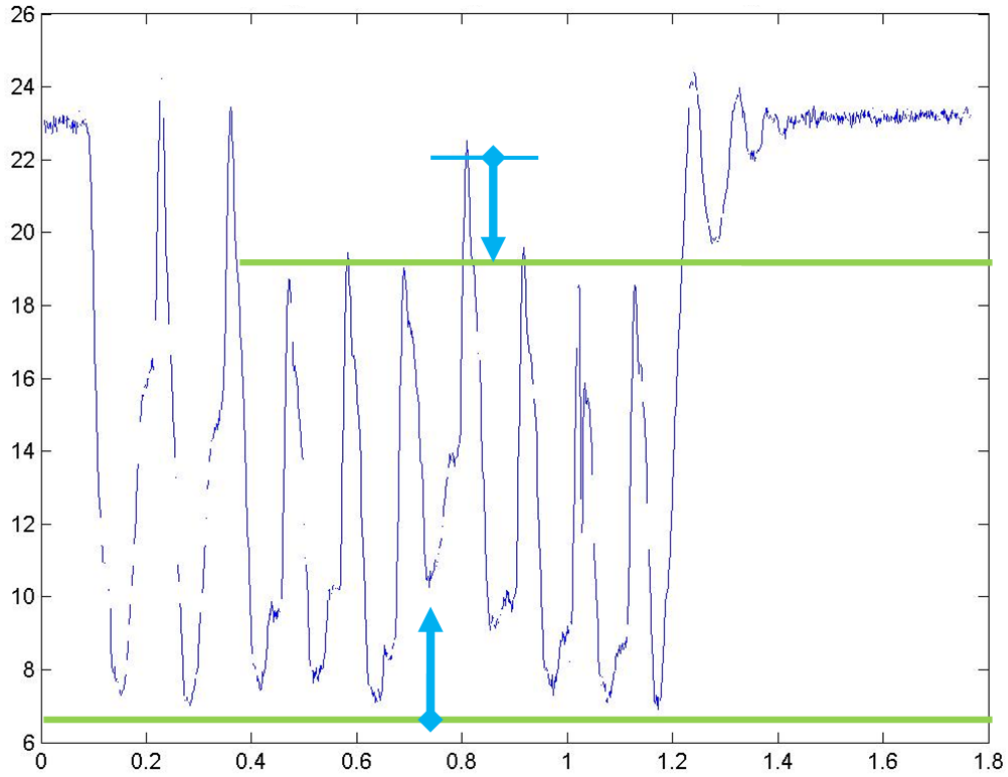

Figure 3-6: Response of Weapon Chassis to 10 Series Burst Firing with Shock Absorber of Medium Stiffness

In Table 3-2, hit points of the test and mean point of impact (MPI) is represented. The diameter of the smallest circle enclosing all hit points is found to be 21.4 mm.

Table 3-2: Hit Points of Test Firing with Shock Absorber of Medium Stiffness

	X [mm]	Y [mm]
	-28	-17
	-30	-23
	-17	-17
	-7	-19
	-1	-15
	-6	4
	14	12
	-9	16
	3	35
	1	45
MPI [mm]	9	2.6667
Ø [mm]		21.4314

In the first two firings, it is observed that the gun is able to recover to its initial state. This is explained with the speed of the firing. After the first few firings, gun gets hotter and the viscosity of the lubricants between metal components drops, making parts to move easier on one another. Consequently, speed of the gun increases and in this case after the second round, there is not enough time for the gun to recover to its initial position when the next round is fired. After this point, gun performs in 12.5mm of harmonic response.

Maximum displacement of gun is measured to be 17.3 mm and bending of the mounting plate as in the case of the softer absorbers, is not observed with the medium stiffness shock absorber. Cyclic firing speed of the gun is measured as 504.2 rpm.

When the shock absorber with highest stiffness is mounted and firing test high speed camera videos are analyzed, it is observed that, the available stroke of 19.5 mm backwards is not completed during the 10 series burst.

In Figure 3-7, red line drawn on the top represents the upper limit of stroke while the bottom one represents the rearmost position gun can achieve during the firing test.

It is observed that, the stiffness of the damper is so high that, shock absorber cannot complete its full stroke after the rounds are fired. Furthermore, it accelerates the gun so much during its retraction that, recoil assembly hits its furthermost position. The impact causes the mounting plate to bend and displacement due to bending occurs. Maximum displacement is measured as 19.57 mm whereas the cyclic firing speed of the gun is found to be 503 rpm.

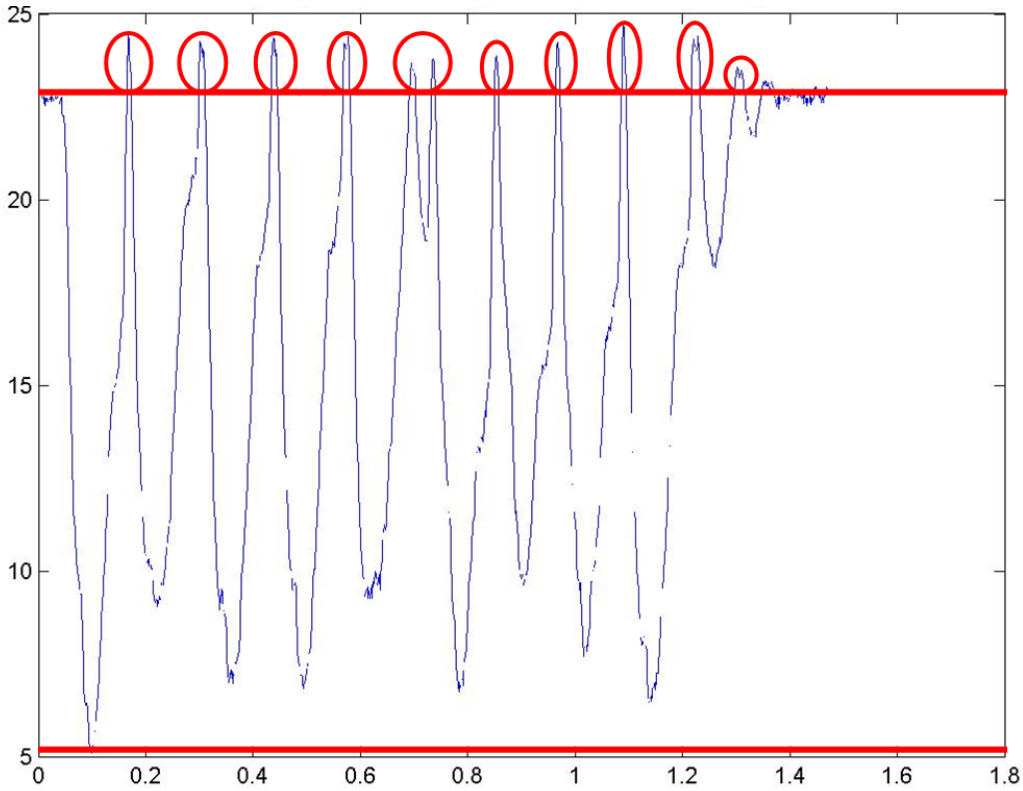

Figure 3-7: Response of Weapon Chassis to 10 Series Burst Firing with Shock Absorber of High Stiffness

Table 3-3: Hit Points of Test Firing with Shock Absorber of High Stiffness

	X [mm]	Y [mm]
	18	70
	4	56
	0	50
	10	48
	9	45
	-19	50
	-24	42
	-31	36
	-11	46
	-3	47
MPI [mm]	8.625	45.5
Ø [mm]		85.4688

CHAPTER 4

MODELLING OF A SHOCK ABSORBER

4.1. Introduction

In this part, the steps of the automated shock absorber design are explained in detail.

Shock absorber design starts with a buckling analysis of piston rod. Piston rod is the part that will serve as the interface to the attached weapon. Therefore, it will directly be subjected to the recoil force and it should sustain high forces. In this step, piston rod length and diameter along with seal cap length are outputs, by inputting frequency of motion, desired damping force, desired stroke and modulus of elasticity of the piston rod.

The second step is the piston design. Piston is the component which generates damping force and is the interface with the viscous fluid. In this step, outputs from buckling analysis are required as inputs. Additionally, fluid and solid material properties, cylinder sizing limits and weapon characteristics are complementary inputs. This step outputs piston parameters, namely, length of piston, length of piston and poppet disk stick together, diameter of piston and diameter and number of capillaries on piston.

Third design step is spring design. This step outputs numerous spring designs with altering winding number, free length, wire diameter and material yielding the same stiffness and preload. User is requested to pick one of the designs to continue to step four. This step requires outputs from buckling analysis and piston design as input, along with desired preload as a complimentary input.

Last design step is cylinder design. Cylinder is designed to be able to sustain the in-cylinder fluid pressure. The inputs are the outputs from previous three steps and material properties of cylinder. It delivers minimum required cylinder thickness as output.

4.2. Buckling Analysis

Piston rod is the most critical part in the design of the viscous damper by means of sustainability and reliability. Piston rod is the interface between the damped system, viscous fluid and spring and therefore, it is subjected to high forces changing direction and magnitude, continuously and rapidly throughout the cycle of firing.

Furthermore, buckling analysis is prior to the other calculations regarding the outputs it delivers. In this step the length of the piston rod, $L_{piston\ rod}$, diameter of the piston rod, $d_{piston\ rod}$ and seal cap length, $L_{seal\ cap}$ are calculated using the dedicated Matlab® function script.

In this study, piston rod is regarded as a compression member, specifically as an Euler column which is fixed at both of its ends. Figure 4-2 shows a section view of the viscous damper, whereby the guidance of the piston rod via the seal cap assembly is shown. Piston rod is screwed into the piston by a threaded hole in the center of the piston and piston is held in its position by the compression spring. These end conditions share the greatest resemblance with the both ends fixed end condition as shown in Figure 4-1.

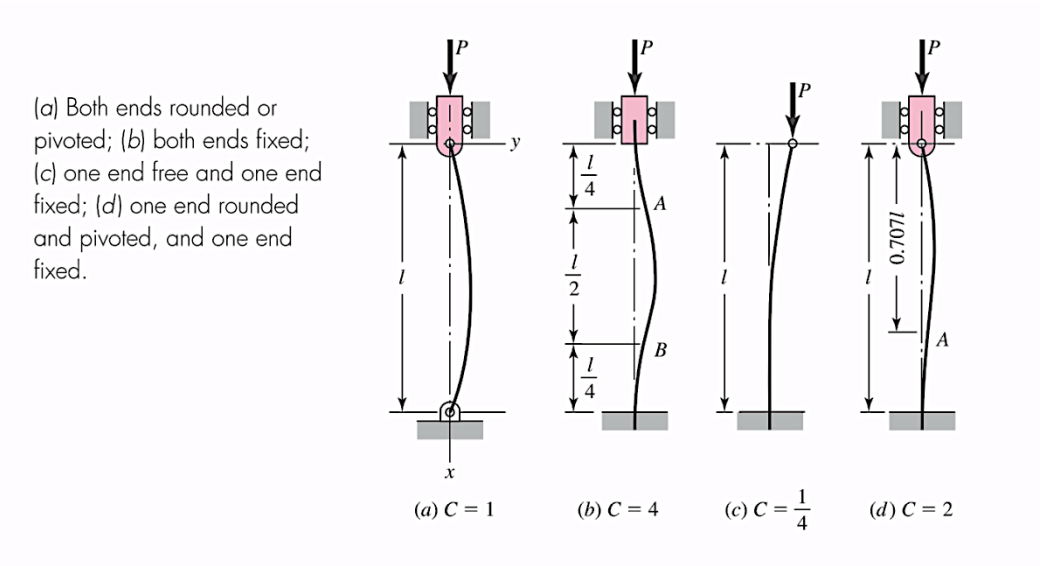

Figure 4-1 : End Conditions for Compression Members [11]

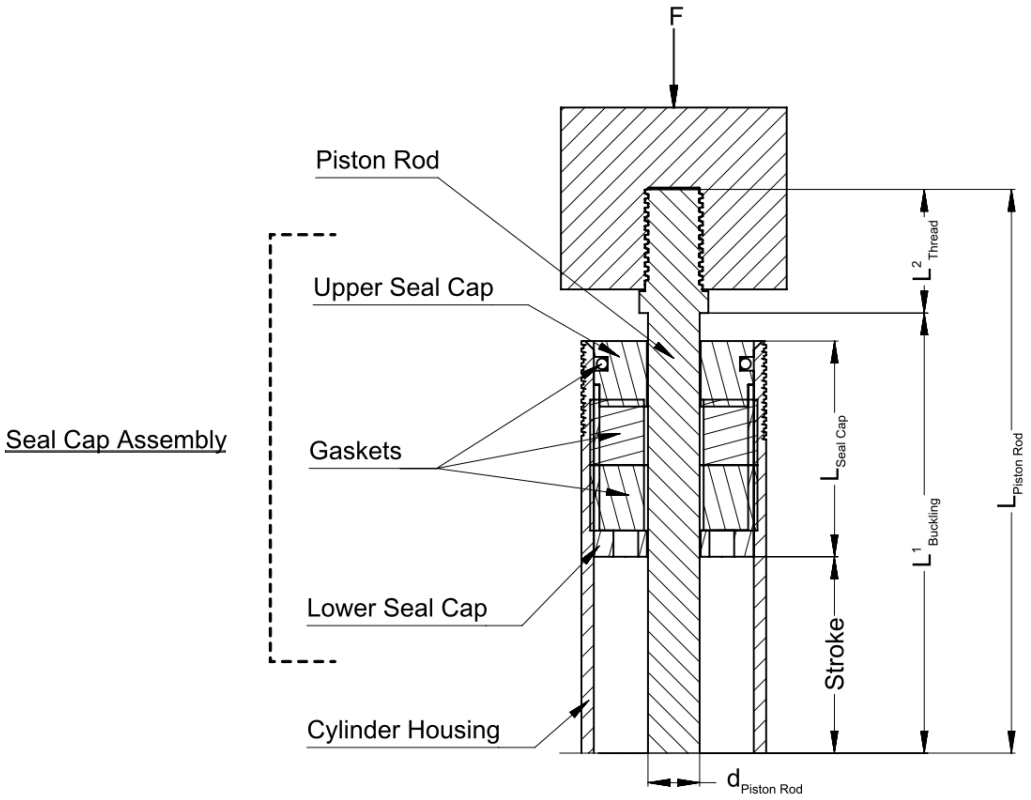

Figure 4-2 : Components of Hydraulic Damper in a Section View

The objective of buckling analysis is to determine the length of the piston rod $L_{Piston\ Rod}$, diameter of the piston rod, $d_{Piston\ Rod}$ and the length of the seal cap assembly $L_{Seal\ Cap}$.

The length and diameter of the piston rod is solved using Euler column formula.

Euler column formula:

$$\frac{F_{cr}}{A}=\frac{(CF)\pi^3 EI}{\left(\frac{L}{\sqrt{I/A}}\right)^2}$$

Equation (4-1)

Since the rod geometry is cylindrical, we can formulate the area, A and the area moment of inertia, I as the following,

$$A=\pi\frac{d^2}{4}$$

Equation (4-2)

$$I=\frac{\pi d^4}{64}$$

Equation (4-3)

The greatest magnitude of the force is to be reached in case of bottom link where the piston rod receives another cycle of recoil force when it has completed its full compression stroke and not yet recovered. It, therefore, is subjected to the recoil force as a compression member. Piston rod should not buckle under the maximum recoil force that it may be subjected to with a factor of safety $n_{buckling}$.

$$F_{cr}=F_{recoil_{max}}n_{buckling}$$

Equation (4-4)

When Equation (4-1), Equation (4-2), Equation (4-3) and Equation (4-4) are combined, minimum piston rod diameter is formulated as Equation (4-5).

$$d_{min}=\left(\frac{64F_{recoil_{max}}n_{buckling}L_{Buckling}^{1}{}^{2}}{\pi^{3}(CF)E}\right)^{1/4}$$

Equation (4-5)

Piston rod should be able travel the distance prescribed by the stroke, through the seal cap assembly. In this study, seal cap assembly length is designed as half the length of the piston rod. The remaining half is to be used for stroke and in order not to get stuck due to production tolerances; stroke is considered to be 90% of the half piston rod length.

$$Stroke=\frac{L_{Buckling}^{1}}{2}0.90$$

Equation (4-6)

To be able to stay on the safe side by means of the sufficiency of stroke, piston rod length is increased by 35%.

$$L_{Buckling}^{1}=\frac{2\ Stroke}{0.90}1.35$$

Equation (4-7)

$$d_{min}=\left(\frac{64F_{recoil_{max}}n_{buckling}\left(\frac{2\ Stroke}{0.90}1.35\right)^{2}}{\pi^{3}(CF)E}\right)^{\frac{1}{4}}$$

Equation (4-8)

Minimum piston rod diameter that is solved by Equation (4-8) is increased by 35% in order to obtain less buckling under the action of recoil force. In Equation (4-9), there is a Matlab® function “ceil(R)” which performs rounding

"R" to the nearest variable that is greater than or equal to "R". All length units are "m", therefore in order to be able to perform rounding, d_{min} should be multiplied with 10^3 first.

$$d_{Piston\ Rod}=ceil(10^3\ d_{min}\ 1.35)\times10^{-3}$$

Equation (4-9)

On top of the piston rod, there is a threaded portion that interfaces the piston with the recoil assembly of the gun. This portion's length is approximated to be twice as large as the diameter of the piston rod. L^2_{thread} is calculated using Equation (4-10), where there is a Matlab® function "floor(R)", which performs rounding "R" to the nearest variable that is less than or equal to "R".

$$L^2_{thread}=floor\left(\frac{10^3\ d_{Piston\ Rod}}{2}\right)\times4\times10^{-3}$$

Equation (4-10)

Last two variables determined by buckling analysis are $L_{Seal\ Cap}$ and $L_{Piston\ Rod}$, calculated in Equation (4-11) and Equation (4-12), respectively.

$$L_{Seal\ Cap}=\frac{L^1_{Buckling}}{2}$$

Equation (4-11)

Total piston rod length is calculated by Equation (4-12). Note that, threaded portion of this length, L^2_{thread} , is sunk into a threaded hole on a plate whereby the recoil force is transmitted. Therefore, the portion of the piston rod that is subjected to buckling due to the compression force is only $L^1_{Buckling}$.

$$L_{Piston\ Rod}=L^1_{Buckling}+L^2_{thread}$$

Equation (4-12)

Considering the above derivation, buckling analysis part of the damper design yields $L_{Piston\ Rod}$,$d_{Piston\ Rod}$ and $L_{Seal\ Cap}$ and requires $F_{recoil_{max}}$, $n_{buckling}$, E and Stroke.

4.2.1. Buckling Analysis for the Piston Rod of Shock Absorber for 12.7 mm Caliber Machine Gun

Table 4-1: Input Parameters for Buckling Analysis

Input Parameter	Value	Unit
$F_{recoil_{max}}$ per piston	5000	N
$n_{buckling}$	2.5	–
$E_{AISI316}$	193	GPa
Stroke	20	mm

$$F_{cr}=F_{recoil_{max}}n_{buckling}=5000N\times2.5=12500N$$

$$L^{1}_{Buckling}=\frac{2\ Stroke}{0.90}1.35=\frac{2\times0.020\ m}{0.90}1.35=0.060\ m$$

$$d_{min}=\left(\frac{64F_{recoil_{max}}n_{buckling}\left(\frac{2\ Stroke}{0.90}1.35\right)^{2}}{\pi^{3}(CF)E}\right)^{\frac{1}{4}}$$

$$=\left(\frac{64\times12500N(0.060m)^{2}}{\pi^{3}193\times10^{9}Pa}\right)^{\frac{1}{4}}=0.0047\ m$$

$$d_{Piston\ Rod}=ceil(10^{3}\ d_{min}\ 1.35)\times10^{-3}$$

$$=ceil(4.7\times1.35)\times10^{-3}=0.007m$$

$$L^2_{thread}=\text{floor}\left(\frac{10^3\ d_{Piston\ Rod}}{2}\right)\times 4\times 10^{-3}$$

$$=\text{floor}(3.5)\times 4\times 10^{-3}=0.012\ \text{m}$$

$$L_{Piston\ Rod}=L^1_{Buckling}+L^2_{thread}=0.072\ \text{m}$$

Table 4-2: Outputs of Buckling Analysis

Output Parameter	Value	Unit
$L_{Piston\ Rod}$	72	mm
$d_{Piston\ Rod}$	Ø 7	mm
$L_{Seal\ Cap}$	30	mm

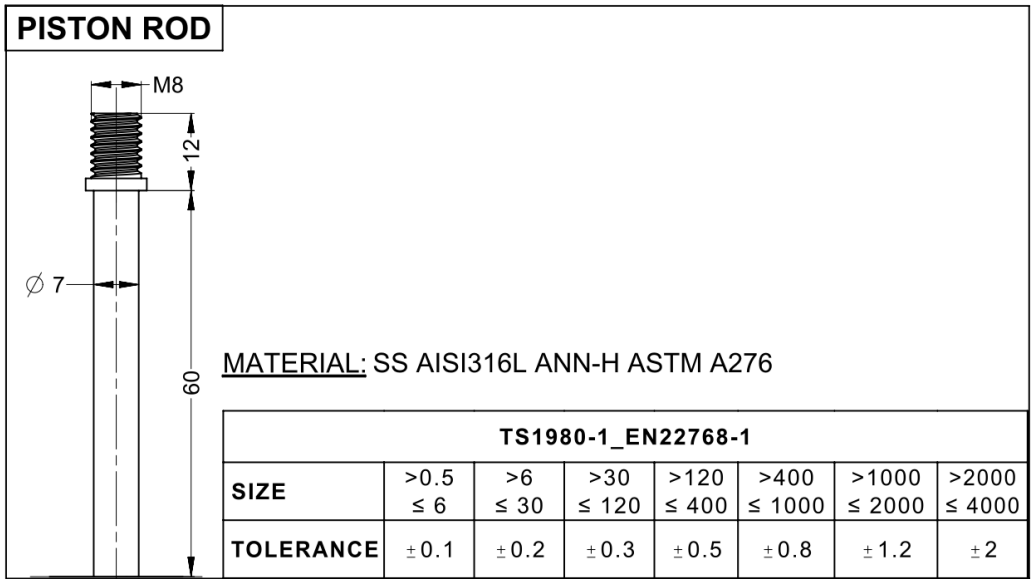

Figure 4-3: Technical Drawing of the Piston Rod Designed

4.3. Piston Design

4.3.1. Damping force

Damping force differs for the compression and retraction strokes of the damper due to a disk attached at the bottom of the piston as shown in Figure 4-4. This disk functions as a poppet and is closed when the piston moves down causing only annular flow. While piston is moving upwards, poppet is opened and capillary flow is introduced along with the annular flow.

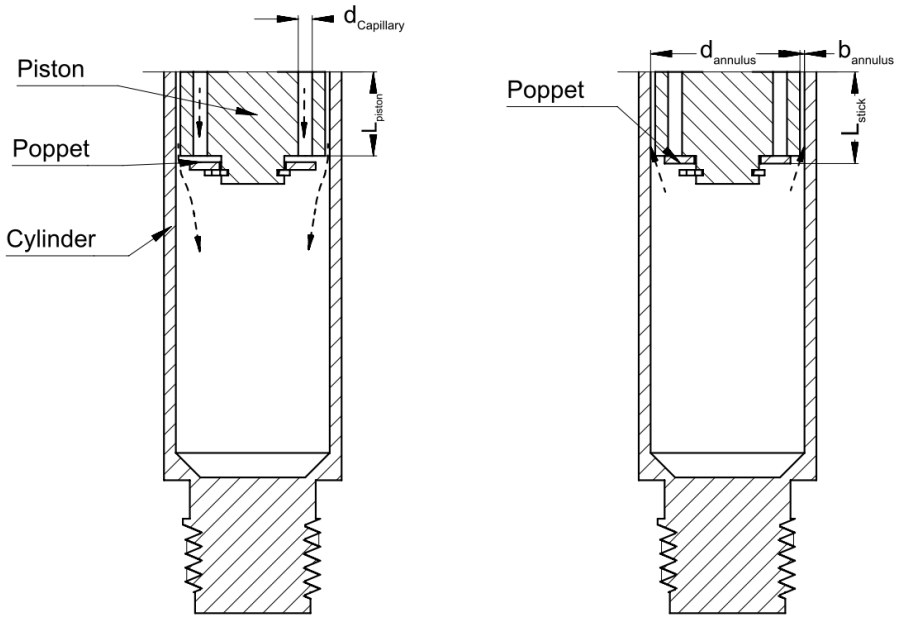

(a) Piston moving up, poppet opened (b) Piston moving down, poppet closed

Figure 4-4: Section View of Piston and Cylinder

For capillary flow, as formulated by Hall [4]:

$$F_{damping}=\frac{128\ \rho\ \vartheta\ L_{capillary}A_{hydraulic}^{2}}{\pi d_{capillary}^{4}}v$$

Equation (4-13)

For annular flow, by Hall [4]:

$$F_{damping}=\frac{12\ \rho\ \vartheta\ L_{annular}A_{hydraulic}^{2}}{\pi d_{annulus}b_{annulus}^{3}}v$$

Equation (4-14)

Piston retraction stroke:

$$v>0$$

$$F_{damping}(t)=\left(\frac{12\ L_{annular}A_{hydr.Ann.}^{2}}{\pi d_{annulus}b_{annulus}^{3}}+\frac{128\ \ L_{capillary}A_{hydr.Cap.}^{2}}{\pi d_{capillary}^{4}}\right)\rho\ \vartheta(t)\ v(t)$$

Equation (4-15)

$$L_{annular}=L_{capillary}=L_{piston}$$

Equation (4-16)

$$A_{hydr.Ann.}=A_{piston}-\left(n_{capillary}\times\frac{\pi\ d_{capillary}}{4}\right)$$

Equation (4-17)

$$A_{hydr.Cap.}=\pi d_{capillary} L_{piston}$$

Equation (4-18)

Piston compression stroke:

$$v<0$$

$$F_{damping}(t)=\frac{12\ L_{annular} A^2_{hydraulic}}{\pi d_{annulus} b^3_{annulus}}\ \rho\ \vartheta(t)\ v(t)$$

Equation (4-19)

$$L_{annular}=L_{stick}=L_{piston}+b_{poppet}$$

Equation (4-20)

$$F_{damping}(t)=\begin{cases}\left(\frac{12\ L_{piston} A^2_{hydr.Ann.}}{\pi d_{annulus} b^3_{annulus}}+n_{capillary}\frac{128\ L_{piston} A^2_{hydr.Cap.}}{\pi d^4_{capillary}}\right)\rho\ \vartheta(t)v(t) & ;\ v>0\\ \frac{12\ L_{stick} A^2_{hydraulic}}{\pi d_{annulus} b^3_{annulus}}\ \rho\ \vartheta(t)v(t) & ;\ v<0\end{cases}$$

Equation (4-21)

4.3.1. Viscous heating

Energy balance can be expressed by

$$m_f c_v \frac{dT}{dt} = F_c(t) \times v - \frac{\lambda(h_r+h)}{\lambda+h_r+h} A(T(t)-T_{air})$$

Equation (4-22)

Assuming there is no forcing at first, Equation (4-22) reduces into Equation (4-23), which is the ordinary differential equation, modeling the cooling as a function of time with initial temperature T_0.

$$m_f c_v \frac{dT}{dt} = -\frac{\lambda(h_r+h)}{\lambda+h_r+h} A(T(t)-T_{air})$$

Equation (4-23)

Initial condition;

$$T(0)=T_0$$

Equation (4-24)

$$T_{cool}(T_0,t) = T_{air_K} - \frac{(T_{air_K}-T_0)}{e^{\frac{A\,\lambda(h_r+h_t)t}{c_v m_f(h_r+h_t+\lambda)}}}$$

Equation (4-25)

When the forcing $F_{damping}(t)$ is included and the differential equation is solved, temperature function takes the form as is stated in Equation (4-26).

$$T(T_0,t)=T_{air_K}-\frac{\left(T_{air_K}-T_0\right)}{e^{\frac{A\,\lambda(h_r+h_t)t}{c_v m_f(h_r+h_t+\lambda)}}}+m_f c_v v\frac{\int_0^t\left|F_{damping}(t)\right|e^{\frac{A\,\lambda(h_r+h_t)t}{c_v m_f(h_r+h_t+\lambda)}}\,dt}{e^{\frac{A\,\lambda(h_r+h_t)t}{c_v m_f(h_r+h_t+\lambda)}}}$$

Equation (4-26)

First iteration starts with;

$$T(0)=T_0=T_{air_K}$$

Equation (4-27)

$$\Delta T=T_{air_K}-T_0=0$$

Equation (4-28)

Using two increments between data points, Equation (4-26) is solved iteratively. In each iteration T_0 is increased by the temperature rise in the previous iteration and the corresponding viscosity value at that T_0 is used for calculating $F_{damping}(t)$.

Viscosity is modeled as a second order polynomial as a function of temperature as shown in Equation (4-29) by using Matlab® function "pol=polyfit([y],[x],n)" and "y(x)=polyval(pol,x)". When all data points of the harmonic excitation are finished, cooling process starts such that including the excitation period, total temperature time span is 100 seconds long.

$$\vartheta(t)=\text{polyval}(\text{polyfit}(\{\vartheta_1,\vartheta_2,\vartheta_3,\ldots,\vartheta_n\},\{T_1,T_2,T_3,\ldots,T_n\},2))$$

Equation (4-29)

Varying viscosity damper part of the damper design yields calculated and desired total forcing according to Equation (4-30) and Equation (4-31), respectively.

$$F_{calc}(t)=m_{Piston\ Rod}\ddot{x}(t)+k_{spring}x(t)+F_{damping}(t)$$

Equation (4-30)

$$F_{desired}(t)=m_{Piston\ Rod}\ddot{x}(t)+c_{desired}\dot{x}(t)+k_{spring}x(t)$$

Equation (4-31)

4.3.1. Iterative piston design

Iterative piston design step solves for L_{piston}, L_{stick}, d_{piston}, $d_{capillary}$ and $n_{capillary}$. However, design process requires an initiation value for each parameter. These initial value assignments are proportional to $L_{piston\ rod}$ obtained in Section 4.2 and user input parameters $d_{cylinder\ outer}$ and $b_{cylinder}$.

As damping force increases, viscous heating it causes increases as well and this results in a drop in viscosity. Decreased viscosity yields lower damping force for the following cycles, which causes the damper to lose its effectiveness when used for higher number of cycles. In order to avoid grandiose variations among cycles, parameters should be selected carefully and throughout this study it is observed that piston parameters L_{piston}, L_{stick}, d_{piston}, $d_{capillary}$ and $n_{capillary}$ each contributed in a different manner to the damping force.

Figure 8-1 to Figure 8-5 illustrate the effects of each individual parameter on a force versus displacement plot. Default values of other parameters are given in Table 4-8 and they are altered for each corresponding parameter to show its effect alone.

In order to investigate the effects of the piston design parameters, system properties must be defined. Solver requires the desired damping and spring stiffness coefficients, preload on spring, viscous fluid and material's thermal properties and geometrical dimensions of other components, which are supplied in tables from Table 4-3 to Table 4-7.

Table 4-3: Desired Shock Absorber Characteristics

Parameter	Value	Unit
$C_{desired}$	1600	$\frac{Ns}{m}$
$K_{desired}$	10000	$\frac{N}{m}$
$F_{preload}$	140	N

Table 4-4: Viscous Fluid Properties for Piston Parameter Analysis

Parameter	Value	Unit
ρ_{fluid}	970	kg/m^3
$[\vartheta_{fluid}(T)]$	$\begin{bmatrix} 20 & 500 \\ 25 & 463 \\ 40 & 289 \\ 50 & 144 \end{bmatrix}$	[°C cSt]
T_{fluid}^{flash}	315	°C
c_v	1370	$\frac{J}{kgK}$

Table 4-5: Thermal Properties for Piston Parameter Analysis

Parameter	Value	Unit
h_{air}	15	$\frac{W}{m^2K}$
h_r	9	$\frac{W}{m^2K}$
λ_{st+fl}	0.139	$\frac{W}{mK}$

Table 4-6: Geometrical Dimensions of Other Damper Components for Piston Parameter Analysis

Parameter	Value	Unit
b_{cyl}	2	mm
$d_{cyl\ outer}$	25	mm
L_{cyl}	145	mm
$L_{piston\ rod}$	70	mm
$d_{piston\ rod}$	7	mm
Stroke	19	mm
$n_{spr\ wnd}$	14	-
$d_{spr\ outer}$	20.5	mm
$d_{spr\ wire}$	3.2	mm
$L_{seal\ cap}$	35	mm

Table 4-7: Miscellaneous Parameters for Piston Parameter Analysis

Parameter	Value	Unit
f_{motion}	10	Hz
n_{Ammo}	100	-
T_{air}	11	^{o}C

Table 4-8: Default Piston Parameter Values

Parameter	Value	Unit
L_{stick}	12	mm
L_{piston}	10	mm
d_{piston}	20.3	mm
d_{cpl}	1	mm
n_{cpl}	7	-

Initial values assigned to these parameters for the initiation of iterative solving are presented in Table 4-9.

Table 4-9: Iterative Piston Design Parameters Initiation

Initiated Parameter	**Value**
L_{stick}	$L_{piston\ rod} \times \frac{1}{100}$
L_{piston}	$L_{piston\ rod} \times \frac{1}{3000}$
d_{piston}	$\left(d_{cylinder\ outer}\text{-}2\ b_{cylinder}\right) \times \frac{97}{100}$
$d_{capillary}$	1 mm
$n_{capillary}$	4

Equation (4-26) is solved for every iteration of Equation (4-21) and the resulting solved force and desired force curves are compared. The following algorithm given in Figure 4-5 is applied to obtain desired damping characteristics.

L_{stick} is increased by four different factors, depending on the difference between the desired damper characteristics and the last iteration. When the difference is above 500N for the maximum force produced and it is the first iteration step, the factor used is 10. If, even after this first increase, difference between desired and iterated piston remains above 500N for the maximum force, the factor used is 5. Unless design tool perceives fine tuning condition, the factor is reduced to 1.1 when the difference is below 500N. Fine tuning condition is when the difference between desired and iterated pistons' maximum forces is less than 4N and any iteration following it. In the fine tuning region, the factor is reduced to 1.01.

L_{piston} is increased by four different factors, like L_{stick}. Depending on the difference between the desired and iterated dampers' minimum forces, used factor is chosen among 5, 2 and 1.1. In fine tuning region, which is when the difference is below 4 N, this factor is reduced to 1.01.

$d_{capillary}$ is increased by factor 1.1 when the difference between the desired and iterated dampers' minimum forces is above 700N. Fine tuning for $d_{capillary}$ is carried out with factor 1.005 if the desired damper's minimum force exceeds the one of the iterated damper's.

$n_{capillary}$ is increased one by one if, again, the difference between the desired and iterated dampers' minimum forces is above 700N.

Lastly, d_{piston} is increased by factor 1.005, when the maximum force of the iterated damper exceeds the one of desired damper's.

All iterations are reverted back one step when there is a risk of exceeding the flashing temperature of viscous oil.

For the parameters given in Table 4-3 to Table 4-7, iterative piston design algorithm in Figure 4-5 is run and the values for piston length, stick length, piston diameter, capillary diameter and number of capillaries are collected. The results of the parameters are presented in Table 4-10 and the hysteresis plot for the designed piston is illustrated in Figure 4-6.

Table 4-10: Outputs of Piston Design

Parameter	Value	Unit
L_{stick}	12.4	mm
L_{piston}	10.1	mm
d_{piston}	20.3	mm
d_{cpl}	1	mm
n_{cpl}	7	-

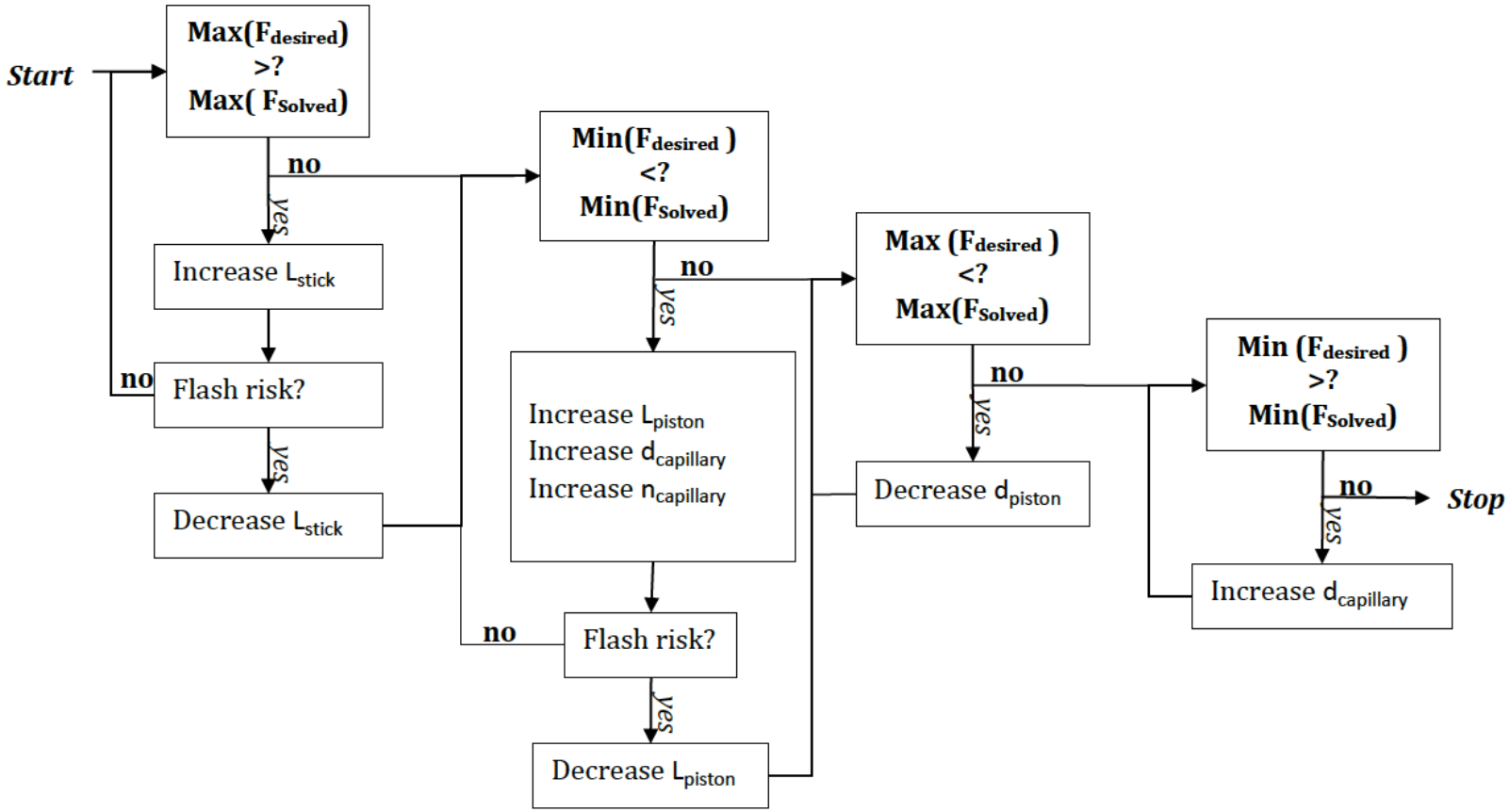

Figure 4-5: Iterative Piston Design Algorithm

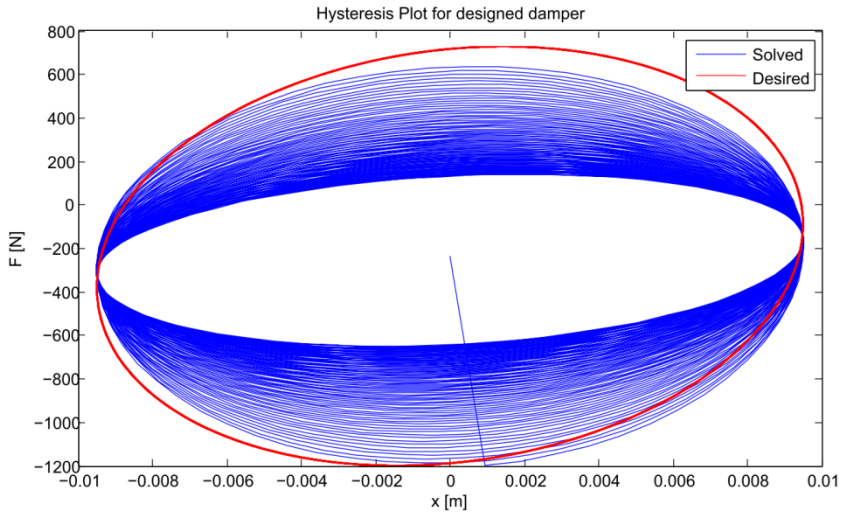

Figure 4-6: Hysteresis Plot for the Designed Piston

4.4. Spring Design

Spring design tool uses the length of seal cap calculated in Section 4.2 and length of the piston calculated in Section 4.3. It produces several possible spring configurations among which different materials, different number of windings and different free lengths are possible.

Materials used for calculations are music wire, ASTM A228, oil-tempered wire, ASTM A229, hard-drawn wire, ASTM A227, chrome-vanadium wire, ASTM A232, chrome-silicon wire ASTM A401, 302 stainless steel wire, ASTM A313 and phosphor-bronze wire ASTM B159.

Most straight forward parameters of spring design are the outermost diameter and free length of spring. Spring is to be assembled between the piston and the cylinder. Cylinder functions as housing and a support for the spring and, assembled, available length for spring determines the preload on it. Spring's

outermost diameter is, therefore, limited by the inner diameter of cylinder, while free length of spring is limited by the lengths of cylinder, piston, seal cap assembly and if desired, the length at preload.

$$d_{spr\ outer}=\left(d_{cyl\ outer}-2b_{cyl}\right)\times 0.95$$

Equation (4-32)

$$F_{preload}=K_{desired}\left(L_{spr\ free}-\left(L_{cyl}-L_{piston}-L_{seal\ cap}-x_{preload}\right)\right)$$

Equation (4-33)

During the travel of the piston through its stroke, spring should not be compressed to its solid length.

$$d_{wire}\left(n_{wnd}+1\right)=L_{spr\ solid}$$

Equation (4-34)

$$L_{spr\ solid}<\left(L_{cyl}-\left(L_{seal\ cap}+L_{piston}+Stroke\right)\right)$$

Equation (4-35)

Number of windings on the spring, n_{wnd}, is changed from 1 to 25. For each iteration of number of windings, equations starting from Equation (4-36) are solved.

$$d_{spr\ wire}^{max}=\frac{L_{cyl}-\left(L_{seal\ cap}+L_{piston}+Stroke\times 1.2\right)}{\left(n_{wnd}+1\right)}$$

Equation (4-36)

$$K_{desired}=\frac{\left(d_{spr\ wire}\right)^4 G_{spr}}{8\left(d_{spr\ outer}-d_{spr\ wire}\right)^3 n_{wnd}}$$

Equation (4-37)

When Equation (4-37) is solved for $d_{spr\ wire}$, each real and positive root of the solution is stored if it is smaller than the maximum possible spring wire diameter in Equation (4-36).

Possible solutions of spring wire diameter considering the solid length should be analyzed for critical frequency. Fundamental frequency for each possible spring solution is obtained from Equation (4-39).

$$W_{spr}=\frac{\pi^2 d_{spr\ wire}^2\left(d_{spr\ outer}-d_{spr\ wire}\right)^2 n_{wnd\ act}\gamma}{4}$$

Equation (4-38)

$$f_{fund}=\frac{1}{2}\sqrt{\frac{K_{desired}g}{W_{spr}}}$$

Equation (4-39)

To avoid resonance, rule of thumb is to obtain fundamental frequency greater than at least 15 times the excitation frequency. Therefore, for instance, for a weapon with 600 rounds per minute, spring should have fundamental frequency at least 150 Hz.

$$15\ f_{motion}<f_{fund}$$

Last step of spring design is to ensure endurance for fatigue. Spring index ζ

$$\zeta=\frac{d_{spr\ outer}-d_{spr\ wire}}{d_{spr\ wire}}$$

Equation (4-40)

$$\kappa_B = \frac{4\zeta+2}{4\zeta-3}$$

Equation (4-41)

$$F_{spr}^{max} = F_{preload} + K_{desired}\text{Stroke}$$

Equation (4-42)

For robust linearity, force on spring at its solid length F_{solid} is calculated as greater than or equal to 15% increased maximum spring force.

$$F_{solid} = 1.15\ F_{spr}^{max}$$

Equation (4-43)

Alternating shear stress component is designated by τ_a.

$$F_a = \frac{F_{spr}^{max} - F_{preload}}{2}$$

Equation (4-44)

$$\tau_a = \kappa_B \frac{8F_a\left(d_{spr\ outer} - d_{spr\ wire}\right)}{\pi d_{spr\ wire}^{\ 3}}$$

Equation (4-45)

Shear stress when the spring is compressed is found by Equation (4-46).

$$\tau_{solid} = \tau_a \frac{F_{solid}}{F_a}$$

Equation (4-46)

Sines failure criterion is used with Zimmerli data S_{sa}=241MPa. Fatigue factor of safety is then formulated as Equation (4-47).

$$n_{fatigue}=\frac{S_{sa}}{\tau_a}$$

Equation (4-47)

Ultimate tensile stress S_{ut} is calculated using Equation (4-48) where constants A and m are obtained from Shigley's[ ].

$$S_{ut}=\frac{A}{d_{spr\ wire}^{m}}$$

Equation (4-48)

Torsional yield strength is calculated by Equation (4-49) as Samonov states and then solid form factor of safety n_{solid} can be calculated.

$$S_{sy}=0.56S_{ut}$$

Equation (4-49)

$$n_{solid}=\frac{S_{sy}}{\tau_{solid}}$$

Equation (4-50)

Among the alternative designs produced by altering the winding number and material, the ones with both fatigue and solid form factors of safety greater than 1 are chosen to be applicable.

Spring design tool requires $L_{seal\ cap}$ as an input from buckling analysis in Section 4.2 and L_{piston} from piston design tool in Section 4.3. Other inputs the tool requires are either system requirements like, $K_{desired}$, Stroke, $F_{preload}$ and f_{motion} or

size limits of the system like L_{cyl}, d_{cyl} and b_{cyl}. Spring design is run for the parameter values supplied in Table 4-11 and some of the resulting possible spring designs are presented in Table 4-12. All possible spring designs are given in Appendix A.

Table 4-11: Input Parameters for Spring Design

Parameter	Value	Unit
$K_{desired}$	10000	N/m
Stroke	19	mm
L_{cyl}	145	mm
d_{cyl}	25	mm
b_{cyl}	2	mm
$F_{preload}$	140	N
f_{motion}	10	Hz
$L_{seal\ cap}$	35	mm
L_{piston}	20.3	mm

Table 4-12: Some of the Possible Spring Designs Calculated

n_{wnd}	L_{free} [mm]	$d_{spr\ wire}$ [mm]	K [kN/m]	Safe Freq [Hz]	Safety Factor	Material
11	118.3000	2.9606	10	20.2696	1.0305	ASTM A401
12	118.3000	2.9727	10	19.3340	1.0428	ASTM A228
13	118.3000	3.0731	10	18.0166	1.1144	ASTM A229
13	118.3000	3.1508	10	17.6089	1.1155	ASTM A313
15	118.3000	3.1413	10	16.4382	1.0388	ASTM A227
16	118.3000	3.2180	10	15.5686	1.3137	ASTM A401
17	118.3000	3.2122	10	15.1288	1.3068	ASTM A228
18	118.3000	3.3029	10	14.3338	1.3559	ASTM A229
19	118.3000	3.4260	10	13.4951	1.3913	ASTM A313

4.5. Cylinder Design

Cylinder should remain intact under the internal pressure that is produced by the viscous fluid under piston excitation.

Damping force is simply given by Equation (4-51).

$$F_{damping}(t)=c_{damping}\, v(t)$$

Equation (4-51)

A damped machine gun's response to firings, conducted in a series manner, can be expressed as sinusoidal harmonic functions. Displacement of such a machine gun is formulated as x(t) in Equation (4-52) for a desired stroke and rounds per minute value.

$$x(t)=\frac{Stroke}{2}\cos(2\pi f_{motion}\, t)$$

Equation (4-52)

Velocity is simply the time derivative of the supposedly formulated displacement.

$$v(t)=-Stroke\ \pi\, f_{motion}\sin(2\pi f_{motion}\, t)$$

Equation (4-53)

In order to obtain a sufficiently rigid cylinder, maximum value of pressure generated should be obtained.

$$F_{damping}^{max}=c_{damping}\, Stroke\ \pi\, f_{motion}$$

Equation (4-54)

Internal pressure is caused by the piston forcing the viscous fluid through its tiny orifices while there is a steady external pressure p_o, which is considered to be atmospheric pressure.

$$p_{in}=\frac{F_{damping}^{max}}{A_{piston}}$$

Equation (4-55)

$$p_o=1atm=101325\ Pa$$

Tangential and radial stresses generated due to pressure difference on cylinder wall are given in Equation (4-56) and Equation (4-57).

$$\sigma_t(r)=\frac{p_{in}r_{in}^2-p_or_o^2-\frac{r_{in}^2r_o^2(p_o-p_{in})}{r^2}}{r_o^2-r_{in}^2}$$

Equation (4-56)

$$\sigma_r(r)=\frac{p_{in}r_{in}^2-p_or_o^2+\frac{r_{in}^2r_o^2(p_o-p_{in})}{r^2}}{r_o^2-r_{in}^2}$$

Equation (4-57)

The stress functions with radius variable have their maximum values at $r = r_i$.

$$\sigma_t^{max}=\sigma_t(r_{in})=\frac{p_{in}r_{in}^2-p_or_o^2-\frac{r_{in}^2r_o^2(p_o-p_{in})}{r_{in}^2}}{r_o^2-r_{in}^2}$$

Equation (4-58)

$$\sigma_r^{max}=\sigma_r(r_{in})=\frac{p_{in}r_{in}^2-p_o r_o^2+\frac{r_{in}^2 r_o^2(p_o-p_{in})}{r_{in}^2}}{r_o^2-r_{in}^2}$$

Equation (4-59)

Maximum allowable shear stress and tensile stress should not be exceeded with given factor of safety.

$$\tau_{max}=\frac{S_y}{2\,n_{cyl}}>\sigma_r^{max}$$

Equation (4-60)

$$\sigma_{max}=\frac{S_y}{n_{cyl}}>\sigma_t^{max}$$

Equation (4-61)

Cylinder design is modified by increasing the outer radius, r_o, from the point of iterative initiation in order to satisfy the conditions given by Equation (4-60) and Equation (4-61). This design requires d_{Piston} calculated in Section 4.3.

Cylinder is designed for an initiation of 1mm cylinder thickness with 25mm outer radius and generic stainless steel of 200MPa yield strength as material. Input parameters for the design process are given in Table 4-13 and the results of the design are tabulated in Table 4-14.

Table 4-13: Input Parameters for Cylinder Design

Parameter	Value	Unit
f_{motion}	10	Hz
$C_{desired}$	1600	Ns/m
Stroke	19	mm
d_{cyl}	25	mm
b_{cyl}	1	mm
$n_{Pressure}$	2.5	-
S_y	200	MPa
d_{piston}	20.3	mm

Table 4-14: Output Parameters of Cylinder Design

Parameter	Value	Unit
$n_{Pressure}$	2.51	-
b_{min}	1.1	mm

CHAPTER 5

PROTOTYPING

5.1. Introduction

This study aims to deliver ease of design for a shock absorber with desired stiffness and damping characteristics and allow localization of the manufacturing process. Prototyping, therefore, constitutes one of the essentials of this study, since it is the method of validation of the mathematical model and the way of providing the know-how for end product manufacturing.

Prior to prototyping, an off-the-shelf product manufactured by Taylor Devices Inc is examined thoroughly. Since the off-the-shelf products obtained from the company are suitable for military applications, choice of material, leakproofness and design aspects are examined.

Figure 5-1: Prototype Pistons

Figure 5-2: Disassembled Off-The-Shelf Shock Absorber

5.2. Manufacturing Know-How's

Piston rod is produced according to the results obtained by the software tool. By means of practicality, piston rod is designed with an additional threaded length at the bottom and is attached to the piston with a corresponding threaded hole on the piston. Design and material choice considerations for piston are explained in Section 4.3.

Piston rod is the part where damper is to be attached to the vibrating system. Therefore, it is required to sustain the loading from the system even if the motion of damper is restrained due to bottom-linking, premature firing of the machine gun before the retraction stroke is completed, or in case piston is stuck somewhere along its stroke.

Piston is the part where the fluid-solid interaction takes place. Since capillaries are to be located on piston and the outer diameter has to stay within very tight tolerance region, piston material is chosen to be free-cutting brass.

Capillaries are positioned at equal distance from the center of the piston and from each other.

At the center of the piston, there is a threaded hole for mounting the piston rod. Since damper is required to yield different damping characteristics between the compression and retraction strokes, a circular disk is to be attached on the piston to function as a poppet. To be able to hold this disk at the end of the piston, a retaining ring is to be used; therefore piston should accommodate both the disk and its retaining ring. Smaller diameter flange is designed at the bottom of the disk for the above-mentioned purposes.

Additionally, piston is the part that slides along the inner surface of the cylinder, which requires it to be guided inside the cylinder. In order to be able

to provide guidance for the piston, the diameter is altered to match the inner diameter of the cylinder at three points separated by equal angular positioning.

Piston cylinder is the part where all the parts are assembled and kept together. It provides piston with guidance, while it is a casing for the parts and the viscous oil. Piston cylinder, among the other parts, has been the one, which required further examination and development.

Piston cylinder is manufactured from 17-4 ph AISI 630 grade stainless steel and then, heat treated to increase hardness from 36HRc to 42HRc. The machining is improved by honing processing following the milling along the length piston moves.

As a casing, piston cylinder should be able to resist corrosion, which is provided with phosphate and oil coating.

Piston cylinder is to be fixed such that it would allow piston to move inside to deliver damping. Therefore piston cylinder is designed with an additional flange at the bottom, which is threaded for suitable mounting.

Seal cap is designed to function as a bearing for the piston rod and provides leakproofness by the round sponge gaskets and the outer O-ring. Seal cap is manufactured from Teflon.

Poppet disk is manufactured from Teflon as well.

5.3. Failing Specimens and Outcomes

The very first prototypes P1301 and P1303 have failed during the tests on servo hydraulic test unit. When the solid length of the spring is reached and piston stopped at its lowest point of compression stroke, due to the continued forcing on piston rod, it functioned as a die and deformed piston hole. Piston rod of P1303 got all the way through the piston and got stuck as seen in Figure 5-3.

Figure 5-3: Damaged Prototype P1303

For piston P1301, after the testing, the collected data was not of the expected kind. When the piston is disassembled and its components are taken out, piston rod was visibly standing at an angle to piston, got askew.

In order to make sure, piston and piston rod are measured in CMM assembled together.

Then, the piston rod is disassembled from the piston and the damage on the piston was observed as in Figure 5-4.

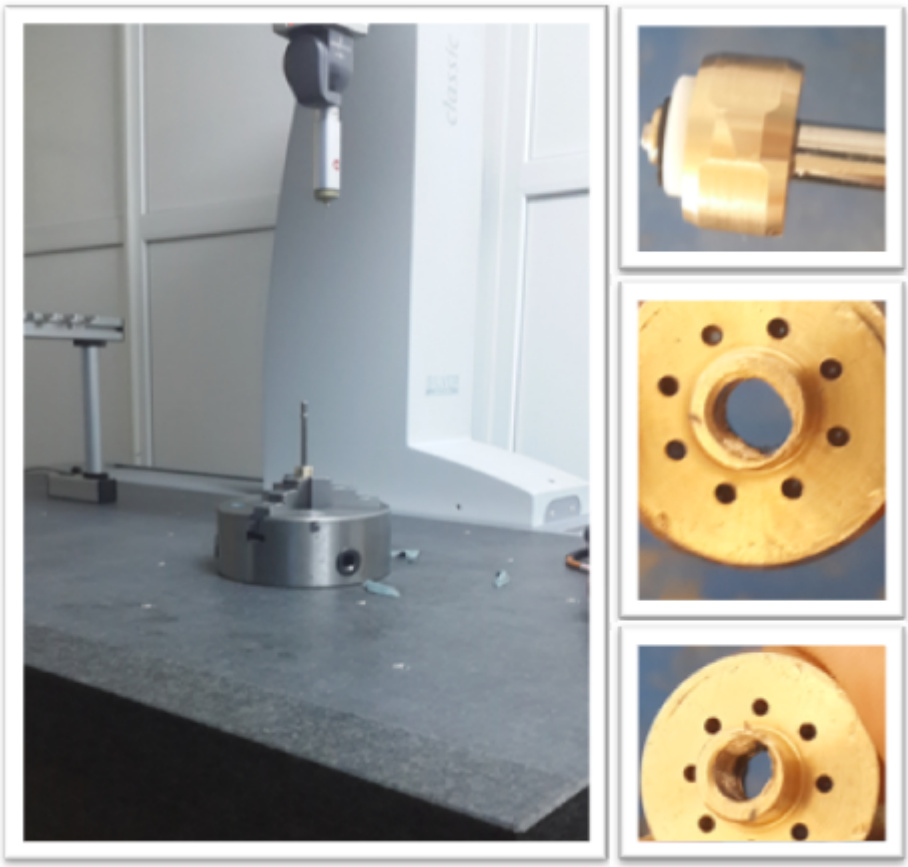

Figure 5-4: Failure of P1301 Brass Piston

Piston material for the first 8 prototypes P1301 to P1308 was selected as brass. After this failure occurred, piston material is updated to bronze. Following this update, failure shown in Figure 5-3 did not repeat. However, the concentricity

was getting disrupted. When investigated further, it was observed that the cylinder was going through small deformations during the motion of the piston inside. Therefore, following prototype P1412, cylinder material is updated to AISI 630.

Another failure on prototypes was concerning the leakproofness. Prototypes P1402 and P1408 which were filled with 350cSt silicone-based viscous fluid, caused leakage as seen in Figure 5-5. Following this incidence, the material of the seal cap is change to Teflon®, from Delrin® POM. Prototypes with seal caps manufactured from Teflon®, as seen in Figure 5-6, have not failed any of the following tests.

Figure 5-5: Leakage of Viscous Oil from Pistons P1402 and P1408

Figure 5-6: Seal Cap Assembly Manufactured from Teflon®

Leakproofness test is introduced for all pistons following P1408. All pistons are kept compressed in a press for 6 hours with a paper placed underneath so that any leakage can be collected.

Leakproofness test prior to cyclic testing on the servo hydraulic test unit is presented in Figure 5-7.

Figure 5-7: Leakproofness Test of a Prototype Piston

5.4. Variations

Table 5-1: Variation of Parameters among Prototypes

<table>
<tr><th></th><th>PN</th><th>Piston Material</th><th>Cylinder Material</th><th>Oil Viscosity [cSt]</th><th>d_{Piston} [mm]</th><th>L_{piston} [mm]</th><th>K [N/m]</th></tr>
<tr><td>1</td><td>P1301</td><td rowspan="8">Brass</td><td rowspan="18">AISI 304</td><td rowspan="4">350</td><td rowspan="8">21.4</td><td rowspan="18">10.1</td><td rowspan="13">1800</td></tr>
<tr><td>2</td><td>P1302</td></tr>
<tr><td>3</td><td>P1303</td></tr>
<tr><td>4</td><td>P1304</td></tr>
<tr><td>5</td><td>P1305</td><td rowspan="4">500</td></tr>
<tr><td>6</td><td>P1306</td></tr>
<tr><td>7</td><td>P1307</td></tr>
<tr><td>8</td><td>P1308</td></tr>
<tr><td>9</td><td>P1401</td><td rowspan="17">Bronze</td><td rowspan="4">100</td><td rowspan="17">20.3</td></tr>
<tr><td>10</td><td>P1402</td></tr>
<tr><td>11</td><td>P1403</td></tr>
<tr><td>12</td><td>P1404</td></tr>
<tr><td>13</td><td>P1405</td><td rowspan="5">350</td></tr>
<tr><td>14</td><td>P1406</td></tr>
<tr><td>15</td><td>P1407</td><td rowspan="12">10000</td></tr>
<tr><td>16</td><td>P1408</td></tr>
<tr><td>17</td><td>P1409</td><td>-</td></tr>
<tr><td>18</td><td>P1410</td><td>350</td></tr>
<tr><td>19</td><td>P1411</td><td rowspan="7">500</td></tr>
<tr><td>20</td><td>P1412</td><td rowspan="6">11</td></tr>
<tr><td>21</td><td>P1413</td><td rowspan="6">AISI 630</td></tr>
<tr><td>22</td><td>P1414</td></tr>
<tr><td>23</td><td>P1415</td></tr>
<tr><td>24</td><td>P1416</td><td rowspan="2">1800</td></tr>
<tr><td>25</td><td>P1417</td></tr>
</table>

Table 5-1 (continued)

	PN	Piston Material	Cylinder Material	Oil Viscosity [cSt]	d_{Piston} [mm]	L_{piston} [mm]	K [N/m]
26	**P1418**	Bronze	AISI 630	500	20.3	11	10000
27	**P1419**						
28	**P1420**					10.1	
29	**P1421**						
30	**P1422**						
31	**P1423**						
32	**P1424**					10.1	10000

CHAPTER 6

VALIDATION OF MODEL

6.1. Introduction

Developed mathematical model is verified by the tests carried out on the prototype pistons using a servo hydraulic test unit by Instron.

Data is collected by a desktop PC connected to the servo hydraulic test unit using built-in Instron data acquisition software. PC is configured with Intel® Core ™ i5-3570 CPU with 3.4 GHz processor speed, 6GB of RAM, 450GB of hard drive capacity and runs on Windows 7 64-Bit operating system.

Outputs are selected as, total time in seconds, elapsed time per cycle in seconds, total number of cycles, elapsed cycle count, current step, loop number, total cycle count, piston position in millimeters and load in kilo Newtons. These values are exported as comma-separated values to be thereby embedded into Matlab®.

While each specimen is tested for its design criteria of stroke and frequency of motion, various test scenarios are implemented as trials for an efficient testing of the specimens, which have yielded into extraordinary hysteresis plots as demonstrated in Figure 6-1.

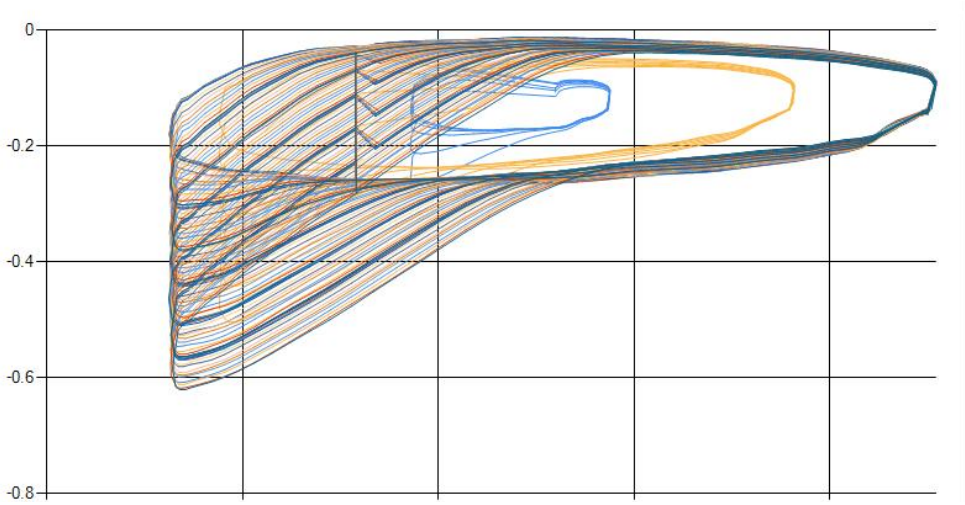

Figure 6-1: Extraordinary Hysteresis Result of Prototype Piston P1401, Displacement in mm vs Force in kN

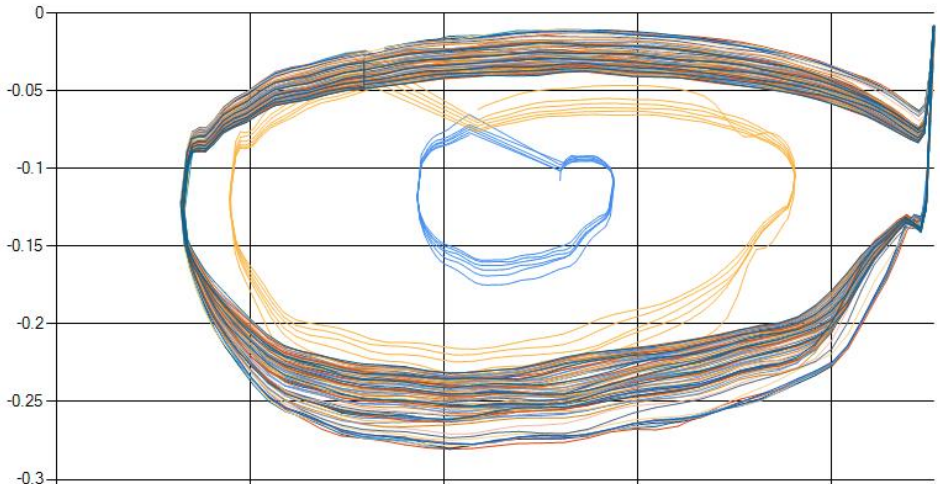

Figure 6-2: Hysteresis Result of Prototype P1408, Displacement in mm vs Force in kN

6.2. Test Scenarios

6.2.1. Frequency Sweep

When the frequency sweep option is checked, WaveMatrix® generates the harmonic motion starting from the specified lowest frequency and sweeps the frequency spectrum up until the specified highest frequency.

Although frequency sweep method is helpful to identify the damper thoroughly, for a weapon of known characteristics, the frequency of motion is known and constant within a range of small deviations.

Damping force is a function of velocity and velocity of the piston is changing when frequency sweep is applied. Since viscous heating does not happen as fast as it would at a given constant frequency when there is a sweep starting from a lower frequency, the viscosity also remains higher and the effect of cyclic firings is not observable. Therefore, not all pistons are investigated with frequency sweep tool in the scope of this study.

6.2.1. 12.7 mm Caliber M2 Machine Gun Configuration

12.7 mm caliber M2 machine gun typically performs about 450-600 rounds per minute and exerts about 9 kN of recoil force. Considering its maximum possible value, 600 rounds per minute corresponds to 10 rounds per second, i.e.: 10 Hz.

In a typical case where the firing is planned to be 5 consecutive burst fires of 20 rounds, shock absorber pistons go through 100 cycles in total per piston.

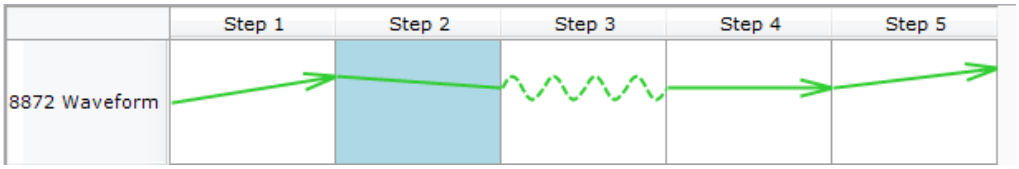

Figure 6-3: Test Sequence Input Screen on WaveMatrix®

6.2.1. Overcycled Piston Scenario

Overcycled piston scenario performs the test in the cyclic rate of fire of 12.7 mm -caliber M2 machine gun. However, this time the firing is planned to be 100 rounds of burst fire, repeated for 6 times.

Practically, M2 is not capable of performing 600 consecutive rounds because its barrel gets overheated and requires replacement before fired rounds reach 600.

Despite the fact that this scenario is practically not possible, overcycling the pistons during the test provides better identification and the ability to see if there is a possible failure point.

Notice the repetition of 100 cycles in Step 3, followed by a very short interval of hold in Step 4, repeats itself, indicated by the arrow on top in Figure 6-4.

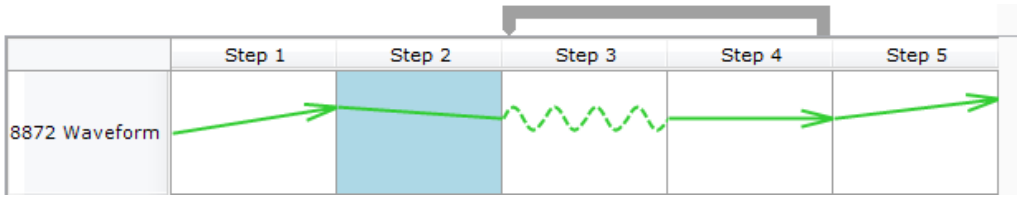

Figure 6-4: Test Sequence of Overcycled Piston Scenario in WaveMatrix®

Position of the test probe at the beginning of Step 1 is such that, probe compresses the piston just a few millimeters. At the end of Step 1, it retracts such that, the probe keeps touching the top of the piston without compressing it. This point is indicated as 'Retracted Piston Position' and shown with the green line in Figure 6-5.

Test probe is then brought down to the center of stroke in Step 2.

When the test unit is programmed to produce a sinusoidal harmonic motion of amplitude equal to half of the desired stroke with its initial position half stroke, it imitates a piston under the action of cyclic firing as seen in Figure 6-5. In Step 3, a sine wave of amplitude half the desired stroke and frequency equal to the frequency of motion is generated.

For a desired stroke of 19mm and a cyclic rate of fire 600 rounds per minute, the sine function given by Equation (6-1) is generated which yields Figure 6-5.

$$x(t)=\frac{19}{2}\sin(10\times 2\pi\times t)\ \text{mm}$$

Equation (6-1)

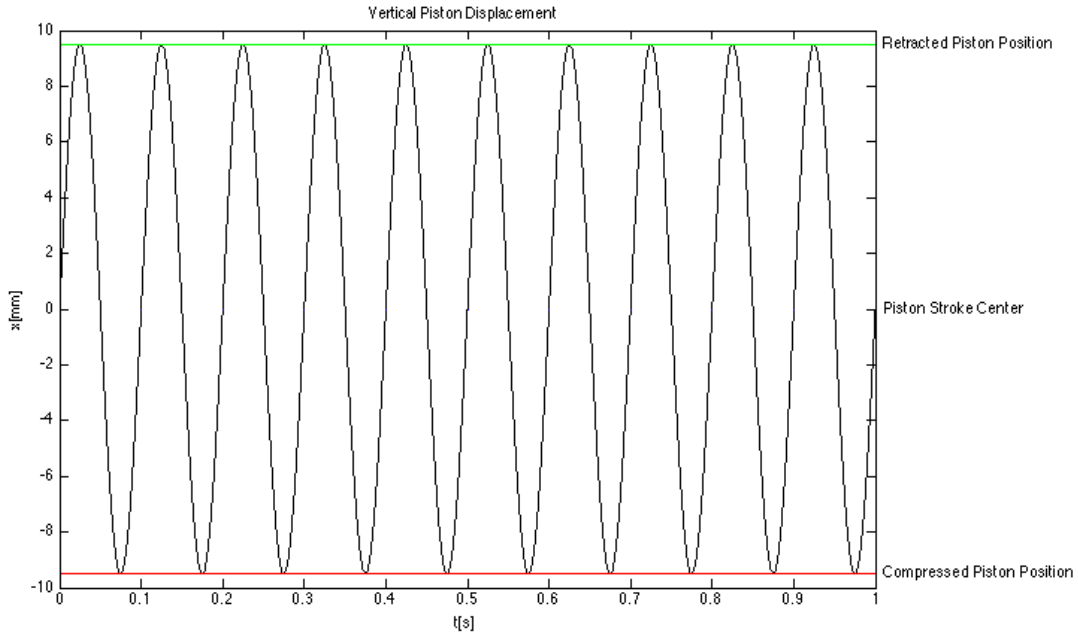

Figure 6-5: Piston Test Displacement Input

6.3. Method

1. Prototype piston is marked with permanent marker and its configuration is recorded.
2. Servo hydraulic test unit is powered on.
3. One thermocouple is positioned away from the piston to measure the ambient temperature during test. Another thermocouple is positioned on the cylinder wall as seen in Figure 6-6.

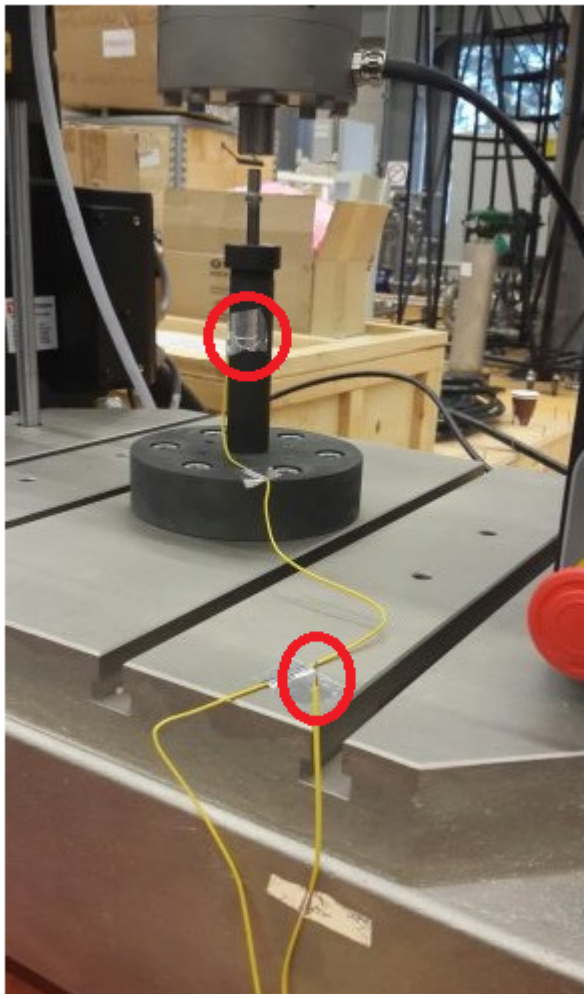

Figure 6-6: Thermocouples Positioned on Piston and Away from Piston

4. Data acquisition unit for thermocouples is connected to PC and its software is programmed to function with the attached thermocouples.
5. WaveMatrix® is programmed to obtain the scenario described in 6.2.1.
6. Test is run and data is recorded in comma-separated value format.

Figure 6-7: Test in Process

7. When 600 rounds are completed, 35 minutes is allowed for the piston to cool down.
8. Temperature as a function of time is plotted using the comma-separated values by Matlab® as seen in Figure 6-8.

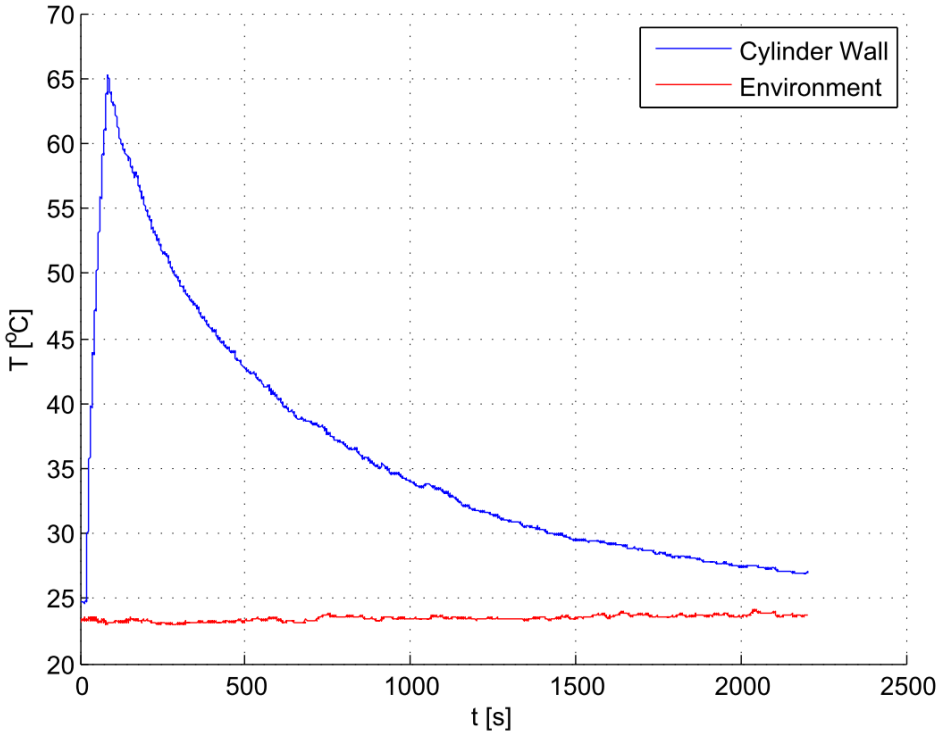

Figure 6-8: Results from Thermocouples

9. Force as a function of displacement is plotted using Matlab® as seen in Figure 6-9.

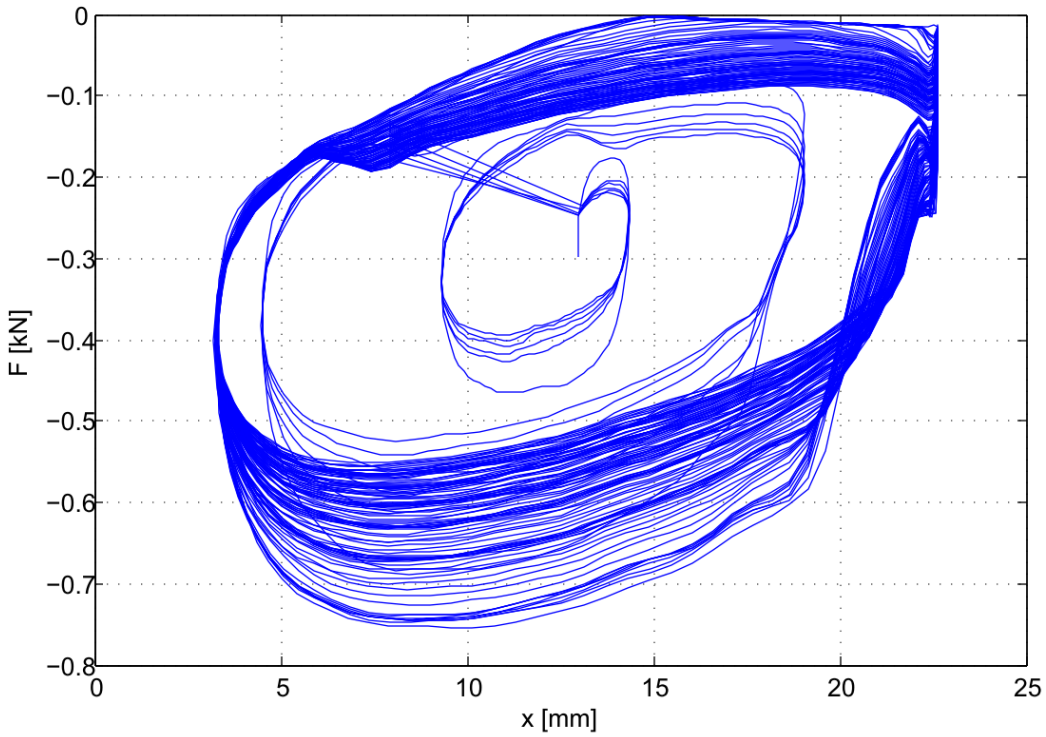

Figure 6-9: Hysteresis Plot for Piston

10. Using the equations obtained in 4.3.1 and 4.3.1, prototype parameters are input into a script on Matlab® and analysis is run. Comparison of the acquired data and the calculation with the given parameters is obtained as seen in Figure 6-10 and Figure 6-11.

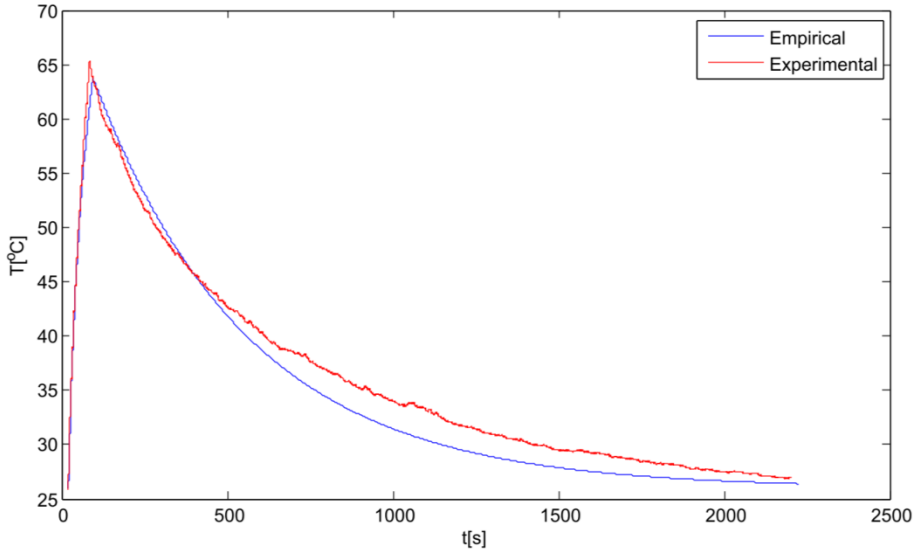

Figure 6-10: Comparison of Empirical and Experimental Temperature on Cylinder Wall

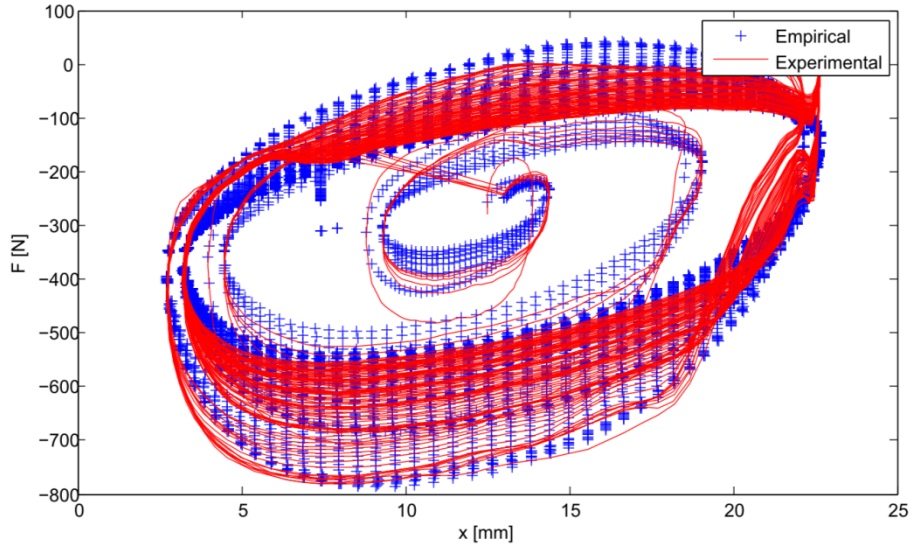

Figure 6-11: Comparison of Empirical and Experimental Hysteresis

CHAPTER 7

SOFTWARE DEVELOPMENT

Software tools for design purposes provide ease of access to qualified, filtered and tailored information and calculation capabilities. In this study, calculations and algorithms for design of multi component damper assembly are embedded into software with a graphical user interface.

Software is designed in Visual Studio 2012 in C# programming language. Design steps presented in Part 4 are first embedded into Matlab® and then, their corresponding Matlab® function scripts are deployed as .NET Assemblies.

Matlab® is preferred for constructing functions because of its capabilities and wide spectrum of functions. However, the deploy tool does not support the symbolic calculation toolbox and all its subfunctions. Therefore, many solutions are carried out by constructing iterative loops.

Software designed to have a detachable toolbox, which serves as a flowchart for the user to follow step-by-step. Each toolbox item is checked with a green icon if all the input boxes are filled with appropriately formatted data.

Figure 7-1: Toolbox of Software

First tool requires inputs concerning the spring design. Desired spring stiffness and preload at desired piston stroke is input in this panel.

Second tool requests input concerning the shock absorber in general. Physical limits like available cylinder outer diameter and length input along with an initiative value of cylinder thickness. This is the starting point of the in-cylinder pressure analysis mentioned in Part 4.5.

User is also requested to pick a viscosity value among a list of silicone based viscous fluids. Calculations are carried out according to the fluid properties specific to selected viscosity. Scrolled down, cylinder material properties like yield strength and modulus of elasticity are requested in this panel.

Next toolbox item is concerning the safety of the design. In this panel, user inputs the required safety factor against buckling and in-cylinder pressure.

Weapon parameters are supplied through the next toolbox item and calculator button solves for the shock absorber parameters.

A tutorial is presented in Appendix D.

CHAPTER 8

SUMMARY AND CONCLUSIONS

8.1. Summary

This study aims to develop a shock absorber design to be used in a military weapon station and software capable of delivering a shock absorber design of desired damping and stiffness characteristics for military systems. The software enables to develop custom shock absorbers dedicated to work on a particular system. Furthermore, rather than being obliged to the off-the-shelf products from abroad, local manufacturers are enabled to become providers using the know-how.

In the scope of this study, a 12.7 mm caliber M2HB machine gun is investigated with off-the-shelf shock absorbers of three different spring stiffness, by carrying out firing tests. Data is collected using an image processing algorithm and the effect of spring stiffness on recoil is observed. Image processing is preferred to avoid noisy accelerometer data due to thermo-acoustic shocks on the weapon casing.

In the design of a hydraulic shock absorber, viscous heating is a critical issue to take into consideration. In this study, the temperature rise as a result of viscous heating is regarded as to affect only the viscosity of the hydraulic fluid. Thermal expansion of piston, cylinder and other components and heat generation due to the friction between the components are assumed to be negligible.

8.2 Conclusions

Considering the results of the image processing, it is concluded that for the lowest and highest stiffness springs, due to the impacts of recoil assembly to

back and to front, respectively, the cyclic regime of the gun is affected. Each round in a 10 series burst firing is, therefore, fired at a different position of the gun and the mounting plate received different amplitudes of recoil force.

It is observed that the medium stiffness spring performed satisfactorily. After the first 2 rounds, regime is stabilized within a shorter stroke without impacts to neither back nor front recoil plate.

The characterization study showed that, although the cyclic rate of firing does not vary, response of weapon casing to cyclic recoil force varies. This causes the weapon to fire each round at different positions, velocities and accelerations along its travel. The phase difference between the internal dynamics of the weapon and its casing affects ballistics. It is concluded that, machine gun should fire each round at around close proximity to a constant point, along its back-and- forth motion, for better dispersion characteristics.

Viscous heating of the designed damper is investigated thoroughly in this study by conducting tests on prototypes. It is observed that for viscous oils with higher viscosity values, heat generated by the action of piston is higher. It is concluded that, unless the physical dimension limits require elsewise, lower viscosity oils should be preferred to avoid radical changes in forcing after continuous use.

Using the mathematical model, each piston parameter is investigated for its effect on damping. L_{stick}, effective piston length for annular only flow type, as shown in Figure 4-4 is initiated with a very small number that is 1% of $L_{piston\ rod}$. Piston length is directly proportional with the damping force as it is stated in Equation (4-21) and damping force's contribution to viscous heating is given by Equation (4-26). It is observed that, when L_{stick} is increased, the retraction stroke of damper has more dispersive hysteresis behavior along the cycles of sinusoidal harmonic motion as shown in Figure 8-1.

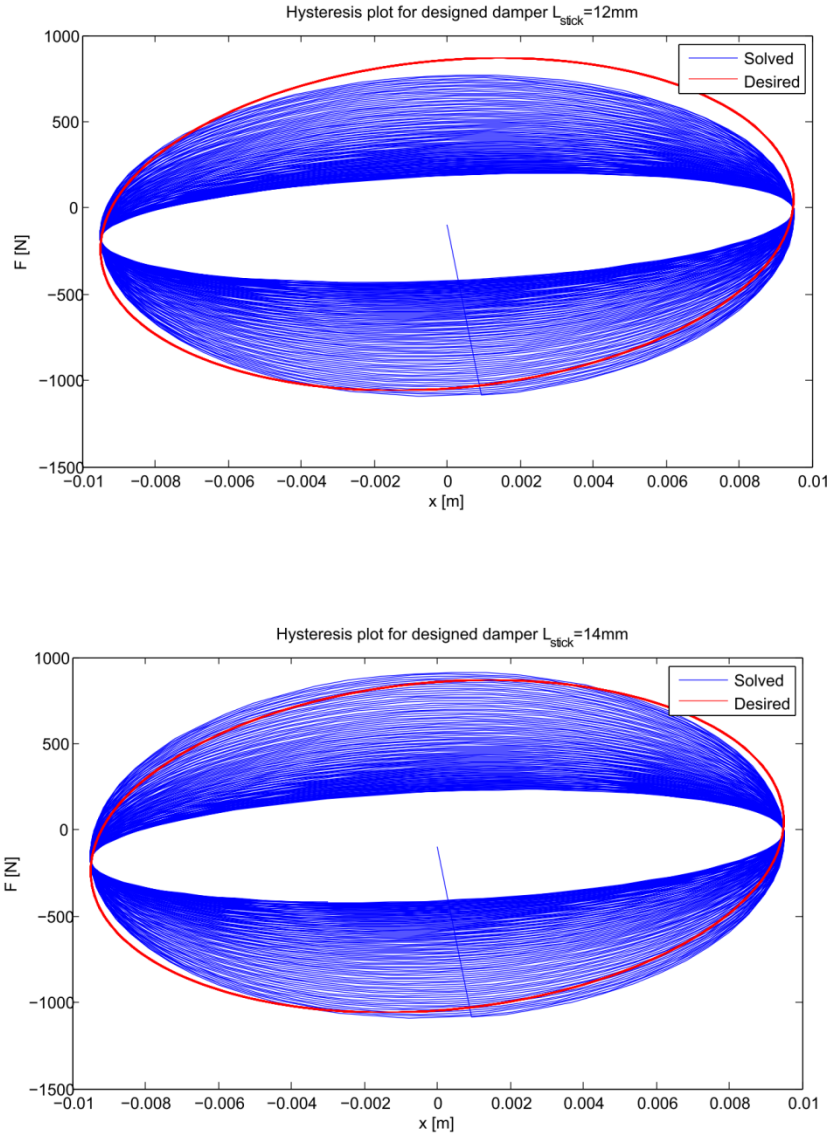

Figure 8-1: Hysteresis Plot Comparison for the Increase in Combined Length of Piston and Poppet Disk

L_{piston}, piston length, as shown in Figure 4-4 is initiated such that it occupies only the 3.33% of L_{stick}. It is observed that, when piston length alone is increased, compression stroke of damper has more dispersive hysteresis behavior along the cycles of sinusoidal harmonic motion as shown in Figure 8-2.

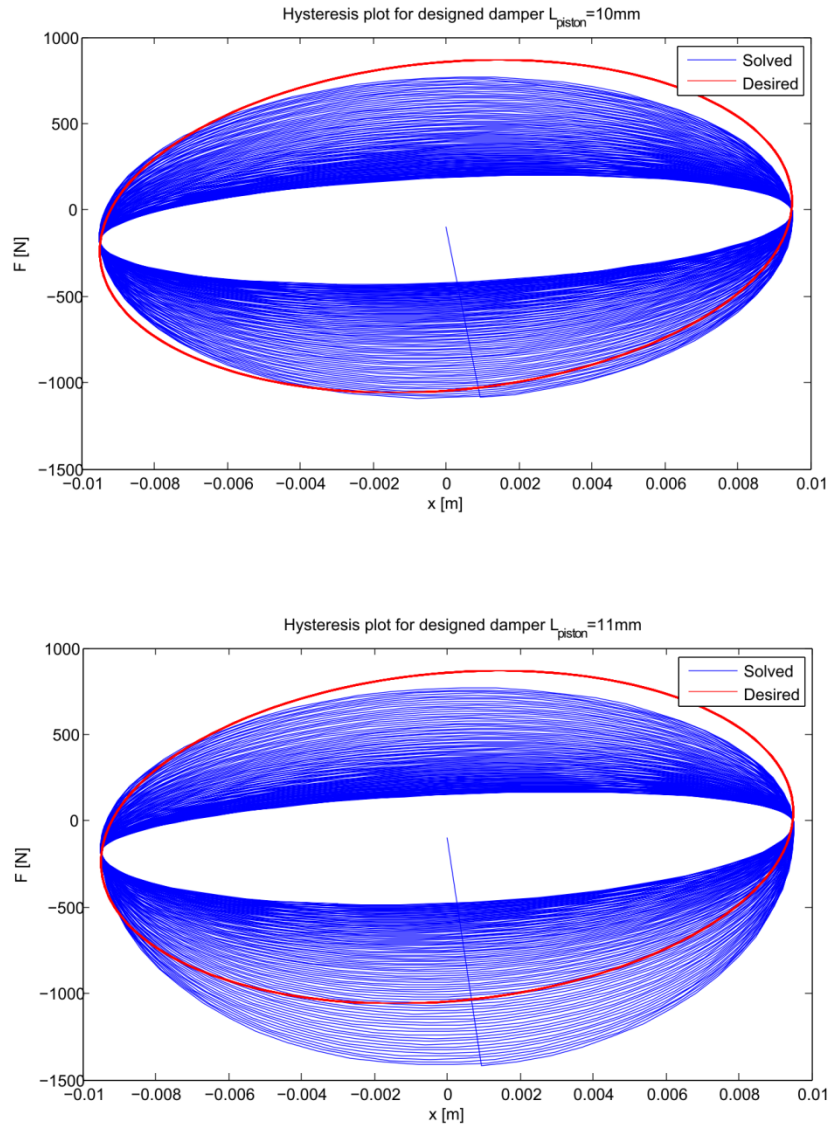

Figure 8-2: Hysteresis Plot Comparison for the Increase in Length of Piston

d_{piston}, piston diameter, provides very fast lowering of the denominator of the annulus flow terms in Equation (4-21), thereby increases the damping force very fast. Increased piston diameter has more pronounced effect on the compression stroke of damper, like piston length, as shown in Figure 8-3.

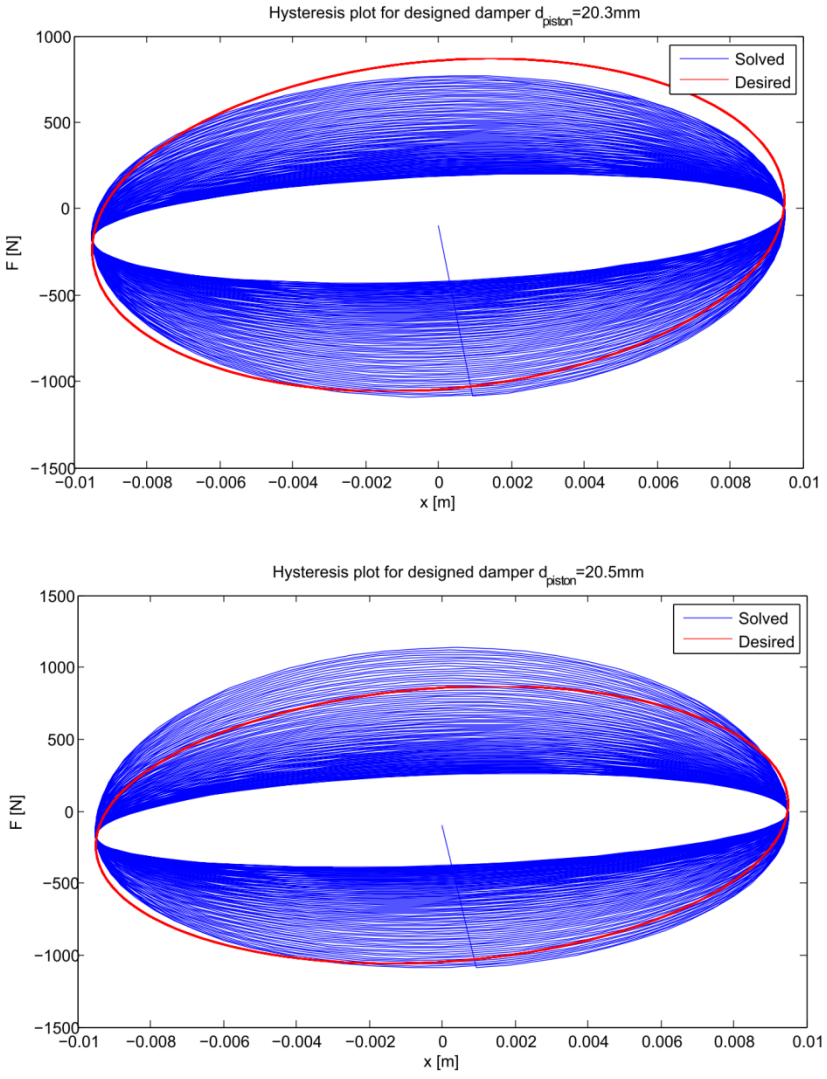

Figure 8-3: Hysteresis Plot Comparison for the Increase in Diameter of Piston

$d_{capillary}$, capillary diameter, is effective only for the retraction stroke of damper because of the poppet. Smaller capillary diameter provides more damping force during the retraction as shown in Figure 8-4.

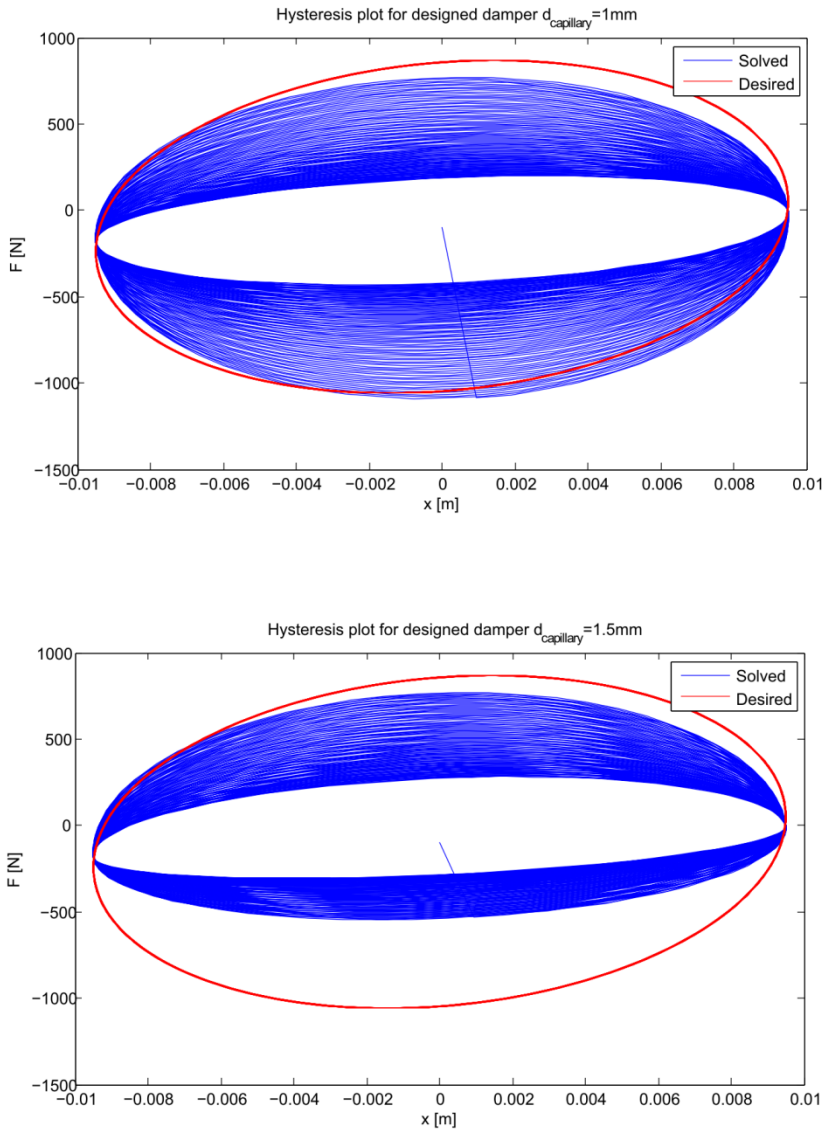

Figure 8-4: Hysteresis Plot Comparison for the Increase in Diameter of Capillaries

Last piston parameter, $n_{capillary}$, number of capillary orifices spread on the piston, is likewise effective only for the retraction stroke of damper. When the number of capillaries is increased, the hydraulic area for the annular flow is decreased and therefore compression stroke has lower damping force. On the other hand, capillary flow along the increased number of capillaries indicates increased friction, thus, providing more damping force for the retraction. Effect of increasing number of capillaries on a piston from 7 to 9 is presented in Figure 8-5.

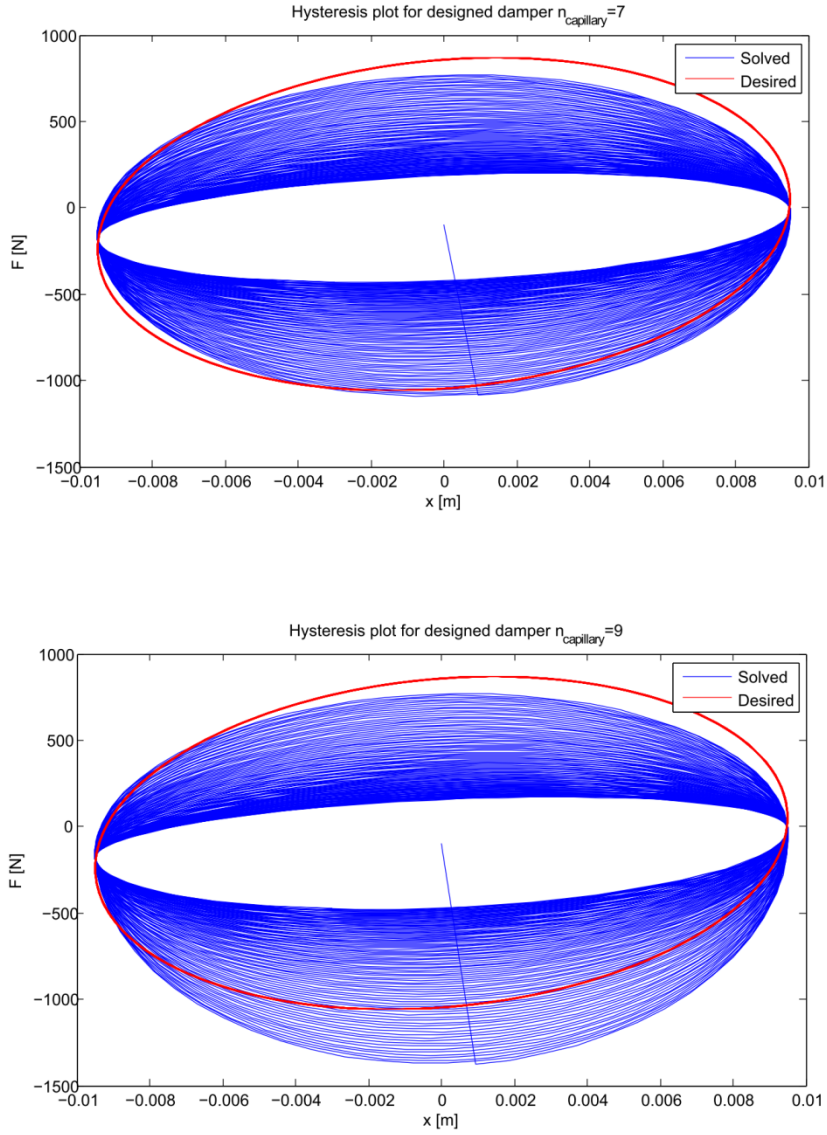

Figure 8-5: Hysteresis Plot Comparison for the Increase in Number of Capillaries

Validation carried out in Chapter 6 concludes that viscous heating model and assumptions are valid. Empirical and experimental temperature changes as shown in Figure 6-10 are coherent both in manners of trend and value.

Damping, in the scope of this study, is regarded as a linear function of velocity. It is modeled in the form of capillary and annulus flow. Calculations validated the method used to obtain damping force as presented in Figure 6-11.

Design of a shock absorber by the input of desired shock absorber characteristics, material properties and weapon characteristics is automated via a software package with graphical user interface, developed in Visual Studio 2012 ®. The algorithm behind the software is composed of several design steps.

Design is initiated with the buckling analysis of the piston rod. Piston rod with sufficient strength against buckling under the loading conditions is designed at first, followed by the design of a piston which is supposed to yield the desired damping coefficient at a user-defined frequency of motion. Spring design is the next step of design and this process produces several possible springs with different geometrical and material properties. User may select one of the many possible spring configurations to carry on with the design. Last step of design algorithm considers the in-cylinder pressure due to damping and suggests cylinder geometry accordingly.

Designs are validated through prototype pistons manufactured in various geometric configurations that are specified in Table 5-1. Manufacturing process required further attention on component-wise properties when the validation tests ended up in failures of the first few prototypes.

Materials of components are updated as failures occurred. It is concluded that, as spring stiffness increases or when bottom-linking is expected, piston material

should be altered to obtain higher yield strength at the cost of increasing the effort and the costs to manufacture.

Cylinder is found out to be demanding material of higher hardness values and it should be concentric with the piston rod and piston assembly.

Leakproofness is concluded to be satisfied with ease for higher viscosity fluids. However, for the less viscous fluids, sealing is of important concern. Seals should be manufactured from Teflon® and O-rings should be used to improve the leakproofness.

8.3 Future Work

This study can be improved by implementing further capabilities:

- Elastic coupling of the weapon station and weapon for better performance of the gun,
- Including viscous fluids other than silicone based ones,
- Including the thermal expansion of metallic components,
- Performing overduty tests to estimate time before failing,
- Investigating the effects of poppet disk geometry.

REFERENCES

[1] Chant, C., 2003, Small arms: over 250 of the world's finest personal weapons., Edison, N.J.

[2] 2002, "Manroy Heavy Machine Gun M2HB and M2QCB General & Technical Information, Illustrated Parts Catalogue, Maintenance Manual," M. E. Ltd, ed.East Sussex.

[3] He, L., Zheng, G.T., 2007, "Effect of viscous heating in fluid damper on the vibration isolation dampers," Mechanical Systems and Signal Processing(21), pp. 3060-3071.

[4] Hall, H., 1967, "Some Theoretical Studies Concerning Oleo Damping Characteristics," Ministry of Technology Aeronautical Research Council, Her Majesty's Stationery Office, London.

[5] Elaldı, F., Akçay, M., 1996, "Design and testing of a recoil mechanism used for self propelled Howitzers," Bulletin of the Technical University of Istanbul, 49(3-4), pp. 301-316.

[6] Duflot, P., Taylor, D., 2008, "Experience and Practical Considerations in the Design of Viscous Dampers," Footbridge.

[7] Mercimek, Ü., 2010, "Shock Failure Analysis of Military Equipments By Using Strain Energy Density," Master of Science, Middle East Technical University, Ankara.

[8] Defense, D. o., 2008, "Environmental Engineering Considerations and Laboratory Tests,"USA.

[9] 2012, "MaxGryro(R) Angular Rate Sensor," Watson, ed.US.

[10] bobcat-B1410, R., 2014, "BOBCAT 2.0 CCDCAMERAS SPECIFICATIONS," IMPERX, ed.US.

[11] Budynas, R. G., Nisbett, J. K., 2008, Shigley's Mechanical Engineering Design, McGraw-Hill.

[12] 2012, "Silikonöl D," MOLYDUVAL, ed., MOLYDUVAL.

[13] Amiri, M., Khonsari, M. M., 2010, "On the Thermodynamics of Friction and Wear — A Review," Entropy, 12, pp. 1021-1049.

[14] Bardos, C., Levermore, C.D., UKAI, S., Yang, T., 2008, "Kinetic Equations: Fluid Dynamical Limits and Viscous Heating," Bulletin of the Institute of Mathematics Academia Sinica, 3(1), p. 49.

[15] Costa, A., Macedonio, G., 2003, "Viscous heating in fluids with temperature-dependent viscosity: implications for magma flows," Nonlinear Processes in Geophysics, 10, pp. 545-555.

[16] Klopcic, J. T., Robinson, W. T., Petty, D. W., Sivack, M. R., 1997, "An Experiment, Analysis, and Model of Ballistic Shock," Aberdeen.

[17] Koreisova, G., 2006, "Identification of viscous damping coefficient of hydraulic motors," Scientific Papers of the University of Pardubice, 12, p. 10.

[18] Liberty, J., 2001, Programming C#, O'Reilly Media Inc., Sebastopol.

[19] M22-15283-EN-G, 2012, "Console Software - Version 8.7 Onwards Reference Manual," INSTRON, ed.

[20] M22-16102-EN-C, 2012, "WaveMatrix Software - V1.5 Onwards," INSTRON, ed.

[21] Makris, N., Roussos, Y., Whittaker, A. S., Kelly, J. M., 1998, "Viscous Heating of Fluid Dampers II: Large-Amplitude Motions," Journal of Engineering Mechanics, 124, pp. 1217-1223.

[22] Makris, N., 1998, "Viscous Heating of Fluid Dampers I: Small-Amplitude Motions," Journal of Engineering Mechanics, 124, pp. 1210-1216.

[23] Öztürk, A. R., 1988, Silah Mekaniği ve Mermilerin Hedef Üzerindeki Etkileri, MKEK, Ankara.

[24] Papasaika-Hanush, H., "Digital Image Processing Using Matlab," Institute of Geodesy and Photogrammetry, ETH Zurich.

[25] Samet, H., 1995, Applications of Spatial Data Structures; Computer Graphics, Image Processing and GIS (Geometric Information System), Addision-Wesley Publishing Group, Massachusettes.

[26] Sharp, J., and Jagger, J., 2002, Microsoft Visual C\# Step by Step, Microsoft Press.

[27] Sherwood, B. A., Bernard, W.H., 1984, "Work and Heat Transfer in the Presence of Sliding Friction," American Journal of Physics, 52(11), pp. 1001-1007.

[28] Taylor, D., Duflot, P., "Fluid Viscous Dampers Used For Seismic Dissipation in Structures."

[29] Wallaschek, J., 1990, "Dynamics of nonlinear automobile shock absorbers," International Journal of Non-Linear Mechanics, 12(2/3), pp. 299-308.

[30] Walter, P. L., 2007, "Selecting Accelerometers for Mechanical Shock Measurements," P. Piezotronics, ed.New York.

APPENDICES

A. ALL POSSIBLE SPRING CONFIGURATIONS

Table A-1: All Possible Spring Configurations

N_{coil}	L_{free}[mm]	D_{wire}	K_{stiff} [kN/m]	Safe Freq	Safety Factor	Material
14	118.3000	2.8666	10	19.5127	1.0193	Music Wire; ASTM A228
15	118.3000	2.9108	10	18.5889	1.0657	Music Wire; ASTM A228
16	118.3000	2.9527	10	17.7651	1.1108	Music Wire; ASTM A228
17	118.3000	2.9925	10	17.0253	1.1549	Music Wire; ASTM A228
18	118.3000	3.0304	10	16.3566	1.1979	Music Wire; ASTM A228
19	118.3000	3.0667	10	15.7488	1.2399	Music Wire; ASTM A228
20	118.3000	3.1015	10	15.1936	1.2811	Music Wire; ASTM A228
21	118.3000	3.1349	10	14.6840	1.3214	Music Wire; ASTM A228
22	118.3000	3.1670	10	14.2145	1.3610	Music Wire; ASTM A228
23	118.3000	3.1980	10	13.7802	1.3998	Music Wire; ASTM A228
24	118.3000	3.2279	10	13.3771	1.4379	Music Wire; ASTM A228

Table A-1 (continued)

N_{coil}	L_{free}[mm]	D_{wire}	K_{stiff} [kN/m]	Safe Freq	Safety Factor	Material
14	118.3000	2.9106	10	19.2420	1.0442	Oil-tempered Wire; ASTM A229
15	118.3000	2.9554	10	18.3318	1.0884	Oil-tempered Wire; ASTM A229
16	118.3000	2.9979	10	17.5203	1.1314	Oil-tempered Wire; ASTM A229
17	118.3000	3.0382	10	16.7915	1.1732	Oil-tempered Wire; ASTM A229
18	118.3000	3.0767	10	16.1327	1.2139	Oil-tempered Wire; ASTM A229
19	118.3000	3.1135	10	15.5339	1.2536	Oil-tempered Wire; ASTM A229
20	118.3000	3.1487	10	14.9869	1.2923	Oil-tempered Wire; ASTM A229
21	118.3000	3.1825	10	14.4848	1.3302	Oil-tempered Wire; ASTM A229
22	118.3000	3.2151	10	14.0222	1.3673	Oil-tempered Wire; ASTM A229

Table A-1 (continued)

N_{coil}	L_{free}[mm]	D_{wire}	K_{stiff} [kN/m]	Safe Freq	Safety Factor	Material
23	118.3000	3.2464	10	13.5942	1.4036	Oil-tempered Wire; ASTM A229
24	118.3000	3.2767	10	13.1970	1.4391	Oil-tempered Wire; ASTM A229
17	118.3000	3.0087	10	16.9416	1.0033	Hard-drawn Wire; ASTM A227
18	118.3000	3.0468	10	16.2765	1.0382	Hard-drawn Wire; ASTM A227
19	118.3000	3.0833	10	15.6719	1.0721	Hard-drawn Wire; ASTM A227
20	118.3000	3.1182	10	15.1196	1.1053	Hard-drawn Wire; ASTM A227
21	118.3000	3.1518	10	14.6128	1.1377	Hard-drawn Wire; ASTM A227
22	118.3000	3.1841	10	14.1457	1.1695	Hard-drawn Wire; ASTM A227
23	118.3000	3.2152	10	13.7136	1.2006	Hard-drawn Wire; ASTM A227

Table A-1 (continued)

N_{coil}	L_{free}[mm]	D_{wire}	K_{stiff} [kN/m]	Safe Freq	Safety Factor	Material
24	118.3000	3.2452	10	13.3127	1.2310	Hard-drawn Wire; ASTM A227
13	118.3000	2.8632	10	20.2711	1.0158	Chrome-vanadium Wire, Aircraft-quality Tempered or Annealed; ASTM A232
14	118.3000	2.9106	10	19.2420	1.0655	Chrome-vanadium Wire, Aircraft-quality Tempered or Annealed; ASTM A232
15	118.3000	2.9554	10	18.3318	1.1139	Chrome-vanadium Wire, Aircraft-quality Tempered or Annealed; ASTM A232
16	118.3000	2.9979	10	17.5203	1.1610	Chrome-vanadium Wire, Aircraft-quality Tempered or Annealed; ASTM A232

Table A-1 (continued)

N_{coil}	L_{free}[mm]	D_{wire}	K_{stiff} [kN/m]	Safe Freq	Safety Factor	Material
17	118.3000	3.0382	10	16.7915	1.2069	Chrome-vanadium Wire, Aircraft-quality Tempered or Annealed; ASTM A232
18	118.3000	3.0767	10	16.1327	1.2517	Chrome-vanadium Wire, Aircraft-quality Tempered or Annealed; ASTM A232
19	118.3000	3.1135	10	15.5339	1.2955	Chrome-vanadium Wire, Aircraft-quality Tempered or Annealed; ASTM A232
20	118.3000	3.1487	10	14.9869	1.3383	Chrome-vanadium Wire, Aircraft-quality Tempered or Annealed; ASTM A232

Table A-1 (continued)

N_{coil}	L_{free}[mm]	D_{wire}	K_{stiff} [kN/m]	Safe Freq	Safety Factor	Material
21	118.3000	3.1825	10	14.4848	1.3803	Chrome-vanadium Wire, Aircraft-quality Tempered or Annealed; ASTM A232
22	118.3000	3.2151	10	14.0222	1.4215	Chrome-vanadium Wire, Aircraft-quality Tempered or Annealed; ASTM A232
23	118.3000	3.2464	10	13.5942	1.4618	Chrome-vanadium Wire, Aircraft-quality Tempered or Annealed; ASTM A232
24	118.3000	3.2767	10	13.1970	1.5015	Chrome-vanadium Wire, Aircraft-quality Tempered or Annealed; ASTM A232

Table A-1 (continued)

N_{coil}	L_{free}[mm]	D_{wire}	K_{stiff} [kN/m]	Safe Freq	Safety Factor	Material
13	118.3000	2.8632	10	20.2711	1.0158	Chrome-silicon Wire, Tempered to Rockwell C49; ASTM A401
14	118.3000	2.9106	10	19.2420	1.0655	Chrome-silicon Wire, Tempered to Rockwell C49; ASTM A401
15	118.3000	2.9554	10	18.3318	1.1139	Chrome-silicon Wire, Tempered to Rockwell C49; ASTM A401
16	118.3000	2.9979	10	17.5203	1.1610	Chrome-silicon Wire, Tempered to Rockwell C49; ASTM A401
17	118.3000	3.0382	10	16.7915	1.2069	Chrome-silicon Wire, Tempered to Rockwell C49; ASTM A401

Table A-1 (continued)

N_{coil}	L_{free}[mm]	D_{wire}	K_{stiff} [kN/m]	Safe Freq	Safety Factor	Material
18	118.3000	3.0767	10	16.1327	1.2517	Chrome-silicon Wire, Tempered to Rockwell C49; ASTM A401
19	118.3000	3.1135	10	15.5339	1.2955	Chrome-silicon Wire, Tempered to Rockwell C49; ASTM A401
20	118.3000	3.1487	10	14.9869	1.3383	Chrome-silicon Wire, Tempered to Rockwell C49; ASTM A401
21	118.3000	3.1825	10	14.4848	1.3803	Chrome-silicon Wire, Tempered to Rockwell C49; ASTM A401
22	118.3000	3.2151	10	14.0222	1.4215	Chrome-silicon Wire, Tempered to Rockwell C49; ASTM A401

Table A-1 (continued)

N_{coil}	L_{free}[mm]	D_{wire}	K_{stiff} [kN/m]	Safe Freq	Safety Factor	Material
23	118.3000	3.2464	10	13.5942	1.4618	Chrome-silicon Wire, Tempered to Rockwell C49; ASTM A401
24	118.3000	3.2767	10	13.1970	1.5015	Chrome-silicon Wire, Tempered to Rockwell C49; ASTM A401
13	118.3000	2.9354	10	19.8145	1.0046	302 Stainless Steel Wire; ASTM A313
14	118.3000	2.9839	10	18.8103	1.0490	302 Stainless Steel Wire; ASTM A313
15	118.3000	3.0296	10	17.9221	1.0920	302 Stainless Steel Wire; ASTM A313
16	118.3000	3.0730	10	17.1301	1.1337	302 Stainless Steel Wire; ASTM A313
17	118.3000	3.1142	10	16.4188	1.1741	302 Stainless Steel Wire; ASTM A313
18	118.3000	3.1535	10	15.7758	1.2135	302 Stainless Steel Wire; ASTM A313

Table A-1 (continued)

N_{coil}	L_{free}[mm]	D_{wire}	K_{stiff} [kN/m]	Safe Freq	Safety Factor	Material
19	118.3000	3.1911	10	15.1913	1.2518	302 Stainless Steel Wire; ASTM A313
20	118.3000	3.2270	10	14.6574	1.2892	302 Stainless Steel Wire; ASTM A313
21	118.3000	3.2616	10	14.1673	1.3257	302 Stainless Steel Wire; ASTM A313
22	118.3000	3.2948	10	13.7156	1.3614	302 Stainless Steel Wire; ASTM A313
23	118.3000	3.3268	10	13.2978	1.3963	302 Stainless Steel Wire; ASTM A313

B. SHOCK ABSORBER DESIGN TUTORIAL

Table B-1: Input of Spring Design Tutorial

Parameter	Value	Unit
$C_{desired}$	1600	$\frac{Ns}{m}$
$K_{desired}$	10000	$\frac{N}{m}$
$F_{preload}$	140	N
f_{motion}	10	Hz
n_{Ammo}	100	-
T_{air}	11	^{o}C
h_{air}	15	$\frac{W}{m^2K}$
h_r	9	$\frac{W}{m^2K}$
λ_{st+fl}	0.139	$\frac{W}{mK}$
ρ_{fluid}	970	kg/m^3
$[\vartheta_{fluid}(T)]$	$\begin{bmatrix} 20 & 500 \\ 25 & 463 \\ 40 & 289 \\ 50 & 144 \end{bmatrix}$	[^{o}C cSt]
T_{fluid}^{flash}	315	^{o}C
c_v	1370	$\frac{J}{kgK}$
$F_{recoil_{max}}$ per piston	5000	N
$n_{cylinder}$	2.5	–
$E_{AISI630}$	200	GPa
$S_{y,AISI630}$	1	GPa
Stroke	19	mm

Table B-2: Output of Spring Design Tutorial

Parameter	Value	Unit
$n_{winding}$	16	-
$d_{spr\ wire}$	2.95	mm
d_{spr}	21.85	mm
L_{free}	118.3	mm
Spring Material	Music Wire; ASTM A228	-
L_{stick}	12.2	mm
d_{piston}	20.3	mm
L_{piston}	9.9	mm
$d_{capillary}$	1	mm
$n_{capillary}$	7	-
$L_{piston\ rod}$	69	mm
$d_{piston\ rod}$	6	mm
d_{cyl}	25	mm
$d_{cyl\ bore}$	21	mm
L_{cyl}	145	–

C. WAVEMATRIX® TEST SETUP

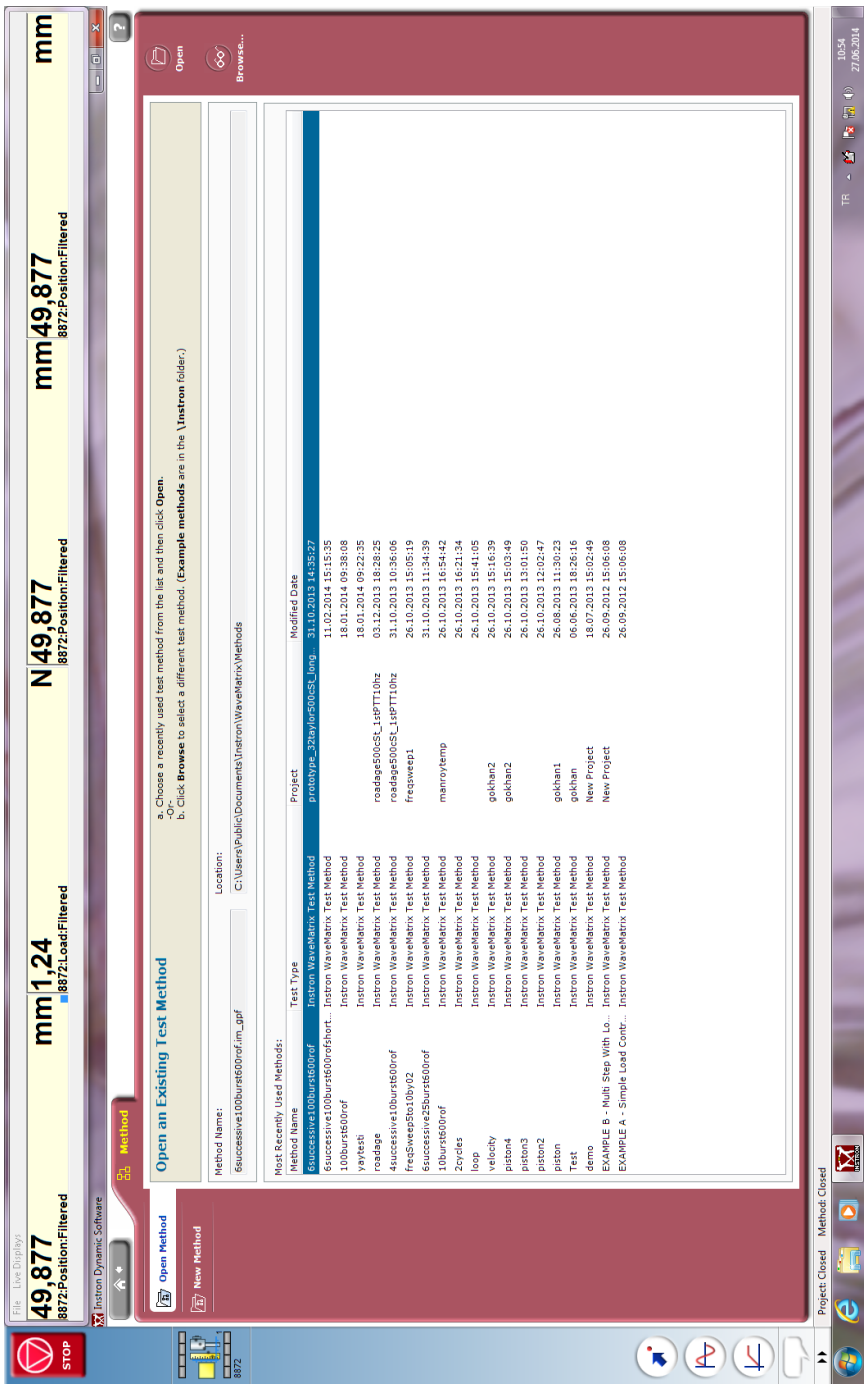

Figure C-1: WaveMatrix® Test Setup Step 1

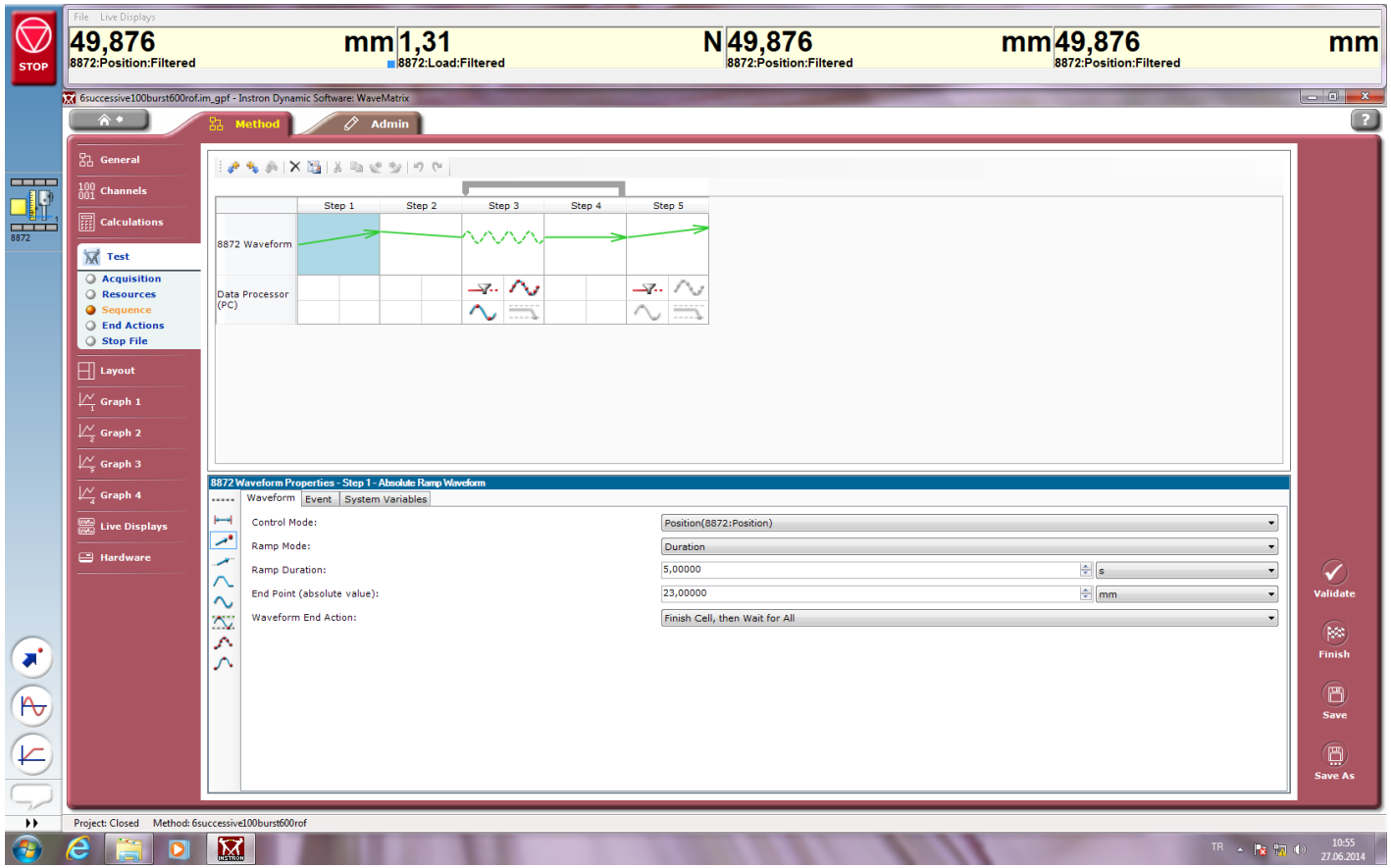

Figure C-2: WaveMatrix® Test Setup Step 2

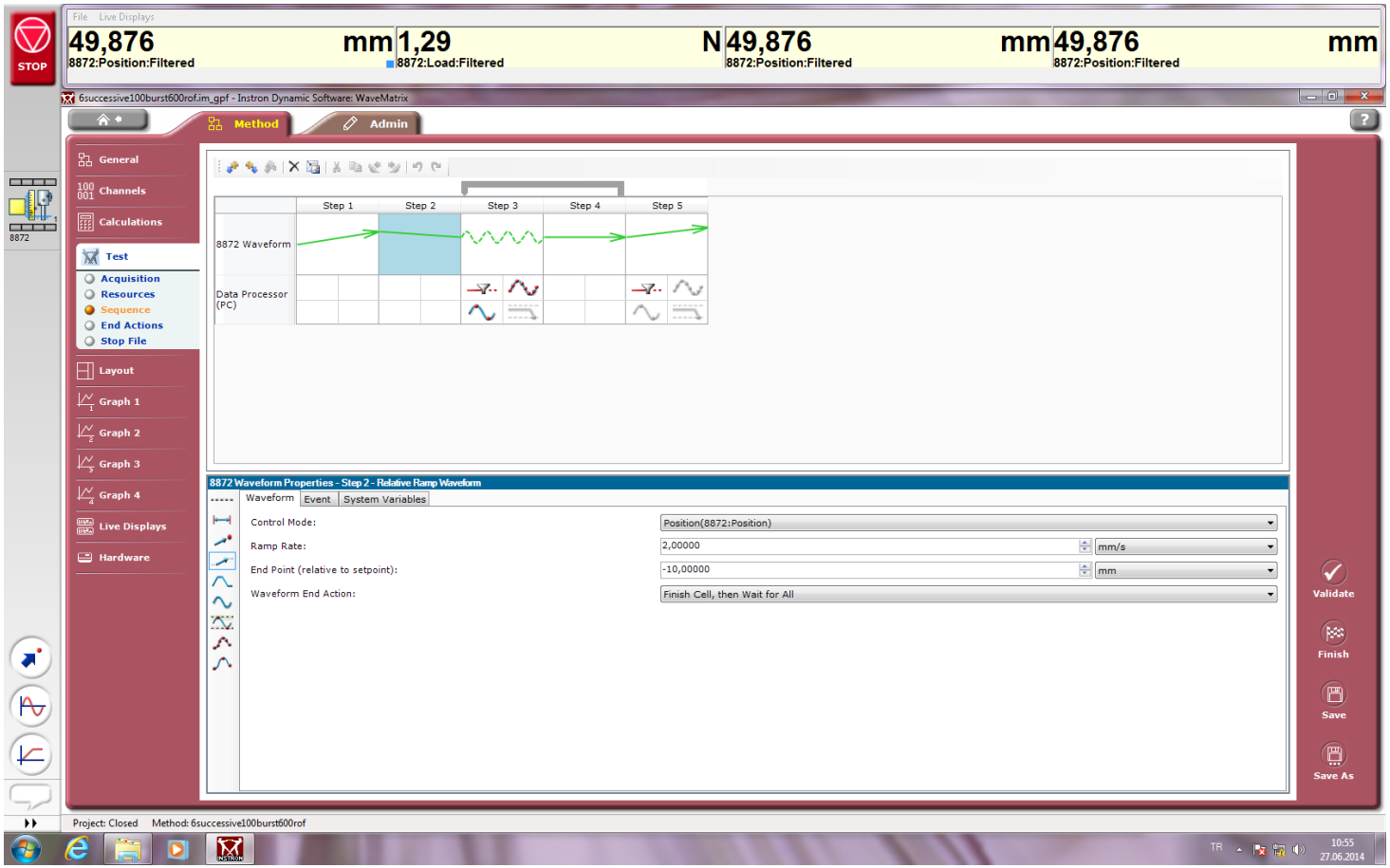

Figure C-3: WaveMatrix® Test Setup Step 3

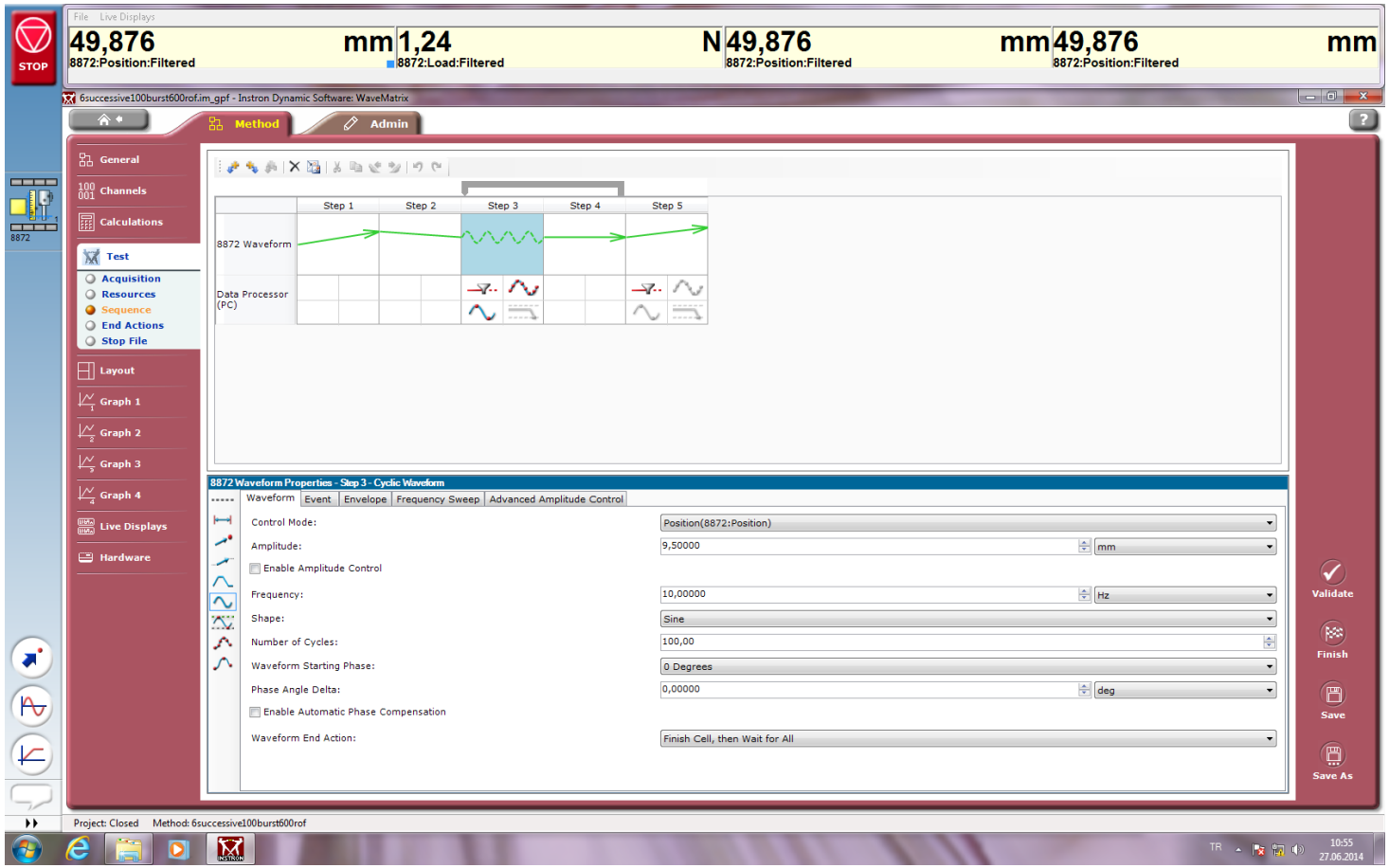

Figure C-4: WaveMatrix® Test Setup Step 4

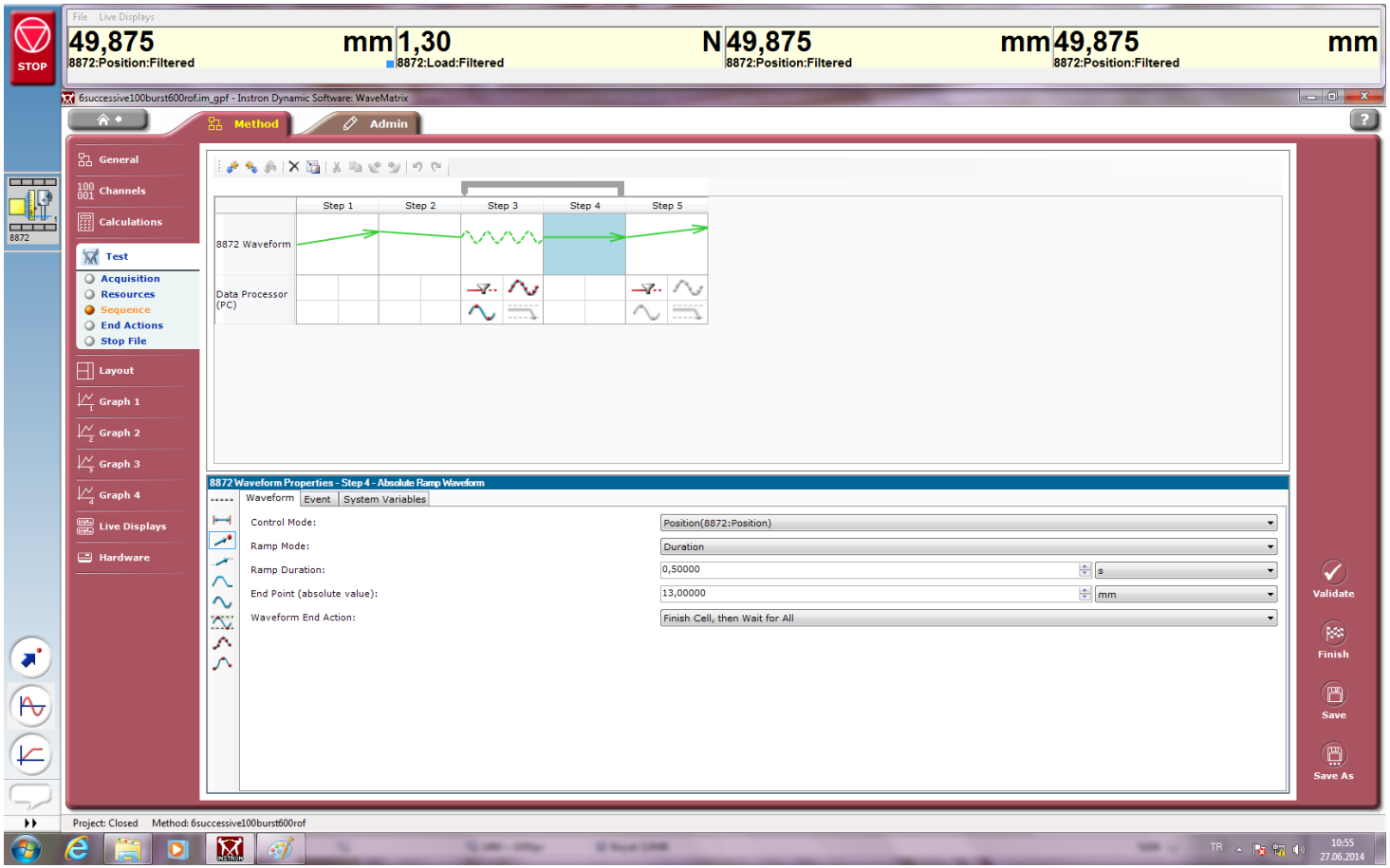

Figure C-5: WaveMatrix® Test Setup Step 5

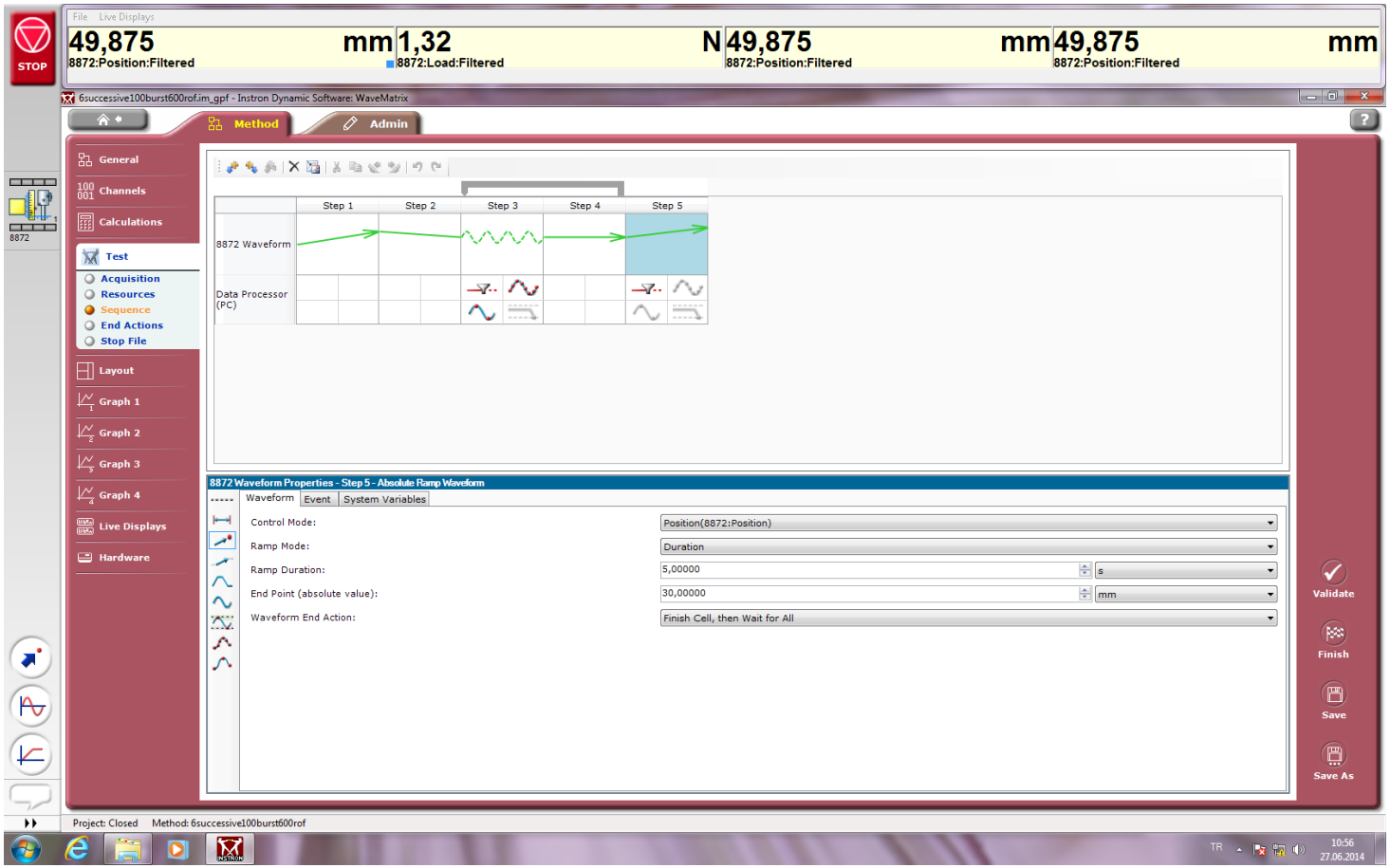

Figure C-6: WaveMatrix® Test Setup Step 6

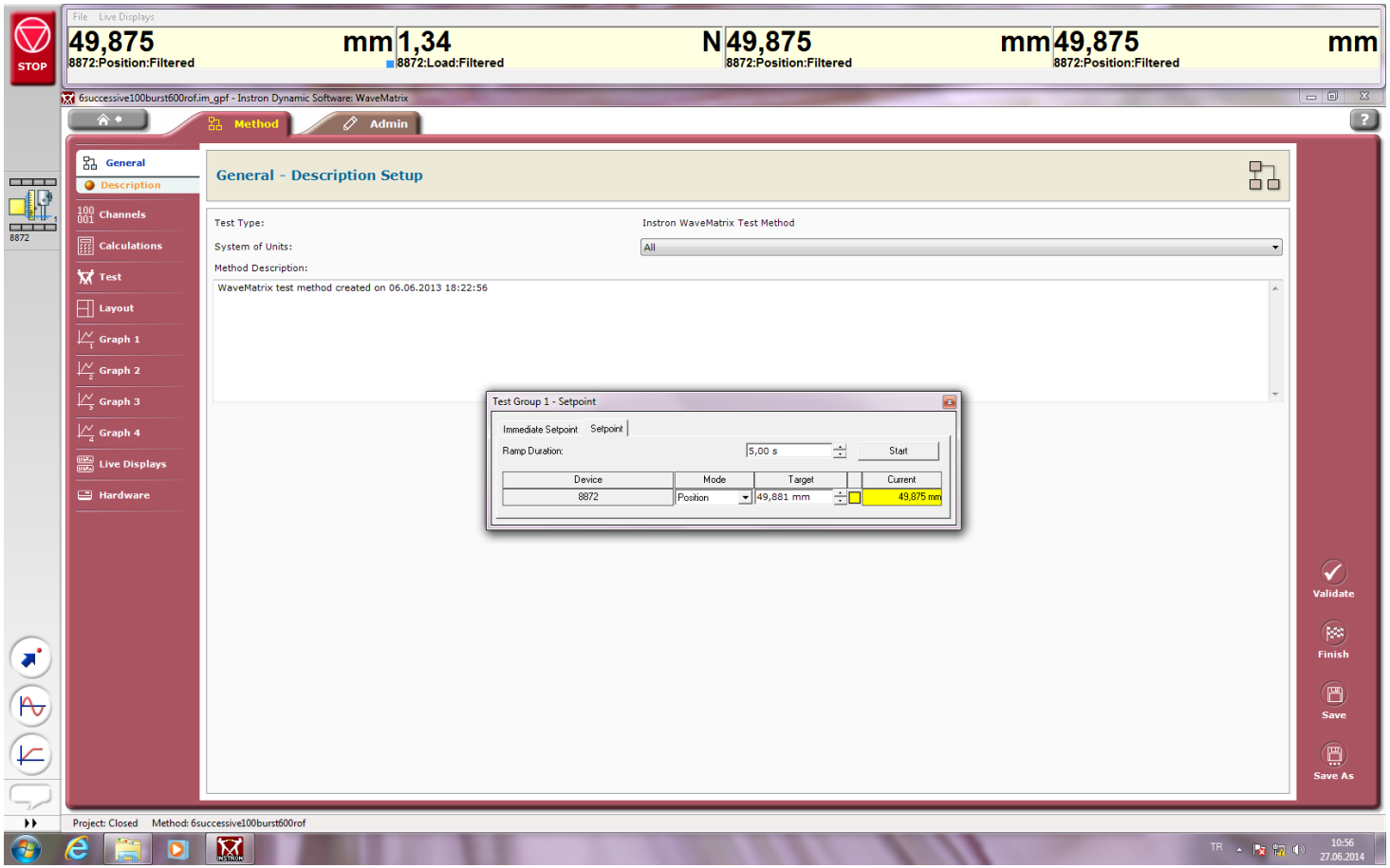

Figure C-7: WaveMatrix® Test Setup Step 7

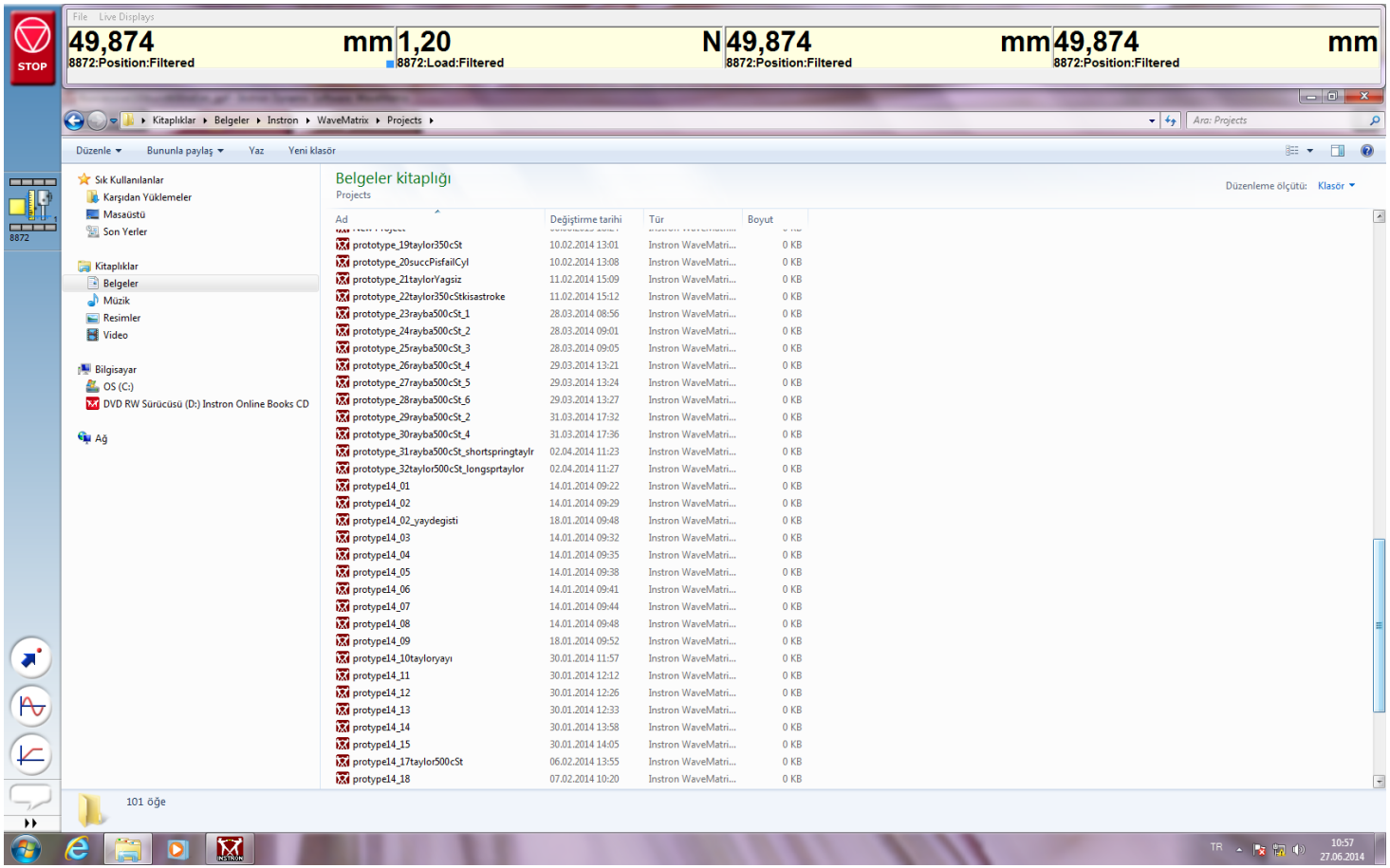

Figure C-8: WaveMatrix® Test Files Directory

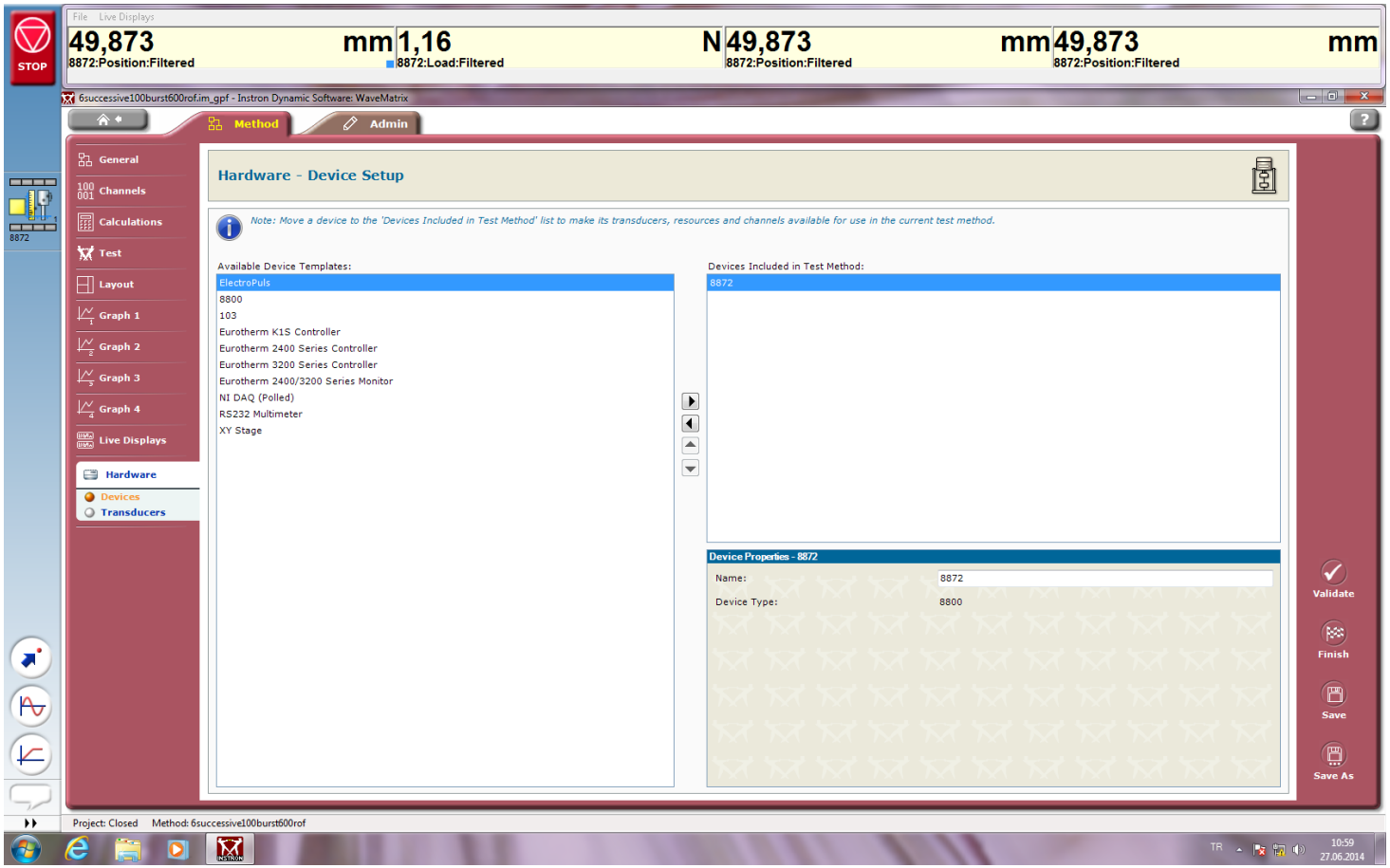

Figure C-9: WaveMatrix® Hardware Setup

D. SOFTWARE TUTORIAL

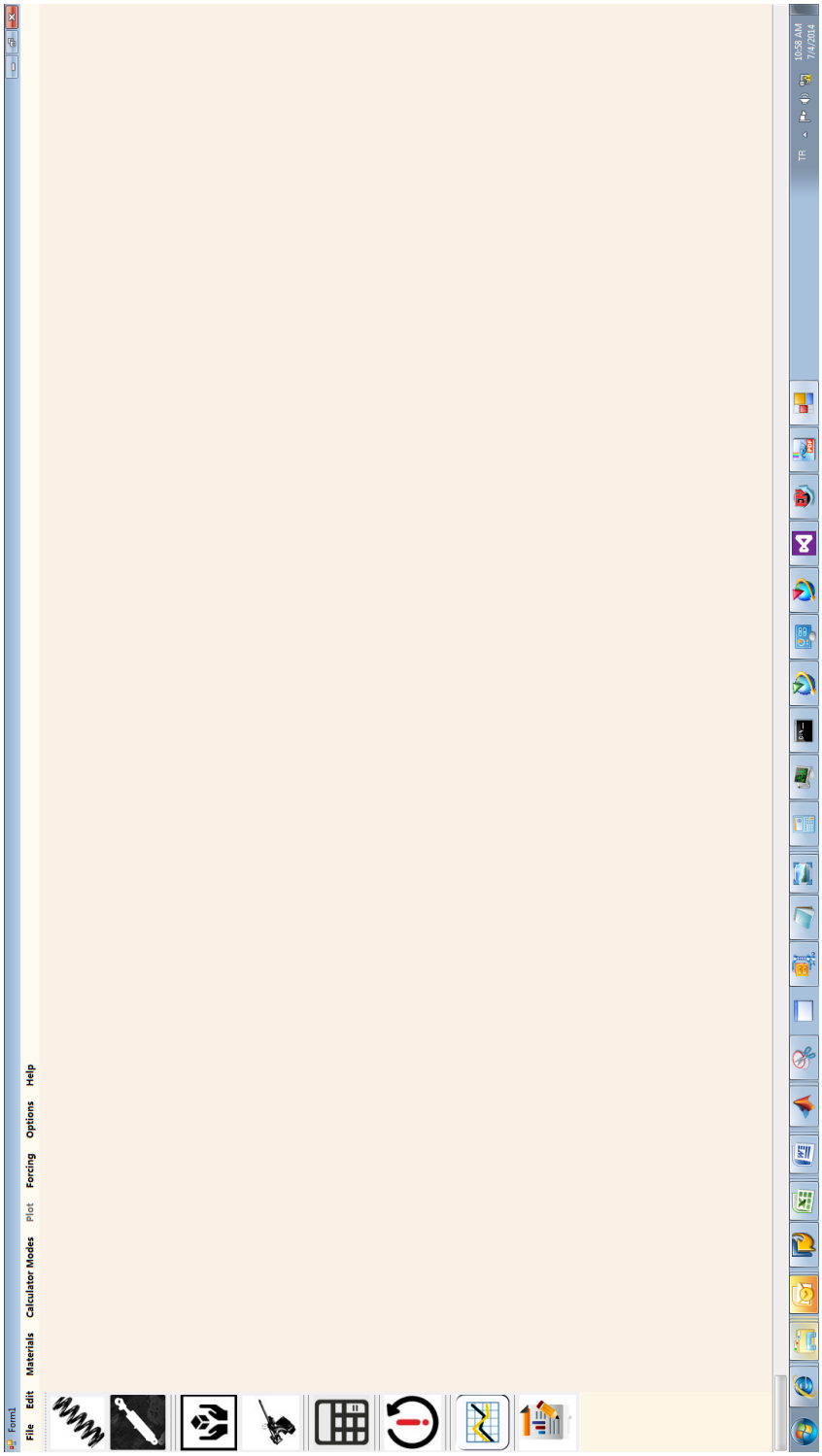

Figure D-1: Fresh Start of Software

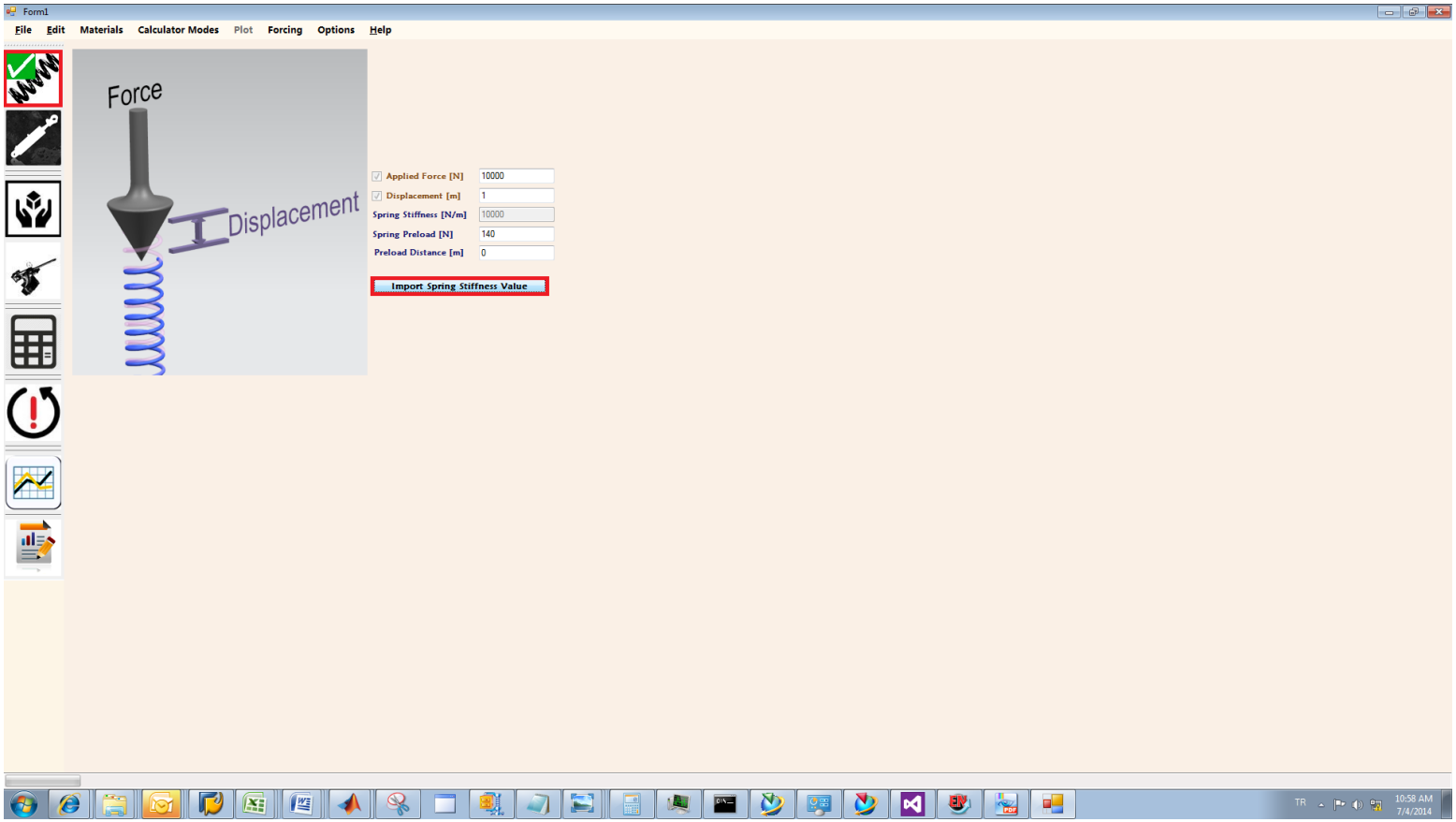

Figure D-2: Spring Parameters Input Panel of Software

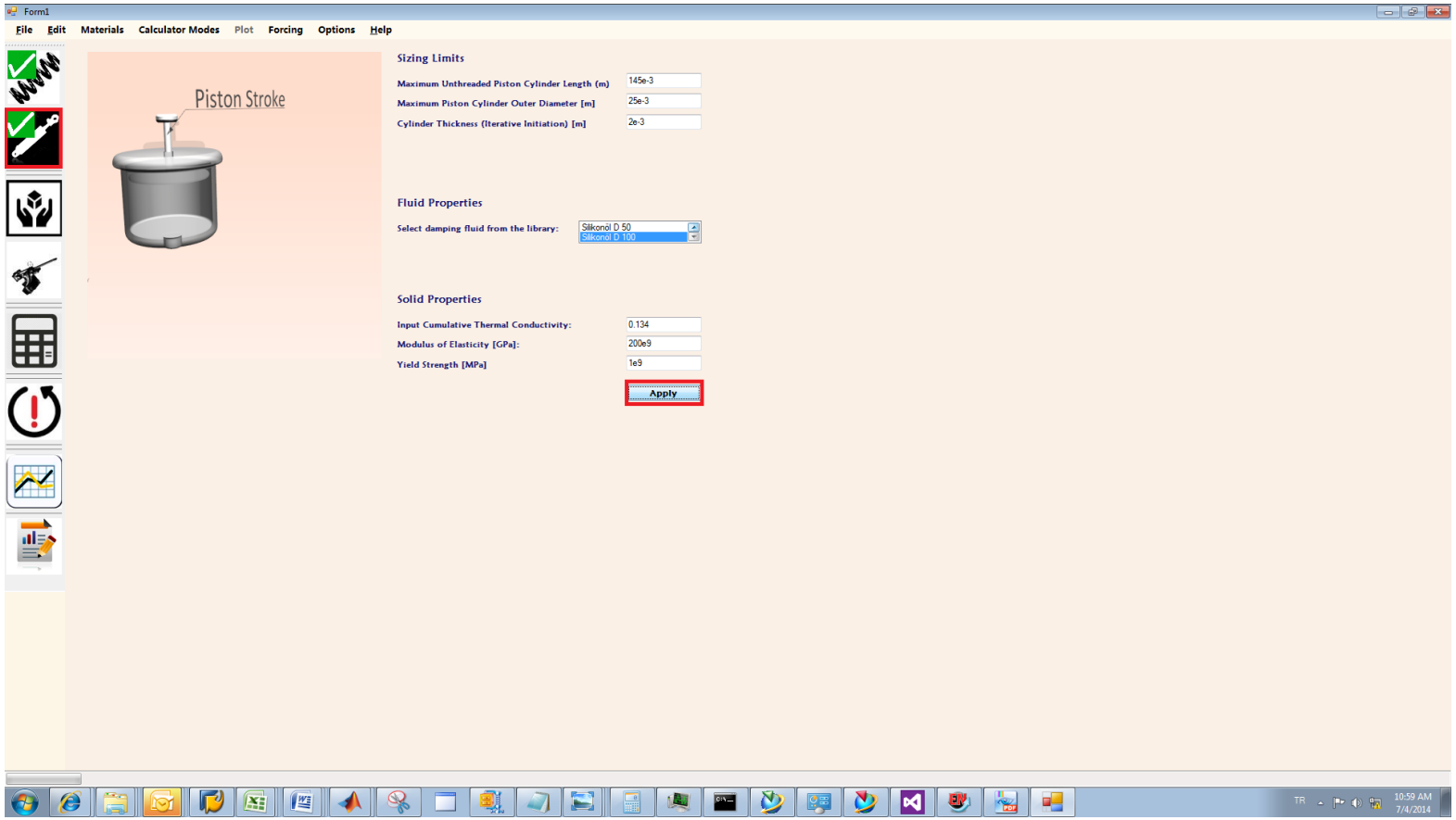

Figure D-3: Piston Parameters Input Panel of Software

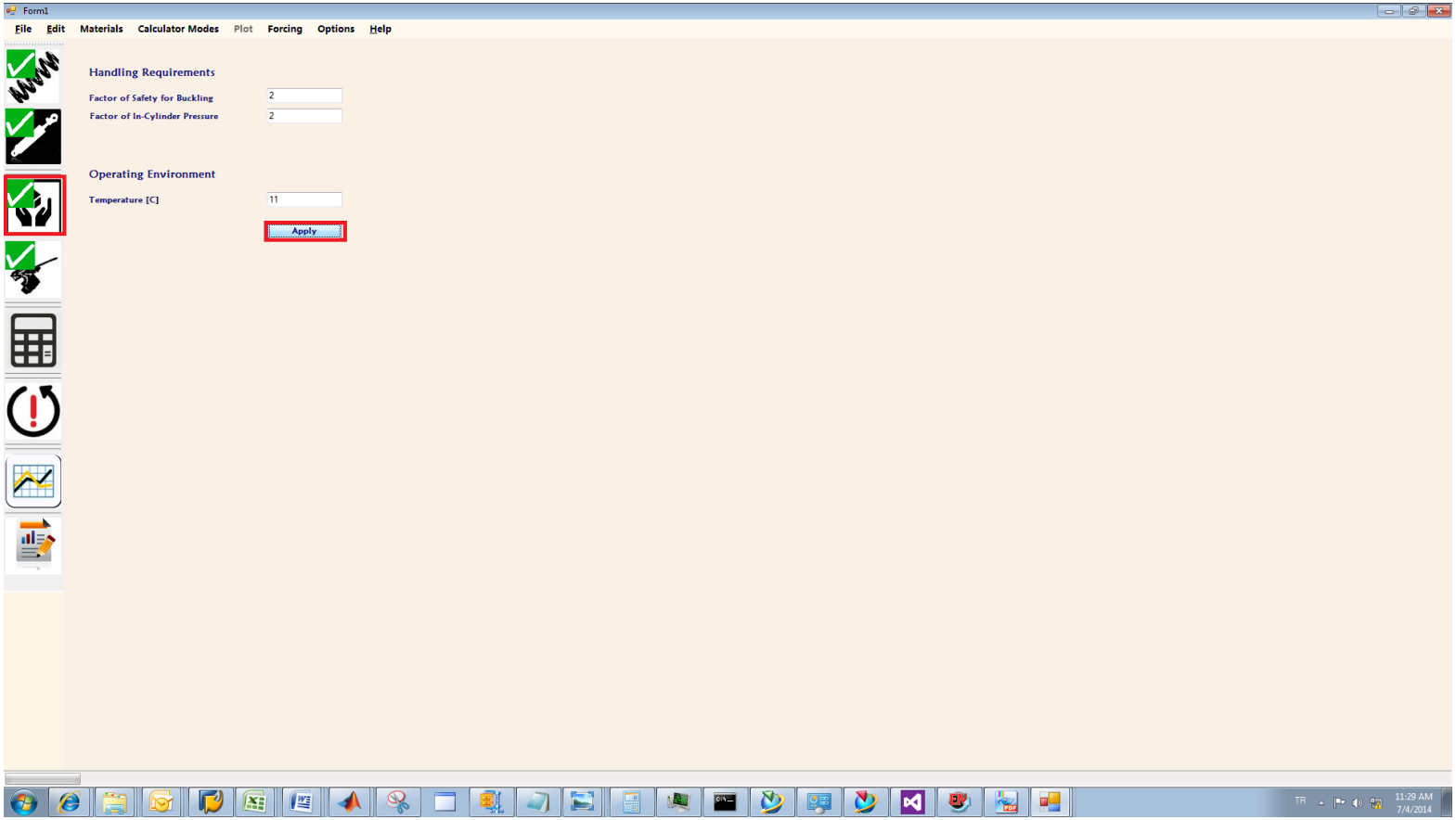

Figure D-4: Safety Factors and Operation Temperature Input Panel of Software

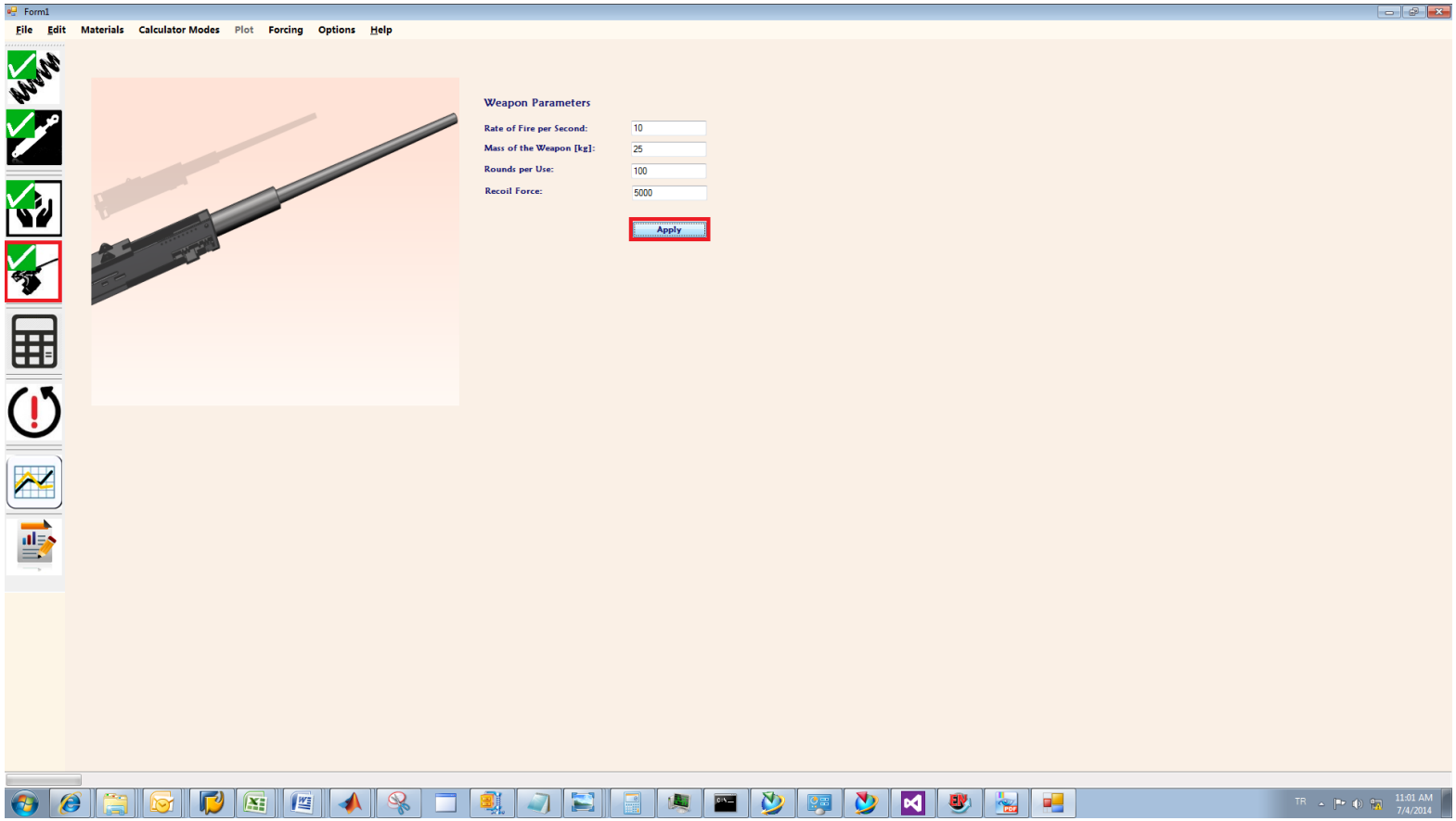

Figure D-5: Weapon Parameters Input Panel of Software

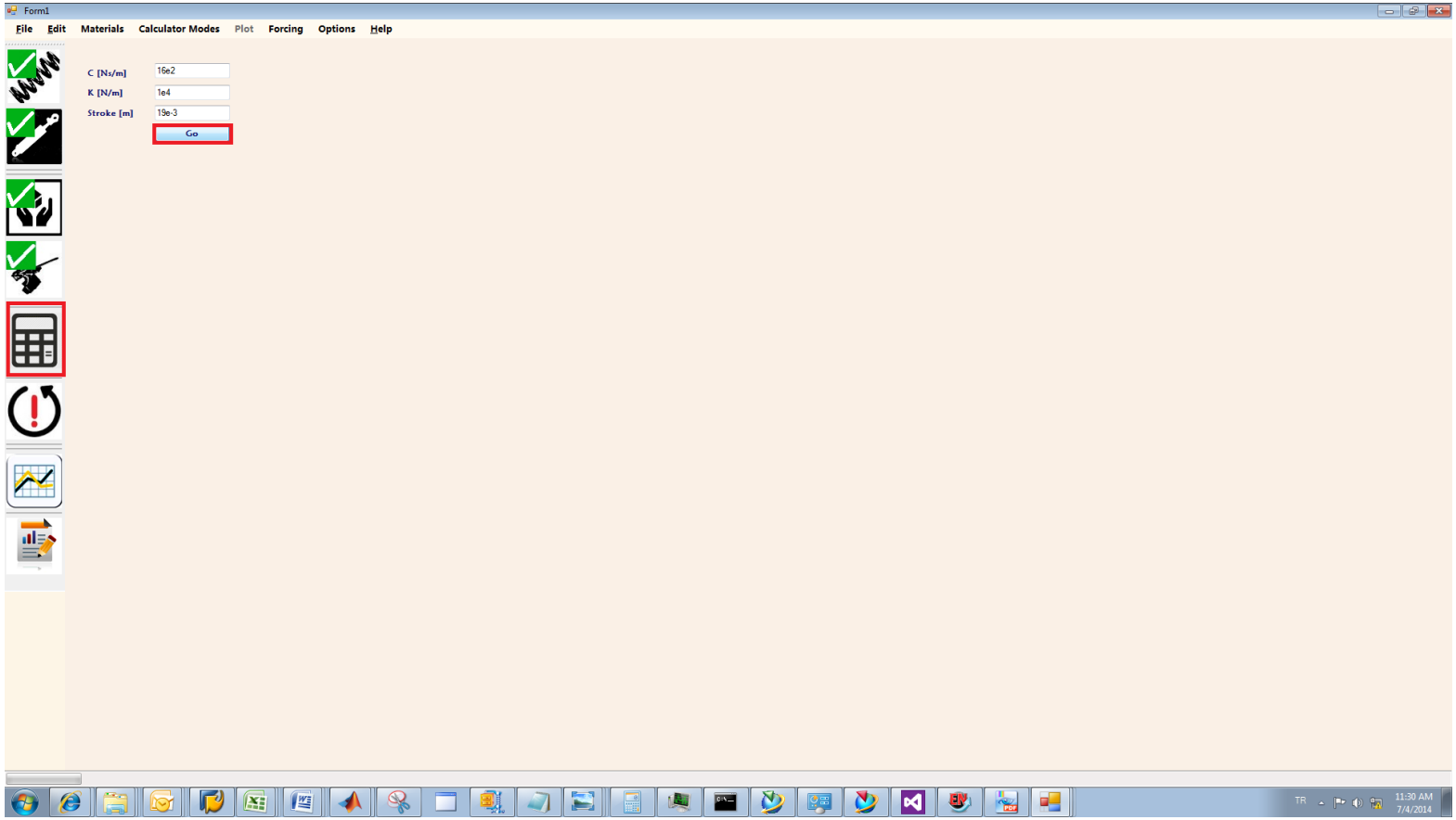

Figure D-6: Desired System Characteristics Input Panel of Software

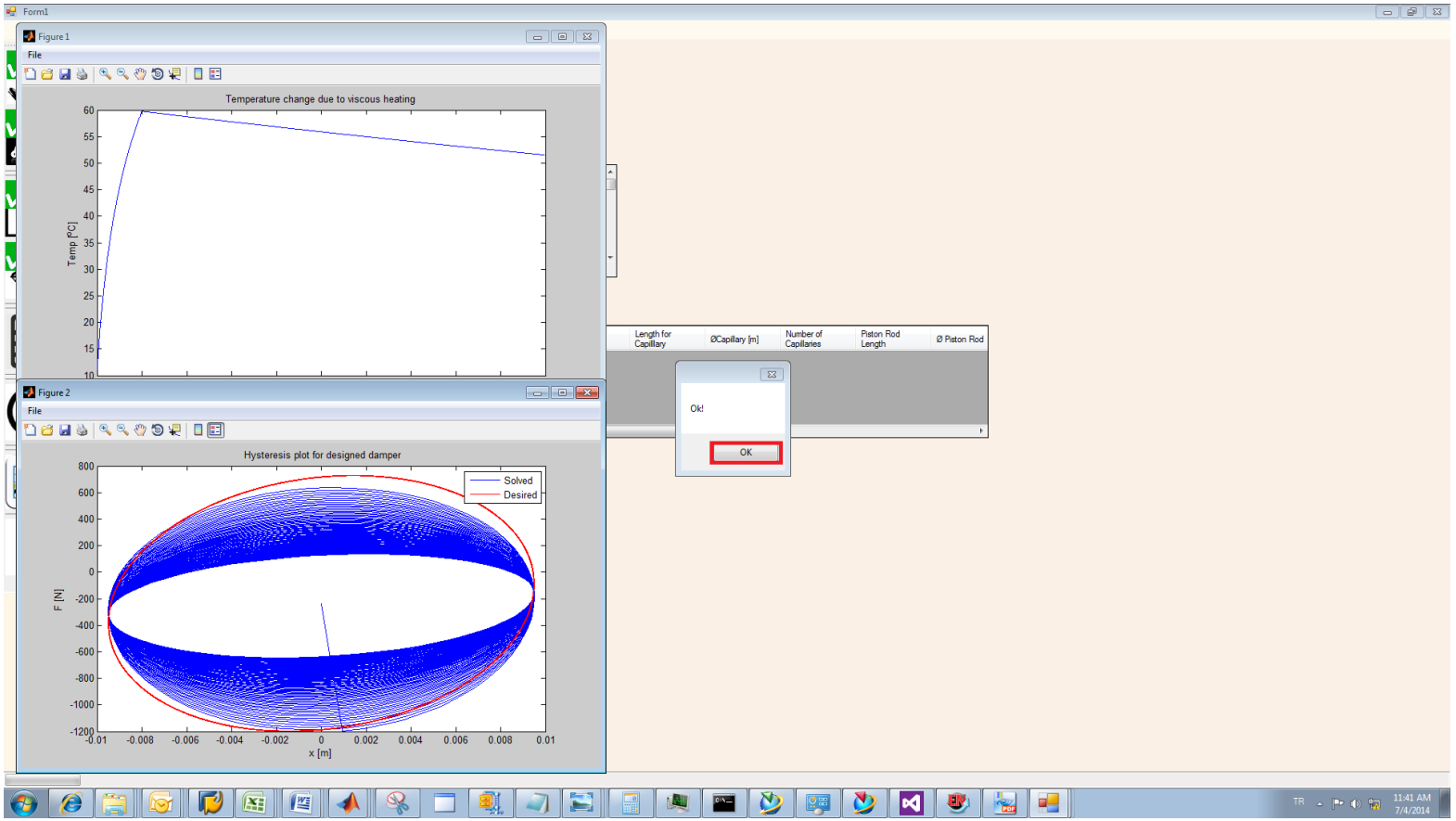

Figure D-7: Temperature on Cylinder Wall and Hysteresis Output for Successful Solution

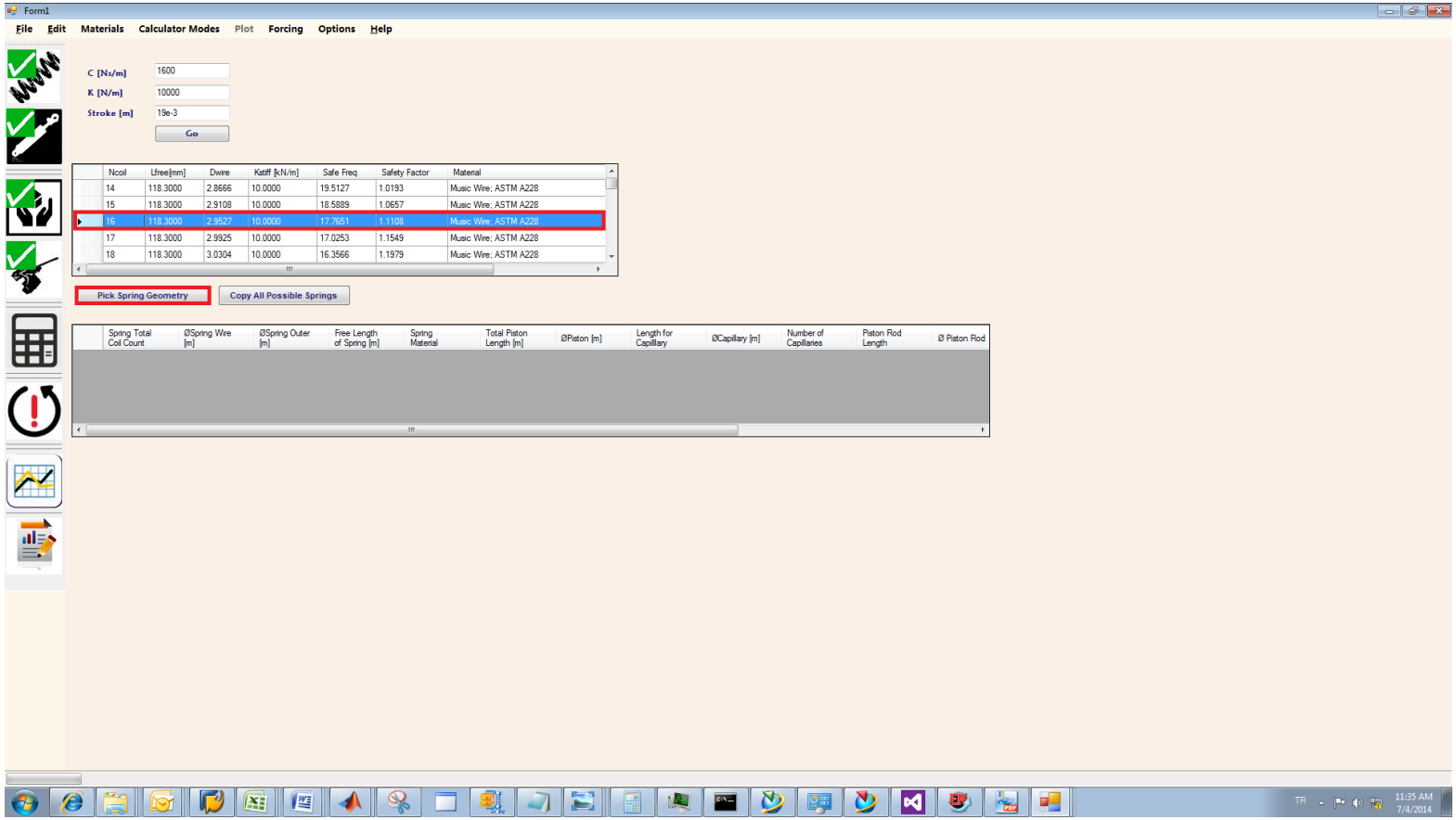

Figure D-8: Spring Selection Panel of Software

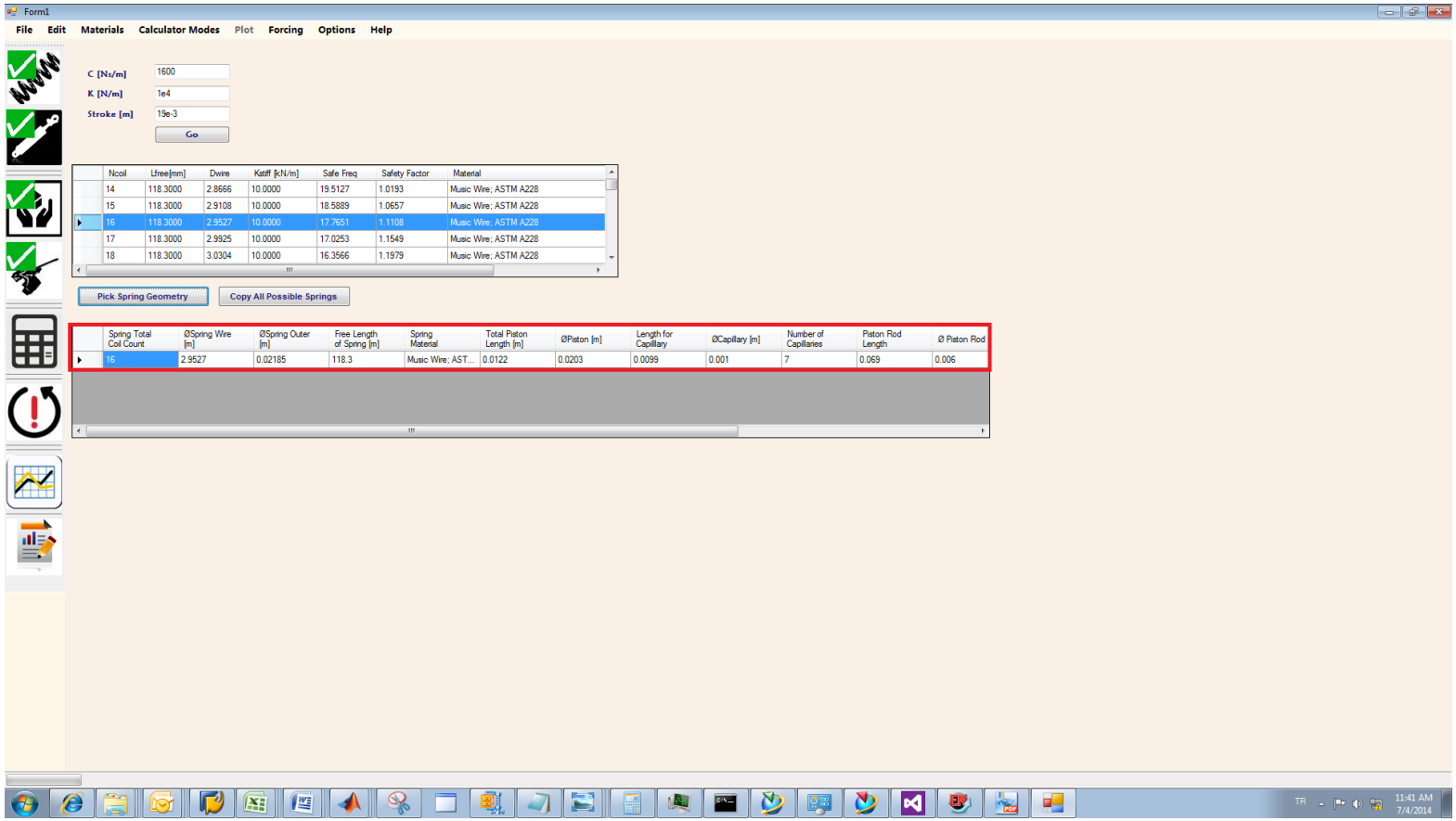

Figure D-9: Piston Parameters Output Panel of Software